

Proposal No. 281

Spokesman: G. A. Smith  
Michigan State University

PROPOSAL TO STUDY HIGH ENERGY PROTON-PROTON AND  
PI-MINUS PROTON INTERACTIONS WITH THE  
FNAL 30-INCH BUBBLE CHAMBER-WIDE GAP  
SPARK CHAMBER HYBRID SYSTEM

By

E. W. Anderson, H. B. Crawley, W. J. Kernan  
Iowa State University

R. G. Glasser, D. G. Hill, G. McClellan, G. A. Snow,  
B. Sechi-Zorn, G. T. Zorn  
University of Maryland

Z. M. Ma, W. Morris, B. Y. Oh, D. L. Parker, G. A. Smith, J. Whitmore  
Michigan State University

L. Voyvodic, R. J. Walker  
Fermi National Accelerator Laboratory

and

J. M. Bishop, N. M. Biswas, N. M. Cason, V. P. Kenney, W. D. Shephard  
University of Notre Dame

ABSTRACT

A review of the present instrumental measurement capabilities of the FNAL 30-inch bubble chamber-wide gap spark chamber hybrid system is presented. Numerous examples of physics coming from the system are given. A request is made for 700K pictures, including 300K pictures of protons on hydrogen at 300 GeV/c, 100K pictures of  $\pi^-$  on hydrogen at 100 GeV/c and 300K pictures of  $\pi^-$  on hydrogen at 375 GeV/c. Based on previous triggering rates which are characteristic of the hybrid system, only ~560K actual beam pulses need be photographed.

## TABLE OF CONTENTS

	<u>Page</u>
I. INTRODUCTION	1-3
II. WIDE-GAP HYBRID SYSTEM	3-9
III. PHYSICS	9-33
1. Exclusive Channel Analyses	11
2. Study of Diffractive Dissociation into Multi-Neutral Systems	19
3. Study of Single Pion Production	22
4. Long Range Correlations and the Nature of the Pommeranchuk Singularity	23
5. Inclusive and Semi-Inclusive Charged-Charged Rapidity Correlations in 200 GeV/c $\pi^-p$ Interactions	24
6. Gamma-Gamma and Gamma-Charged Particle Mueller Correlation Parameters for 200 and 300 GeV/c Proton-Proton Interactions	26
7. Inclusive and Semi-Inclusive Charged-Charged and Charged-Gamma Rapidity Correlations in 200 and 300 GeV/c Proton-Proton Collisions	30
8. Leading Particle Effects in $\pi^-p$ Interactions at 100 and 200 GeV/c	32
IV. REQUEST	33-39
1. Proton-Proton Interactions at 300 GeV/c	33
2. Pi-Minus Proton Interactions at 100 GeV/c	34
3. Pi-Minus Proton Interactions at 375 GeV/c	35
4. Summary	35

	<u>Page</u>
5. Correspondence concerning agreement to utilize E-215 data	37-39
V. REFERENCES	40-41
VI. FIGURE CAPTIONS	42-45
VII. FIGURES	After text

## I. INTRODUCTION

In 1971, the ANL, FNAL, ISU, Maryland and MSU groups were approved to build a hybrid bubble chamber-spark chamber system utilizing the 30-inch bubble chamber at FNAL. Approval was given for 250K pictures (100K protons at 200 GeV/c, 100K protons at 300 GeV/c, and 50K  $\pi^-$  at 100 GeV/c) to be taken by these groups and 200K pictures (120K  $\pi^-$  at 200 GeV/c and 80K  $\pi^+$  at 100 GeV/c) to be taken by groups from Duke, Notre Dame and Toronto ( $\pi^-$ ) and Purdue, Wisconsin ( $\pi^+$ ). These ten groups constitute the present E-2B collaboration. The downstream facility was completely tested and installed behind the bubble chamber in May 1972, according to the agreement with FNAL. Picture taking for approved "bare" experiments began in July 1972, and, as approved by FNAL, Experiment 2B began its running, primarily of a preliminary testing nature at first, behind the sequence of "bare" experiments.

Valuable experience was gained in terms of learning how to optimize spark chamber conditions and triggering schemes. However, during this period, only the spark chamber photographs were available, which somewhat limited our ability to truly optimize the entire system. By the fall of 1972, reasonably reliable operating conditions were realized and a short run of 10K proton pictures at 200 GeV/c was taken in November-December 1972.

The immediate availability of these correlated bubble chamber and spark chamber pictures was of immense value and permitted a full scale attack on the problems of spark chamber track reconstruction and track hookup with bubble chamber tracks. For the first six months of 1973, full attention was given to these tasks, as well as continuing to run in a parasitic mode behind "bare" experiments. The additional opportunity to run

the system under actual run conditions again proved valuable in terms of perfecting the use of the downstream equipment. As the program of "bare" experiments approached completion, the remaining approved running for E-2B (440K pictures) was completed in the period from November 1973 to April 1974.

In addition to the downstream apparatus, the E-2B group supplied a fast beam kicker (Duke) for the N-3 beamline, carried on studies of the cerenkov counter system (Purdue, Wisconsin) and completed a precision map of the bubble chamber magnetic field (Notre Dame-Toronto). Each of these contributions has had an important impact on the overall "bare" and hybrid 30-inch program.

According to the terms of the agreement between FNAL and E-2B, many of the bubble chamber photographs taken by the "bare" experiments have reverted to the E-2B collaboration. At this time, these include: 50K from E-125 ( $\pi^-$ -p @ 100 GeV/c); 50K from E-137 ( $\pi^-$ -p @ 200 GeV/c); 50K from E-37A (p-p @ 300 GeV/c) and 50K from E-121A ( $\pi^+$ -p @ 100 GeV/c). An additional 50K pictures from E-143A ( $\pi^-$ -p @ 280 GeV/c) are anticipated this fall. Some of these photographs, particularly those taken in the early part of the 30-inch "bare" program, are of limited value since operating conditions of the downstream system were being tested and varied at that time.

Since the completion of the approved E-2B running, the downstream system has been utilized as a "facility" by several other groups. In all, 300K pictures have been run or are in progress at this time in this mode, including 50K for E-161 (p-p and Ne @ 300 GeV/c), 50K for E-163A ( $\pi^-$ -p and Ne @ 200 GeV/c), 100K for E-209 (p-D @ 300 GeV/c), and 100K for E-280 (p-D @ 200 GeV/c).

It is our opinion that the data taken to the present demonstrate that the hybrid system is an extremely valuable instrument and, in fact, in many ways render the "bare" chamber somewhat obsolete. In the following discussion we present a careful study of the hybrid system's properties, including resolution, triggering versatility and uniqueness in the detection of gamma rays.

## II. WIDE GAP HYBRID SYSTEM

The physical layout of the E-2B hybrid system is shown in Figure 1. In this configuration the 30-inch bubble chamber is used as a detector of the event vertex and for measuring the momentum and angles of low momentum charged tracks ( $< 15$  GeV/c) and the wide-gap optical spark chambers are used to measure the momentum and angles of forward, high momentum secondary charged tracks and the numbers and angles of forward gamma-rays.

The downstream apparatus consists of four dual wide-gap (8 inches) optical spark chambers each with an active area of 30 x 40 inches (horizontal x vertical). The chambers are approximately one meter apart and the most upstream chamber is approximately four meters from the center of the bubble chamber. Each of the four chambers is fired by a ten-stage Marx generator producing typically a 280 KV pulse with a width of 60 nanoseconds. With such a pulse as input and chamber termination of 100-150 ohms, track widths of 2-3 millimeters in space are achieved. In Figures 2 and 3 we show a plot of track width in space versus delay from coincidence and track width in space versus Marx voltage respectively. Although the indicated voltage and termination conditions, as well as film, are not those in use currently, the trend and scale of the data in Figure 2 are typical of current conditions, namely a chamber life-time of  $\sim 5$  microseconds. Similarly, Figure 3 shows the sensitivity of track width versus Marx voltage for single tracks.

For multitrack events of interest at FNAL, 28 KV per stage typically produces 3 mm tracks.

In Figure 4 we show a plot of the single gap efficiency, defined as the ratio of the number of times the first or second gap fires less the number of times the first gap does not fire but the second gap does, divided by the number of times the first or second gap fires, versus the observed track multiplicity, averaged over the four chambers. The efficiencies are quite high ( $> 97\%$ ) and only weakly dependent on multiplicity.

The chambers and optical recording system can be multipulsed easily with a cycle time of 250 milliseconds. The spark chambers have been successfully quadruple fired under actual run conditions for several hundred thousand pulses separated by 250 milliseconds, with beam pulses down to 40 microseconds in length. The system is therefore capable of collecting large amounts of data in conjunction with multipulse operations of the 30-inch bubble chamber. It is further possible to fire the chambers in pairs to photograph two triggers during each beam pulse.

Photography is done with two 35 millimeter Flight Research cameras using Kodak S0121 film with a new anti-halation base. Each frame contains three views of the tracks: (1) a direct view, (2) a 90-degree mirror view and (3) a 10-degree mirror view. The direct and 10-degree views are photographed at  $f/11$  with a demagnification of  $\sim 50$  and the 90-degree views are photographed at  $f/8$  with a demagnification of  $\sim 60$ . Comparing reconstructions using the three view-pairs removes ambiguities one normally gets from simple two-view reconstruction.

The trigger for the spark chambers is also shown in Figure 1. A trigger is generated if an incoming beam track either produces two or more forward secondary tracks as detected in a set of three  $dE/dx$  counters or

is deflected from a normal beam trajectory as detected by two sets of aligned counters, one upstream and one downstream of the bubble chamber. The  $dE/dx$  counters are each  $8 \times 14 \times 1/16$  inches and are viewed at two ends by RCA 8575 photomultiplier tubes. Each of the three counters is required to produce a signal larger than the minimum signal produced by the simultaneous passage of two minimum-ionizing particles. The upstream and downstream counters divide the beam into five 5 mm and 6.5 mm horizontal slices respectively (Figure 1 indicates only three of the five counters), the difference in size being such as to compensate for beam divergence and multiple scattering. These dimensions give a lower momentum transfer squared cut-off of  $-0.02 \text{ GeV}^2/c^2$ , enabling us to trigger on a large fraction of low multiplicity (2-prong) elastic and inelastic events with a low momentum target recoil particle. Logic is used to determine whether a given particle stays in the appropriate slice. If not, a trigger is generated. The two triggering systems complement each other in two respects: (1) the  $dE/dx$  trigger efficiency increases with increasing beam momentum, whereas the beam deflection trigger efficiency falls somewhat with increasing beam momentum; (2) the  $dE/dx$  trigger has high efficiency for high multiplicity events, whereas the beam deflection trigger has high efficiency for low multiplicity events (particularly elastic and quasi-elastic two-prong events). Typical efficiencies, assuming an OR combination of the  $dE/dx$  and deflection signals, exceed 95%.

A typical event is shown in Figure 5. The bubble chamber view shows two slow tracks and six forward tracks which are detected and photographed in the spark chambers. Only the upstream chambers are shown in the figure. Immediately adjacent to and on each side of the data box one



sees the direct view of the two upstream chambers, with the 10-degree view overlaid (short track segments). The 90-degree view of the two upstream chambers is farthest from the data box. As can be seen, each camera-based optical system has many fiducials. Survey measurements give the relative coordinates of the fiducials in space. Subsequent film measurements and fits to the fiducials give spatial X-Y R.M.S. deviations of ~150 microns in the direct views and 400 microns in the 90-degree views.

The bubble chamber magnet deflects particles vertically and the direct views record this deflection. For a 200 GeV/c track the deflection from the center of the bubble chamber to the center of the first two spark chambers is 19 millimeters with the bubble chamber central magnetic field set at 30 Kg.

The software system for the Experiment 2B FNAL hybrid spectrometer has three basic components: (1) reconstruction in the bubble chamber; (2) reconstruction in the spark chambers, and (3) the track hookup between the two detectors. Reconstruction in the bubble chamber is done with the standard program TVGP.

In Figure 6 we show a block diagram of the logic flow in the spark chamber reconstruction program. The film plane measurements are first transformed to the ideal film plane in much the same way that TVGP does for the bubble chamber. Then each direct view track is paired with the 90-degree mirror view tracks and each resulting view-pair reconstruction is rejected unless there is a corresponding 10-degree mirror view track image. This procedure is continued until all tracks have been reconstructed without ambiguities. Figures 7 and 8 show point scatter (FRMS) distributions in space for a sample of beam tracks. The direct views (Figure 7) measure the momentum determining coordinate ( $y$ ) and the indirect views

(Figure 8) measure the equivalent of the bubble chamber depth ( $z$ ) coordinate. Since each dual gap spark chamber has a separate 90-degree mirror view, this process is repeated four times and the four resulting track segments are subjected to a least squares fit to obtain a best determination of the physical quantities of interest for each track. These quantities are: (1) two angles corresponding to azimuth ( $\phi$ ) and the dip ( $\lambda$ ) in the usual bubble chamber terminology, and (2) two transverse beam-coordinates ( $y, z$ ), all calculated at a fixed value of  $x$ , the coordinate along the beam direction.

Pursuant to the hookup with the bubble chamber, the track coordinates and angles are then transformed to the bubble chamber coordinate system. The matrix used to carry out this transformation is obtained from a sample of magnet off, straight-through tracks. Figure 9 shows, for example, the distribution of the difference between the  $y$  coordinate of the last point measured on the track in the bubble chamber and the  $y$  coordinate of the spark chamber track extended back to the bubble chamber. The width of this distribution ( $\pm 1$  mm) results from the propagation of bubble chamber and spark chamber errors, and possibly other effects such as fluid motion, magnetic field uncertainties, etc.

The track hookup program now combines the bubble chamber and spark chamber results. Figure 10 shows a block diagram of the logic flow of this program. Each bubble chamber track with angles and momentum approximately consistent with the spark chamber acceptance is propagated to the no field region using a Runge-Kutta stepping method, then drifted to the point  $x_0$  at which the spark chamber coordinates and angles are known. At this point, one of two options is elected: (1) if there is no track candidate in the region of acceptability the track is completed with

only the bubble chamber information for it; or (2) if there is a track candidate, then the program proceeds to iterate angles and momentum repeating the bend-drift until a best fit is obtained.

We have measured forward tracks with the spark chamber-bubble chamber hybrid system having momenta between 15 GeV/c and 300 GeV/c. The momentum distribution for a sample of 200 GeV/c beam tracks is shown in Figure 11. We note that the FWHM of the distribution is 25 GeV/c, considerably smaller than the ~90 GeV/c value obtained with the bubble chamber data alone in the same film. We show similar results in Figure 12 for 300 GeV/c beam tracks. These results are consistent with the fact that the percentage error on momentum scales as the momentum.

In Figure 13 we show a  $\pm\Delta p/p$  vs.  $p$  scatterplot for a sample of secondary tracks as measured in the bubble chamber alone and as measured in the combined hybrid system. The pull-quantities on the four variables ( $\phi$ ,  $\lambda$ ,  $y$ ,  $z$ ) used in the hook-up are normal ( $\pm$  unit half-width) and hence we believe our error estimations have been realistic and quoted errors are accurate. The straight line indicates our original estimated expectations for the system, with a form

$$\pm \frac{\Delta p}{p} (\%) = 0.07 p \text{ (GeV/c)} \quad (1)$$

Our results indicate a more realistic representation of the form

$$\pm \frac{\Delta p}{p} (\%) \approx 0.04 p \text{ (GeV/c)} \quad (2)$$

At all values of momentum the accuracy of the hybrid system is vastly superior to that of the bubble chamber alone.

The hybrid system has proven itself to be a highly efficient detector of gamma-rays. This has been achieved by inserting 2.27 radiation lengths of lead between the last two spark chambers. Up to as many as ten

gamma-ray showers have been successfully and unambiguously identified and measured in spark chamber #4. This technique adds a new dimension to the study of gamma-ray production in high energy bubble chamber experiments with the addition of an efficient gamma converter to a pure hydrogen target system. In Figures 14 and 15 we show two examples of shower production indicating one and five showers respectively. Because of the relatively high yield of gamma-rays in collision processes at FNAL energies (typically six per event), the wide-gap spark chambers with their inherent high multi-track efficiency are ideally suited to this problem.

### III. PHYSICS

In this section we discuss several physics problems which illustrate the power of the hybrid system. In each instance, the detection of gamma-rays and/or improved momentum resolution on charged tracks is involved in a special way. Because we are requesting further proton and  $\pi^-$  running, the topics have been kept to these areas.

Before turning to specific physics discussion, we list in Table 1 the progress to date on scanning and measuring of bubble and spark chamber photographs from the proton and  $\pi^-$  exposures of E-2B.

Table 1. Scanning and Measuring Progress

<u>Particle</u>	<u>Momentum</u>	<u>Exposure</u>	<u>#BC Pictures Scanned</u>	<u>#BC Events Measured</u>	<u>#SC Pictures Measured</u>
p	200 GeV/c	100 K	82 K	14 K	9 K
p	300	100	78	12	8
$\pi^-$	100	50	48	5	4
$\pi^-$	200	120	82	9	11
		<hr/>	<hr/>	<hr/>	<hr/>
		370 K	290 K	40 K	32 K

Unless specifically indicated, the data presented in this section are based on event samples with good spark chamber triggers and hooked-up tracks. We note that 50% of all visible interactions in hydrogen have good triggers. Since the beam burst is  $\sim 100$   $\mu$ sec long and the minimum recharging time of the system is  $\sim 250$  msec, it is possible for beam interactions in the bubble chamber windows, which occur before the desired interaction in hydrogen, to trigger the system and leave the high voltage systems incapable of being triggered on a subsequent interaction. The triggered hydrogen events are easily identified, by (1) requiring spatial and time coincidence of the upstream PWC beam trajectory with the beam track which triggered the system or (2) requiring good hook-ups on bubble chamber tracks in the spark chambers. By grouping the four spark chambers into independent sets (for example, two groups of (1) spark chambers #1, 3, 4 and (2) spark chamber #2) we can trigger on two events per beam burst, in which case the hydrogen signal is enriched to 60% of all visible interactions. This mode of triggering has been tested and used in the past, although for only a small portion of the E-2B runs. In either case, as stated previously the system can cycle with the multi-pulse mode of bubble chamber operation, provided the time between beam bursts does not fall significantly below 250 msec.

Finally, we note that our triggered system permits substantial savings of bubble chamber film and development costs. Based on past performance with  $\sim 6$  beam tracks,  $\sim 20\%$  of the beam bursts have not yielded triggers, corresponding to instances where no event occurs, either in the hydrogen or adjacent materials. For these cases, the bubble chamber flash can be inhibited.

## 1. Exclusive Channel Analyses

### (a) Introduction

A summary of the existing data on the exclusive four and six body four-constraint final states in pp and  $\pi^-p$  interactions at incident momenta above 20 GeV/c is shown<sup>1,2</sup> in Table 1 and Figure 16. Two of the more interesting aspects of these data are (a) whether the four (and six) body final states are entirely diffractively produced, in which case one might expect that the cross sections should show little or no energy dependence, and (b) how big is the contribution to these exclusive final states from the Double Pomeron exchange process (see Figure 17)? Table 1 shows that, at present, there is no information on the six body final state and only preliminary answers can be given regarding the four body reactions. This is partly a result of the low level of statistics in the bare bubble chamber experiments but, more importantly, the accuracy attained on high momentum tracks in the bare chamber experiments results in large systematic errors in the estimation of background contamination in these samples due to final states with one or more neutral particles. In this proposed experiment we expect to overcome both of these difficulties.

In Figures 18-20 we show some preliminary results based on the 200, 300 GeV/c pp data and the 100 GeV/c  $\pi^-p$  data. The following specific reactions have been considered:

$$pp \rightarrow pp \quad (3)$$

$$\pi^-p \rightarrow \pi^-p \quad (4)$$

$$pp \rightarrow pp\pi^+\pi^- \quad (5)$$

$$\pi^-p \rightarrow \pi^-p\pi^+\pi^- \quad (6)$$

$$pp \rightarrow pp\pi^+\pi^-\pi^+\pi^- \quad (7)$$

and  $\pi^-p \rightarrow \pi^-p\pi^+\pi^-\pi^+\pi^- \quad (8)$

Table 1. Summary of Existing Data on Exclusive Four and Six Body Four-Constraint Final States

<u>Beam</u>	<u>Final State</u>	<u>Events</u>	<u>(<math>\mu\text{b}</math>)</u>	<u>Double Pomeron (upper limit) (<math>\mu\text{b}</math>)</u>	<u>(events)</u>
205 GeV/c pp	$p\bar{p}\pi^+\pi^-$	191	$680\pm 140$	$44\pm 15$	9
100 GeV/c $\pi^-p$	$\pi^-p\pi^+\pi^-$	101	$590\pm 70$	$40\pm 20$	8
205 GeV/c $\pi^-p$	$\pi^-p\pi^+\pi^-$	128	$530\pm 65$ ( $630\pm 61$ )	$\leq 50$	
5.52 GeV/c pp	$p\bar{p}\pi^+\pi^-\pi^+\pi^-$		$227\pm 23$		
10. GeV/c pp	"		$460\pm 40$		
19. GeV/c pp	"		$400\pm 200$		
28.5 GeV/c pp	"		380 (no error given)		
3.9 GeV/c $\pi^-p$	$\pi^-p\pi^+\pi^-\pi^+\pi^-$		$115\pm 11$		
5.48 GeV/c "	"		$210\pm 20$		
5.97 GeV/c "	"		$250\pm 20$		
6.00 GeV/c "	"		$220\pm 20$		
7.00 GeV/c "	"		$260\pm 30$		
10.00 GeV/c "	"		$420\pm 50$		
11.00 GeV/c "	"		$290\pm 30$		
16.00 GeV/c "	"		$250\pm 20$		

Figures 18(a) and 18(c) show the resulting missing mass squared ( $MM^2$ ) for two-prong events which fit the reaction (3) when no use of the downstream system has been employed. When we use the data resulting from the fast track which hooks up in both spark chamber and bubble chamber (shaded events) we obtain Figures 18(b) and 18(d). Similar data for reaction (4) are shown in Figures 20(a) and 20(b). The increased resolution is apparent and, furthermore, the background visible, particularly in Figures 18(a) and 18(c), has been considerably reduced. For the events fitting the elastic channel (3), we have also examined whether there are  $\gamma$ -rays detected in the fourth spark chamber following the 2.27 radiation lengths of lead. We find that  $7.2 \pm 1.4\%$  of the events have at least one photon shower, presumably generated by the interaction of the fast forward proton in the downstream bubble chamber windows. An independent analysis of triggers on single beam tracks predicts this rate should be  $6.8 \pm 0.9\%$ . Hence, we conclude that the percentage of inelastic background in the elastic sample is  $\approx (0.4 \pm 1.7\%) \times 1.6 = 0.6 \pm 2.7\%$ , where the factor of 1.6 corrects for gamma-ray acceptance. Presumably background in reaction (4) is somewhat less.

Figure 19 shows similar distributions for reactions (5) and (7). In each case, as expected, the distributions using information from the downstream system show better resolution and lower background levels than the corresponding bare chamber measurements. In these distributions, we have required that the resulting kinematic fit be consistent with the observed ionization for the slow particles in the bubble chamber and that the Feynman  $x$  variable ( $x = 2P_L^*/\sqrt{s}$ ) for the  $\pi^+$  in reactions (5) and (7) be  $x \leq 0.6$ , as was found to be necessary in a previous 205 GeV/c pp experiment.<sup>3</sup> After applying these criteria, we find that the  $x$  distributions



for  $p$ ,  $\pi^+$  and  $\pi^-$  (shown in Figures 21 and 22) each show the required symmetry of the  $pp$  center-of-mass system, thus indicating no obvious biases in these samples. Similar  $MM^2$  plots are shown for the 100 GeV/c  $\pi^-p$  data in Figures 20c-f. The shaded events in Figures 19b, d, f, h and 20d, f, are those which have either all, or a significant fraction, of the forward hemisphere tracks which hook up.

For the elastic samples, we have considered the resultant apparent resolution in  $MM^2$ . Referring to the detailed plots of Figures 18(b), 18(d) and 20(b) (see inserts) we note that our estimated half-widths of the  $MM^2$  distributions scale approximately as  $p(\text{beam})$ , according to the relation  $\Delta(MM^2) \sim \pm 0.06 \frac{p(\text{beam})}{100}$  expressed in  $\text{GeV}^2$  units. Because the numerical coefficient in this formula is not small compared to  $M_\pi^2 = 0.02 \text{ GeV}^2$ , kinematics alone cannot be used to rule out some small inelastic contamination in the elastic samples. As discussed previously, our gamma-ray data tell us that the contamination is  $(0.6 \pm 2.7)\%$ .

We have attempted to use gamma-ray data to estimate backgrounds in our samples of events for reaction (5), in a fashion similar to that used for reaction (3). This is somewhat more difficult, since there is more background in the gamma-ray data due to the presence of several charged particles in the vicinity of the downstream windows. Scaling the  $\pi^\pm$  interaction rate down from protons ( $6.8 \pm 0.9\%$ ) by the ratio of total cross sections to ( $4.3 \pm 0.5\%$ ), we find a positive excess of gamma-ray events over calculated background to be  $\leq 11\%$ . Because of the conservative assumptions made to get this estimate, we quote an upper limit. This is to be compared with the estimated background of  $\approx 20\%$  for the "bare" 200 GeV/c experiment.<sup>3</sup>

(b) Physics Discussion

In this section we discuss in more detail some of the physics to be investigated using the four-constraint events that we expect to obtain.

(1) Four-prong events: As indicated above, the most interesting aspects in the four-body final states are the investigation of the Double Pomeron (DP) exchange process and the question of the amount of diffraction in these final states. The bare chamber experiments have set upper limits of  $\sim 40 \mu\text{b}$  to the DP contribution to reactions (5) and (6). With this proposed experiment, we would like to investigate this topic with 1 event/ $\mu\text{b}$ , i.e., we would have  $10 \pm 3$  events if the DP contribution were to be as small as  $10 \mu\text{b}$ .

An interesting study that requires a clean sample of the events is the analysis of diffraction in the four-body final states. Figure 16 shows the four-body cross sections as a function of laboratory momentum. There is an indication that these cross sections are becoming independent of energy as might be expected for a diffractively produced final state. The present errors ( $\sim 15\%$ ) are dominated by background contamination uncertainties. A measurement at 300 GeV/c with  $\pm 5\%$  errors would certainly be most useful.

From studies of the effective mass and rapidity distributions in these final states, it is concluded<sup>1-3</sup> that  $\sim (90 \pm 10)\%$  of the four-body final states is consistent with either proton or pion diffraction excitation. Are the remaining 10% events non-diffractive (including DP) or are they due to the contamination from final states with one or more neutral particles? In the proposed experiment we would hope to be able to answer this question at  $\lesssim 5\%$  level.

Bare chamber studies of reaction (6) have indicated that pion and proton dissociation seem to contribute equally to this final state. However, the pion diffraction contribution, resulting in fast charged particles in the laboratory system, is the most difficult to extract reliably in the kinematic fitting procedure. We therefore expect that the pion dissociation sample be the one most likely to be improved significantly by the use of the hybrid system.

Other topics which will be studied in detail include:

- (1) We expect to be able to study the two and three-body effective mass distributions and possibly to isolate various quasi-two body processes such as  $pp \rightarrow N^{**}(1680)p$  and  $\pi^-p \rightarrow A_1^-p$ . Comparison of these cross sections and mass distributions with similar ones found at lower energies could be most illuminating.
- (2) Having a large sample of the four-body final state produced in  $pp$  and  $\pi^-p$  interactions at a similar energy will permit the study of factorization in a specific exclusive reaction (e.g., quasi-two body) as well as in an inclusive reaction. In particular, one will be able to study Pomeron factorizability if the reactions (5) and (6) are indeed dominated by diffractively produced three-body systems. Bare chamber data indicate factorization is good to  $\pm 30\%$ .
- (3) We will be able to investigate the contribution of the four-body state to
  - (a) inclusive low mass diffraction studies,
  - (b) single particle distributions, inclusively and semi-inclusively,
  - (c) two particle semi-inclusive correlation data  $R_{12}^n$ ,

- (d) the possible leading particle effect in  $\pi^-p \rightarrow \pi^- + X$
- (e) inclusive  $\Delta^{++}$  production and  $\rho^0$  production.

(ii) Six-prong events: Very little data presently exist<sup>4</sup> on the six-body 4c final states reactions (7) and (8), as seen in Table 1, so it is hard to predict what these channels will yield. Much of the analysis possible on the four-body final state can also be duplicated on the six-body. These are, however, the following topics specific to the latter:

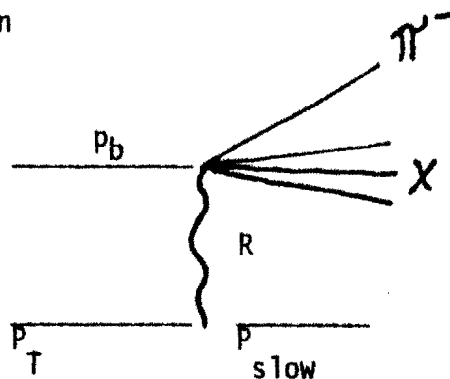
- (1) With the availability of increased resolution on invariant mass combinations of the forward hemisphere, we expect to be able to look for double diffraction dissociation e.g.:



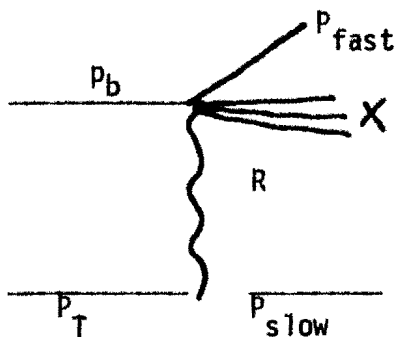
and compare the observed cross sections with those expected on the basis of Pomeron factorization.

- (2) We will study the ratio of double to single dissociation and again measure how much (all?) of the 6-prong 4c final state is diffractively produced and the ratio of  $\pi$  and p dissociation.
- (3) Double Pomeron exchange is likely to occur in two forms in the six-prong final states, as shown in Figure (17b). The first diagrams in Figure (17b) should be related by Pomeron factorization.

- (4) Is there evidence for double  $\Delta^{++}$  production?  
 (5) Bare chamber studies have shown<sup>5</sup> that by studying the properties of inclusive  $\pi^-$  production recoiling off a slow proton



in the overall C.M. of the  $R-p_b$  system one finds that the shape of the  $\pi^-$  invariant differential cross section is very similar to that observed in  $\gamma p \rightarrow \pi^- + \text{anything}$  when the CMS energies of the  $\gamma p$  and  $R-p_b$  system are similar. It would be very interesting to continue these studies by examining the contribution to this process from the exclusive reactions (5) and (7). In particular, with the increased accuracy on the fast proton in reactions (5) and (7) it will be of interest to study the properties of the X system in the process:



in order to look for diffraction of the exchanged particle R.

(111) Summary of Exclusive channel Analysis:

Much of the interest in the exclusive channels lies in investigating the diffractive properties of these final states and in measuring their contribution to the various inclusive distributions that have become fairly well known from previous experiments at FNAL or ISR. Furthermore, the study of double Pomeron exchange is of great interest at the present time.

2. Study of Diffractive Dissociation into Multi-Neutral Systems

While elastic scattering has now been well studied at incident beam momenta above 50 GeV/c, for the studies of diffraction, inclusive single particle distributions and multiparticle correlations it is important to be able to study the inelastic two-prong events on an event-by-event basis. This requires a reliable separation of the elastic and inelastic samples. In the bare chamber pp experiments at 100, 200, and 400 GeV/c this separation in the two-prong samples has presented problems. For example, at 205 GeV/c, the quoted uncertainty<sup>6</sup> in the inelastic sample for  $M_x^2 \leq 10 \text{ GeV}^2$  is  $(36 \pm 5)\%$ . Such an uncertainty must be taken seriously, since the inelastic two-prong events form a substantial fraction of the total inelastic diffractive cross section. In Figures 18 and 20(a,b) we have shown that a very much improved separation of elastic events is possible by incorporating information from the downstream system. With such a system, errors which dominate the bare chamber analyses should be reduced enough to permit a detailed study of the cross section and diffractive component of the inelastic two-prong final states.

In Figure 23 we show the measured differential cross sections for elastic and inelastic two-prong events. For purposes of comparison, both the "bare" and complete hybrid data are shown. It should be noted that

the loss of events for  $-t \lesssim 0.05 \text{ (GeV/c)}^2$  is expected on the basis of the geometry of the five deflection counter triggering system. With the recently installed new five counters (which are smaller counters than used for the present data) we estimate that the lower bound on  $-t$  should be  $\sim 0.02 \text{ (GeV/c)}^2$ .

In Figure 24 we have plotted the  $M_x^2$  distribution for the combined inelastic two-prong samples at 200 and 300 GeV/c for events which have a slow proton ( $< 1.5 \text{ GeV/c}$ ). We have also completed a scan for  $\gamma$ -rays associated with these events and they are shown as the shaded area in Fig. 24. We find that 43% of the inelastic two-prongs with  $M_x^2 < 40 \text{ GeV}^2$  have one or more  $\gamma$  showers. The  $\gamma$ -ray data may be used to estimate elastic contamination in this sample. In the region of  $M_x^2 \approx 0.88 \text{ GeV}^2$  (one proton mass squared) where elastic contamination would be expected to be most pronounced, we observe that after correcting for  $\gamma$ -ray acceptance 69% of the events have associated  $\gamma$ -rays. The background due to window interactions is 6.8%, leaving 62% to be identified with multi- $\pi^0$  production. Arguments developed in the next section of this proposal show that the  $p\pi^+$  final state is  $\sim 19\%$  of the total inelastic two-prong cross section. We estimate that the  $n\pi^+\pi^+$  final state represents another  $\sim 10\%$ , thus the anticipated multi- $\pi^0$  contribution to the inelastic two-prongs is  $\sim 71\%$ . It then follows that the elastic contamination in the inelastic two-prong sample, after full utilization of the hybrid data, is  $\sim 9\%$ , substantially improved over the estimated  $36 \pm 5\%$  for the "bare" experiment at  $205 \text{ GeV/c}^6$ .

Since the primary motivation of this high statistics, increased accuracy bubble chamber-spark chamber experiment is to investigate the various components that build up the inclusive distributions which have

been studied in the bare chamber experiments, the study of a clear sample of two-prong inelastic events will have important consequences on the following topics:

1. Improved inelastic charged multiplicity distribution and the resulting moments derived from the distribution;
2. The study of the magnitude and shape of the diffractive component and the multiplicity dependence thereof;
3. It is particularly important to remove elastic events when studying a possible leading particle effect in the inclusive reaction  $\pi^-p \rightarrow \pi^- + (p + \text{neutrals})$ . This will be discussed in more detail later;
4. In order to study distributions semi-inclusively, i.e., for fixed number of charged final state particles, a large sample of inelastic two-prongs would be most useful, e.g., two-particle correlation function  $R_{12}^{++}(y_1, y_2)$ .

With the proposed experiment we would like to continue our studies of  $\pi^0$  production in the low mass diffractive component. Bare chamber experiments have shown<sup>2</sup> that there appears to be a strong correlation between the average number of  $\pi^0$ 's,  $\langle \pi^0 \rangle$ , and the number of charged particles,  $n_C$ , for inclusive  $\pi^0$  production. In a recent study<sup>5</sup> in the "bare" chamber, shown in Figure 25, the values of  $\langle \pi^0 \rangle$  vs  $n_C$  have been separated for those events which can be considered diffractive, i.e., the  $M_x^2$  recoiling off a slow proton should be less than  $25 \text{ GeV}^2$ , and the remaining, i.e., non-diffractive, sample. One observes that a much weaker correlation (perhaps none?) is found for each component. In the hydrogen bubble chamber the average conversion efficiency per  $\gamma$ -ray is less than 2%. As a preliminary study of



the  $\gamma$ -rays that convert in the downstream Pb plate, we show Figure 26 which presents the rapidity distributions for  $\gamma$ -rays associated with different numbers of charged particles. The shaded events correspond to a sample of beam dissociation interactions. It is clear that, with those events and with the distributions based on the  $M_X^2$  recoiling from a fast proton, we will be able to make a much more detailed examination of  $\pi^0$  production in the diffractive and non-diffractive components than has been possible in the bare chamber.

### 3. Study of Single Pion Production

As a final project, we hope to be able to isolate an enriched sample of one constraint events, e.g.,  $pp \rightarrow pn\pi^+$  (11)

$$pp \rightarrow pp\pi^0 \quad (12)$$

$$\pi^-p \rightarrow \pi^-p\pi^0. \quad (13)$$

Preliminary data<sup>7</sup> from the ISR show that the cross section for reaction (11) at 1500 GeV is  $270 \pm 80 \mu\text{b}$  and appears to continue to fall with the same energy dependence ( $p_{1ab}^{-.4}$ ) as the cross sections at energies below 30 GeV/c. This would appear to be somewhat surprising since one would expect a large fraction of reaction (11) is due to diffractive production of  $N_{1/2}^*$  states (see for example, the corresponding discussion of the four-body final state reactions (5) and (6), which are almost entirely diffractively produced at FNAL energies).

Assuming the aforementioned energy dependence, we would anticipate observing a cross section for reaction (11) of  $\sim 550 \mu\text{b}$  at 200 GeV/c. This represents 19% of the total inelastic two-prong section (2.85 mb). Assuming diffraction dominance ( $N_{1/2}^*$  production), we would correspondingly expect a cross section for reaction (12) which is one-half that for (11),

or  $\sim 275 \mu\text{b}$ . Hence,  $\sim 28\%$  of the total inelastic two-prong cross section would be one-constraint final states.

The aforementioned results (see Section 1(a)) on  $\Delta(\text{MM}^2)$  (for elastic events) imply simple one-constraint fitting may be difficult, particularly at the highest FNAL energies. However, by making cuts on the number of observed gamma-rays and ionization we can enrich the sample before fitting. For reaction (12) we estimate the ratio of signal to all events will go from 9% to  $\sim 24\%$  after removing events with three or more gamma-rays and selecting events with slow protons. For reaction (11) the enrichment is  $\sim 27\%$ , up from 19% after eliminating events with one or more gamma-rays. In each case,  $\sim 7\%$  of the signal will be lost in the gamma-ray cuts due to interactions of the fast, forward track in the bubble chamber windows. Similar arguments can be made for the  $\pi^-$  induced reaction (13).

#### 4. Long Range Correlations and the Nature of the Pomeranchuk Singularity

One of the major advantages of the hybrid system is that rather accurate measurements of momenta and angles of particles in the forward energetic cone can be made for the same event in which accurate measurements of the slow particles in the bubble chamber are also available. This allows detailed correlation studies to be made between particles that are separated by large rapidity gaps in events of arbitrary multiplicity. This capability can be applied to examine the nature of the Pomeranchuk singularity as described below.

Several years ago, Freedman, Jones, Low and Young<sup>8</sup> proposed the measurement of reactions of the type  $p_1 + p_2 \rightarrow q_1 + q_2 + \text{anything}$  at high energy in the region in which the produced particles  $q_1$  and  $q_2$  can be

regarded as "fragments" of the incident particles  $p_1$  and  $p_2$ , respectively. They pointed out that the dependence of the cross section on the angle between transverse parts of the vectors  $\vec{q}_1$  and  $\vec{q}_2$  would indicate that the Pomeranchuk singularity contains Regge-cut contributions, since a pure pole would imply independence in the variable  $\cos \phi = \hat{q}_{1\perp} \cdot \hat{q}_{2\perp}$ . This measurement is particularly interesting provided one can isolate two secondary particles  $\vec{q}_1$  and  $\vec{q}_2$  in the fragmentation region of  $p_1$  and  $p_2$  from average or high multiplicity ( $n$ ) events in which the invariant mass formed from the  $(n-2)$  particles, other than  $q_1$  and  $q_2$ , is large. This can be done in the high energy pp and  $\pi^-p$  exposures proposed here in the following way. For pp events at 300 GeV/c one selects for  $\vec{q}_1$  positive tracks measured with the downstream spark chambers to have large  $x \geq +0.5 \cdot (p \geq \frac{p_0}{2})$ . This sample will predominantly consist of protons from fragmentation of the incident particle. In the same event one searches for an identified proton in the bubble chamber ( $p_p \lesssim 1$  GeV/c). Such a proton will be a fragmentation particle from the target proton. From this sample one then studies the  $\phi$  correlation for various subsets of the data making cuts on  $t_1, t_2$  and  $x_1, x_2$ . In  $\pi^-p$  collisions the forward energetic track with  $x \geq 0.5$  is required to be negative, while the slow track in the bubble chamber is still taken to be an identified proton. Without the downstream apparatus one cannot measure  $q_1$  accurately enough to obtain a relatively pure "fragmentation" sample.

5. Inclusive and Semi-Inclusive Charged-Charged Rapidity Correlations in 200 GeV/c  $\pi^-p$  Interactions

The existence of strong positive inclusive correlations in 200 GeV/c  $\pi^-p$  interactions has been clearly established<sup>9</sup> by members of the E-2B

collaboration. Fig. 27 shows contour plots of  $R(y_1, y_2)$  for charged-charged,  $\pi^- \pi^-$ ,  $\pi^+ \pi^+$ , and  $\pi^- \pi^+$  pairs. The rapidity density function  $R(y_1, y_2)$  is defined as

$$R = \rho_{12} / \rho_1 \rho_2 - 1, \quad (14)$$

where  $\rho = (d\sigma/dy) / \sigma_{inel}$  (15)

and  $\rho_{12} = (d^2\sigma / dy_1 dy_2) / \sigma_{inel}$  (16)

In addition to strong positive correlations in the central region, comparable in magnitude to those in pp interactions at the same energy, the data suggest positive correlations in regions where one or both of the particles has a large c.m. rapidity. Plots of  $\pi^{-2} d^2\sigma / dy_1 dy_2$  shown in Fig. 28 also suggest possible enhancements involving particles with large c.m. rapidity. Preliminary studies of semi-inclusive correlations (based on samples selected by charged prong number) suggest that large positive correlations are not present for all topologies or all charge combinations. The importance of diffractive contributions in determining the inclusive and semi-inclusive correlations has been suggested.

The lack of forward-backward symmetry in  $\pi^- p$  interactions is clearly shown in Fig. 27. This inherent lack of symmetry may allow more information in the region of large positive  $y$  and to study the details of pion beam diffraction, accurate measurements of vector momenta for the fast forward particles are essential. Monte Carlo studies of 200 GeV/c  $\pi^- p$  interactions indicate  $\Delta y \approx 0.2$  for pions at  $y_{c.m.} = +4$  from hybrid measurements, as compared to  $\Delta y \approx 0.8$  from bubble-chamber measurements alone. Information on fast forward gamma-rays, available from the hybrid system as described in later sections of this proposal, can also help in the study of charged-neutral correlations.

6. Gamma-Gamma and Gamma-Charged Particle Mueller Correlation Parameters for 200 and 300 GeV/c Proton-Proton Interactions

Recent experiments at the CERN/ISR, FNAL and Serpukhov have revealed the existence of strong correlations between pions produced in proton-proton collisions at high energies. Dao and Whitmore have discussed these effects in a review article.<sup>10</sup> Among those effects considered are: (1)  $\langle n_{\pi^0} \rangle$  may be parameterized in the form  $\alpha n_{-} + \beta$ , where  $n_{-}$  is the number of negative pions and  $\alpha \approx 0.6$  at FNAL energies and higher energies; and (2) values of the Mueller correlation parameter.

$$f_2 = \begin{cases} \langle n(n-1) \rangle - \langle n \rangle^2 & \text{for } n_1 = n_2 = n \\ \langle n_1 n_2 \rangle - \langle n_1 \rangle \langle n_2 \rangle & \text{for } n_1 \neq n_2 \end{cases} \quad (17)$$

are relatively large, positive and ordered according to  $f_2^{CC} > f_2^{+-} > f_2^{-0} > f_2^{--}$ . One implication of the second observation is that neutral charged pairs of pions are more strongly correlated than singly or doubly charged pairs. Dao and Whitmore have studied the  $f_2$  parameter in terms of a simple fragmentation model<sup>11</sup> and a critical fluid model<sup>12</sup>. Their analysis shows that the presently available data agree fairly well with the critical fluid model in its predicted energy dependence  $\{(\ln s)^{3/2}\}$ , whereas the fragmentation model gives a stronger energy dependence ( $s^{1/2}$ ) than allowed by the data. Furthermore,  $f_2^{00}$  is predicted to be equal to  $f_2^{+-}$  for the fragmentation model and  $f_2^{-0}$  for the critical fluid model. At 200 GeV/c, the measured values of  $f_2^{+-}$  and  $f_2^{-0}$  are  $3.64 \pm 0.09$  and  $1.84 \pm 0.61$  respectively<sup>5</sup>. At 300 GeV/c, their values are  $4.89 \pm 0.23$  and  $3.25 \pm 1.3$  respectively<sup>6</sup>. A measurement at 69 GeV/c in the Serpukhov hydrogen bubble chamber Mirabelle gave  $f_2^{00} = -2.0 \pm 1.0$ , substantially below the predictions of either model at that energy<sup>13</sup>. Hence, a new measurement of  $f_2^{00}$  and a more precise measurement of  $f_2^{-0}$  at FNAL energies would clearly lend themselves to a better understanding of the mechanisms responsible for multiparticle production at high energies.

We have recently completed a preliminary analysis of ~30,000 bubble chamber photographs taken as part of the 200,000 photographs exposure of protons at 200 and 300 GeV/c. Gamma-rays which are produced at a laboratory angle of approximately  $\pm 4^\circ$  relative to the incident beam direction are detected in the downstream spark chamber system by inserting 1.27 cm of lead (2.27 radiation lengths) between the last two spark chambers. The lead plate has dimensions 86 cm x 101 cm and is located at a distance of 6.84 m from the center of the bubble chamber. The spark chamber photographs were scanned by professional scanners and checked by physicists. A total of 4900 gamma-ray showers were recorded. The overall combined scanning efficiency for the number of showers was estimated at ~98%. The corresponding bubble chamber photographs were scanned in the usual fashion, resulting in 2200 events.

Possible prompt background, produced by the interactions of produced gamma-rays or hadrons in materials between the hydrogen and the lead radiator, has been considered. Particular attention has been given to the possible existence of low energy ( $\gtrsim 200$  MeV) gamma-rays produced by bremsstrahlung of primary gamma-rays in these materials. Because of the multiplicative nature of this process, such events could have serious effects on a measurement of a correlation parameter, particularly  $f_2^{00}$ . Because of the high spatial resolution and multi-track efficiency of the spark chambers, it has been possible to selectively study individual gamma-ray showers according to their electron number. In an average sense this is equivalent to an approximate gamma-ray energy selection. Experimental evidence for low energy gamma-ray background is apparent, based on the observation that the ratio of one electron showers to two electron showers is larger than expected from directly produced gamma-rays. Monte Carlo

studies reveal that, to a very good approximation, such low energy background would be confined to showers with three or fewer electrons. In the subsequent analysis, we have used only showers with four or more electrons.

In Figure 29 we show the geometrical acceptance ( $E_1$ ) of the downstream detector (shaded area) expressed in terms of the gamma-ray C.M. rapidity variable for 200 and 300 GeV/c incident protons. The overall distributions represent an approximation to the expected gamma-ray rapidity distribution where we have explicitly substituted measured  $\pi^-$  tracks for  $\pi^0$ 's, with the subsequent decay  $\pi^0 \rightarrow \gamma\gamma$ . The geometrical efficiencies are estimated by these means to be 37 and 41% at 200 and 300 GeV/c respectively. This efficiency improves with incident beam momentum. Including an 80% transmission ( $E_2$ ) of gamma-rays through materials between the event vertex and lead radiator and a 70% conversion probability ( $E_3$ ) in the lead plate, the overall estimated efficiency of the detector per gamma-ray is  $E_1 E_2 E_3$  -20% (at 200 GeV/c). The measured gamma-ray rapidity distribution is in good agreement with the geometrical distribution of Figure 29, suitably modified to account for the aforementioned transmission and conversion efficiencies. In Figure 30 we show the distribution of events, normalized to the cross section data of previous experiments<sup>14</sup> plotted as a function of the number of gamma-rays per event,  $N(\gamma)$ .

In order to calculate Mueller parameters from the ( $N_\gamma$ ) data, we assume that, for a given  $\pi^0$  multiplicity, the center of mass momentum spectrum of produced  $\pi^0$ 's is the same as that of  $\pi^-$ 's of the same multiplicity. Then we calculate the Monte Carlo probability  $P_{N_\gamma}(j)$  to detect  $N_\gamma$  showers from various  $\pi^0$  multiplicity ( $j$ ) channels. Since the  $\sigma(N_\gamma)$  data are a superposition of these probability functions, we minimize the chi-squared function

$$\chi^2 = \sum_N \left\{ \frac{\sigma(N_\gamma) - \sum_j a_j P_{N_\gamma}(j)}{\Delta\sigma(N)} \right\}^2 \quad (18)$$

to find the  $a_j$  coefficients, which give the weight or cross section for the  $j$ th multiplicity. It is then a straight forward matter to calculate the various quantities  $\langle N_\gamma \rangle$ ,  $\langle N_\gamma(N_\gamma-1) \rangle$ , etc., which enter directly into a calculation of the Mueller parameters.

In this fashion the quantities  $f_2^{-0}$  and  $\langle n_{\pi^0} \rangle$  has been calculated from our data. The results are:

$$\begin{aligned} f_2^{-0} &= 1.89 \pm 0.42 \text{ (200 GeV/c); } \langle n_{\pi^0} \rangle = 3.29 \pm 0.16 & (19) \\ &2.36 \pm 0.45 \text{ (300 GeV/c); } & 3.83 \pm 0.13 \end{aligned}$$

These measurements are consistent with the previously measured values of  $f_2^{-0} = 1.84 \pm 0.61^5$  and  $3.25 \pm 1.6^6$  and  $\langle n_{\pi^0} \rangle = 3.17 \pm 0.32^{15}$  and  $3.95 \pm 0.38^{16}$  at 200 and 300 GeV/c respectively. A more physical interpretation of  $f_2^{-0}$  may be seen in Figure 31, where we show  $\langle n_{\pi^0} \rangle$  versus the number of charged tracks in the event. For comparison, we show similar results from the "bare" experiment at 200 GeV/c<sup>15</sup>. The hybrid data, obviously already very much superior in statistics compared to the "bare" experiment, indicate a turnover for  $n_c > 10$  (as expected from energy conservation considerations) which was not apparent in the "bare" data. With ~ one order of magnitude more events available in existing and requested film, interesting details such as the turnover may be thoroughly studied. Final results on  $f_2^{00}$  are not yet available. Since  $\gamma$ -ray detection efficiencies enter in this problem quadratically, further checks are required on the efficiencies before final results can be quoted.



7. Inclusive and Semi-Inclusive Charged-Charged and Charged-Gamma Rapidity Correlations in 200 and 300 GeV/c Proton-Proton Collisions

In this section we discuss two particle correlations in proton-proton collisions as a function of the rapidity variable of each particle. In such a way, dynamical information, which has been averaged out in the previous Mueller correlation parameter approach, can be extracted.

The existence of strong inclusive two-particle correlations at ISR and FNAL energies is well established. In the central region,  $R(0,0) \approx 0.6 - 0.7$  for charged-charged pairs (Pisa-Stony Brook<sup>17</sup>) and charged-gamma-pairs (CERN-Hamburg-Vienna<sup>18</sup>). In the absence of momentum identification, the pseudorapidity variable  $\eta_{CM}$  has been used for the ISR experiments. The FNAL "bare" bubble chamber experiments have obtained similar results, only expressed in terms of the true C.M. rapidity,  $y_{C.M.}$ , for charged-charged, positive-positive, positive-negative, and negative-negative pairs<sup>19,20</sup>. Recent studies of these correlations by topology<sup>20</sup> indicate that the large  $R(0,0)$  effect is not shared equally among the topologies, as one would naively suspect. The most dramatic observation is that  $R(0,0)$  is very large in the low multiplicity diffractive events (particularly the four and six prong events) and essentially zero elsewhere. One implication of this is that correlations are associated with the diffractive component. If this is so, then currently popular models which explain large inclusive correlations by the existence of two-particle clusters on the multiparticle chain are questionable.

We have studied charged-gamma rapidity correlations in our 200 and 300 GeV/c pp data. In Figures 32 and 33 we show the inclusive  $R$  distributions for various selections on laboratory pseudorapidity (boosted down by 3.2 and 3.5 respectively at 200 and 300 GeV/c from the laboratory to approximate C.M. pseudorapidity) for the charged particles and various selections

on gamma-ray C.M. rapidity (pseudorapidity and rapidity are identical for gamma-rays; only laboratory angles for gamma-rays are required for this plot). With somewhat better statistics (based on only ~15% of our present data) the data confirm the large correlation observed in the central region by the CERN-Hamburg-Vienna group<sup>18</sup> at the ISR.

In Figures 34 and 35 we show our semi-inclusive charged-charged and charged-gamma data at 200 and 300 GeV/c respectively. We note that the semi-inclusive selection has been made on charged prong count only, without regard to the number of gamma-rays detected. Hence, this plot is semi-inclusive in the usual sense. However, as we improve our statistics we should be able to select on gamma-ray number and reduce the semi-inclusive selection to include at least a rough selection on the number of produced  $\pi^0$ 's. We note that all topologies show an enhancement near  $\eta_1 = 1$ . Since  $\bar{\eta}_2 = 1$ , this means the enhancement is located near  $\Delta\eta = 0$ , in agreement with the results of Singer et al.<sup>20</sup> We also observe that the four and six prong events exhibit the largest enhancements near  $\eta_1 = 1$ . The fact that these effects are not as dramatic as those observed by Singer et al., may be due to (1) the cut  $0.4 < \eta_2 < 1.6$  is not as central as that of Singer et al.; (2) the lack of an explicit diffractive cut on our data, as imposed by Singer et al., or (3) a presently unknown contribution of the  $\pi^\pm - \pi^0$  system to the diffractive component. The first two restrictions can be removed with improved statistics, as mentioned previously. The third point raises an important physics question. That is, what is the overall charge structure of the diffractive component? With our very large acceptance for gamma-rays resulting from  $\pi^0$ 's produced in the forward hemisphere we should be able to deal with this important question.

8. Leading Particle Effects in  $\pi^-p$  Interactions at 100 and 200 GeV/c

It is well known that inclusive production of  $\pi^\pm$  in  $\pi^\pm p$  interactions at energies below about 50 GeV/c exhibits definite "leading particle" effects. The  $\pi^-(\pi^+)$  production in the beam fragmentation c.m. hemisphere is greatly enhanced over that observed in the target c.m. hemisphere in  $\pi^-p(\pi^+p)$  interactions. In addition to the overall asymmetry of the  $\pi^-(\pi^+)$  distributions a strong peaking in the invariant cross section near  $x = +1.0$  is observed for  $\pi^-(\pi^+)$  produced in inelastic events. This has previously been observed in  $\pi^-p$  experiments<sup>21,22</sup> at 16 and 40 GeV/c for the inclusive reaction

$$\pi^-p \rightarrow \pi^- + \text{anything} \quad (20)$$

after removal of elastic events from the sample.

In order to investigate this effect at 100 and 200 GeV/c, we show in Figures 36 - 38 some preliminary data obtained from the hybrid system. Distributions are shown for events in which at least one track is required to hook up between the spark chambers and bubble chamber. In Figure 36 are shown distributions for different charged-multiplicity final states in 100 GeV/c  $\pi^-p$  interactions. A leading particle peak near  $x = +1.0$  is seen in the inelastic two-prong sample as well as in the  $\pi^-p\pi^+\pi^-$  final state. No peak is seen in the  $\pi^-p2\pi^+2\pi^-$  final state. In Figures 37 and 38 are shown inclusive distributions of  $d\sigma/dx$  as a function of  $x$  for  $\pi^-$  produced in inelastic  $\pi^-p$  interactions at 100 and 200 GeV/c. These inclusive distributions also show the peaking near  $x = +1.0$ . These figures also show the effect of the increased resolution of the hybrid system. Distributions have also been shown for the same track samples with momenta from hooked-up tracks replaced by the corresponding momenta from bare bubble chamber measurements. The bare chamber data (open circles) show no peak near  $x = +1$  and,

in fact, show a large "spill-over" in the unphysical region  $x > 1$ .

In Figure 39 we show the normalized invariant cross section

$$F(x) = \int_{\text{all } p_T^2} \frac{2E^*}{\pi\sqrt{s}} \frac{d^2\sigma}{dx dp_T^2} dp_T^2 \quad (21)$$

as a function of  $x$  for the 16, 40, 100, and 200 GeV/c data. The data appear to be in good agreement in the region of large  $x$ . However, higher statistics are needed before any definitive statement can be made about the energy dependence of the peak near  $x \approx +0.95$ .

#### IV. REQUEST

We believe we have demonstrated that the FNAL 30-inch bubble chamber-wide gap spark chamber hybrid system is a proven and unique instrument, capable of doing physics which heretofore in the "bare" mode was either impossible or substantially less precise. In this proposal we have conveyed explicit examples of physics which are coming from the system. With those preliminary data in hand, we have been able to establish realistic goals, which are enumerated in the following request.

##### (1) Proton-Proton Interactions at 300 GeV/c

After careful examination of physics results to date, it appears that the most demanding (from a viewpoint of statistics) topics are:

- 1) Semi-inclusive  $c$ - $\gamma$  correlations: We estimate that 300K additional pictures are required to get  $\pm 10\%$  statistics on  $(-, \gamma)$  data points in a  $y_1, y_2$  plot in the four-prong channel. Similar statistics will be obtained for  $(-, -)$  data points from the six-prong final state. These two channels have been considered since they are the most restrictive from a statistical viewpoint.

- 2) Study of  $\Delta$  production processes: It is difficult to even estimate cross sections for processes such as  $\Delta^{++}\Delta^0$  production. However, 300K additional pictures will yield a total of ~400 non-diffractively produced inclusive  $\Delta^{++}$  events (if pion exchange contributes at the calculated level).
- 3) Study of exclusive channels: For the  $pp\pi^+\pi^-$  and the  $pn\pi^+$  final states, 300K additional pictures will give ~800 events of each kind. We estimate that ~600  $pp2\pi^+2\pi^-$  and 400  $pp\pi^0$  events will be found. This will permit a measurement of the Double Pomeron process in  $pp\pi^+\pi^-$  to  $< 10 \mu\text{b}$ . The choice of 300 GeV/c momentum represents an advantage over previous attempts at this measurement at 100 and 200 GeV/c due to the expanded rapidity scale and separation of the diffractive and central regions.
- 4) Study of Diffraction: We estimate that 300K pictures will yield ~2000 inelastic two-prongs, including 900 correlated gamma-ray triggers. Correspondingly large numbers of diffractive four-prong events will be recorded.

(2) Pi-Minus Proton Interactions at 100 GeV/c

It is clear that leading particle effects, in order to be clearly identified and studied, require the hybrid system even at the lowest FNAL energies. In addition to our existing 50K pictures, we are presently analyzing 50K pictures returned to us by E-125. It is our opinion that these leading particle effects are very important and should be pursued. For this reason, we request an additional 100K pictures, which when combined with existing film will give a total of 200K pictures. This will provide ample data for inclusive studies and ~250  $\pi^-p\pi^+\pi^-$  events for more detailed studies, such as  $\pi^- \rightarrow \rho^0\pi^-$  dissociation effects.

(3) Pi-Minus Proton Interactions at 375 GeV/c:

It is our opinion that the more interesting aspects of studying  $\pi^-p$  interactions at FNAL energies involve the study of the energy dependence of pion diffraction and the Double Pomeron process. We therefore request a total of 300K pictures of 375 GeV/c  $\pi^-p$  interactions to add to the 100K pictures which we shall be receiving from E-215. For purposes of information, the E-2B group requested and was granted approval to run behind E-215 ( $\pi^-p$  @ highest momentum). The terms of this approval are spelled out in three correspondences, copies of which are included at the end of this section.

The factor of  $\sim 9$  increase in CM energy squared over our present 100 GeV/c  $\pi^-p$  is approximately the same as the increase in  $s$  between 40 GeV/c and 100 GeV/c and should be a wide enough spread in  $s$  to permit a conclusive study of the energy dependence of many of the interesting cross sections. The advantages of high beam momentum for a study of the Double Pomeron process have already been pointed out. For example, from the total 400K pictures we expect to obtain  $\sim 800$  events of the  $\pi^-p\pi^+\pi^-$  final state if this cross section remains at the 590  $\mu\text{b}$  level at 375 GeV/c.

(4) Summary

We request a total of 700K pictures of the following beam particles and energies:

$\pi^-p$	100 GeV/c	100K
$\pi^-p$	375 GeV/c	300K
pp	300 GeV/c	300K.

With the previously mentioned inhibit on the bubble chamber flash corresponding to beam pulses with no trigger, ~140K fewer bubble chamber pictures can be taken. We estimate this represents a savings (in terms of film purchases and development costs) of ~\$10,000. For each of these runs, ~6 tracks per picture will be required.

NATIONAL ACCELERATOR LABORATORY 

P.O. BOX 500  
BATAVIA, ILLINOIS 60510  
TELEPHONE 312 840-3211  
DIRECTORS OFFICE

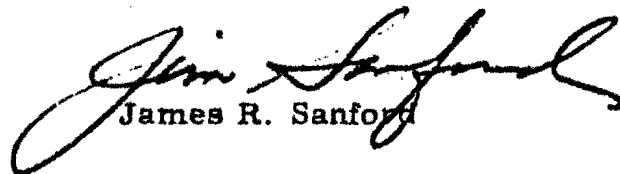
April 18, 1974

Professor Gerson Goldhaber  
University of California  
Lawrence Berkeley Laboratory  
Berkeley, California 94720

Dear Gerson:

I imagine that you are aware of the request that Gerry Smith has made as spokesman of the Hybrid #2B collaboration. Specifically, he wishes permission to run the wide-gap hybrid system behind the 30-inch bubble chamber during the exposure of high energy  $\pi^-$  for Experiment #215. Gerry's wish is that the film be released to the Hybrid #2B experimenters eight months after your exposure. I am asking for your response to this request so that more formal arrangements can eventually be made through an Agreement with the Laboratory.

Sincerely,

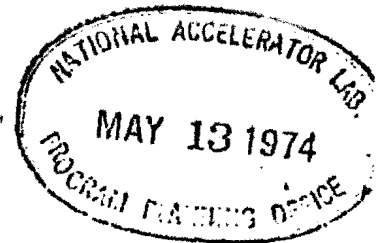
  
James R. Sanford

AFG:jp

cc: F. R. Huson  
G. Smith



-38-  
LAWRENCE BERKELEY LABORATORY  
UNIVERSITY OF CALIFORNIA  
BERKELEY, CALIFORNIA 94720 □ TEL. (415) 843-2740



May 10, 1974

Dr. James R. Sanford  
National Accelerator Laboratory  
P.O. Box 500  
Batavia, Illinois 60510

Dear Jim:

Thank you for your letter of April 18, 1974. We are willing to let Gerry Smith and co-workers run their system behind the 30-inch bubble chamber during our Experiment Number 215, however, it is totally unacceptable to us to release the film after eight months.

In our previous experiment, where we did release the film, the result was that we only measured about one third of the six-prong events and even a smaller fraction of the higher multiplicities. This has severely hampered our physics results from this previous experiment. In Experiment Number 215, the measurements will be more difficult because of the higher energy, and we feel it is totally unrealistic to limit the measuring time as requested. Furthermore, the urgency which one may argue existed in the early days of the NAL running, is no longer there. I understand that the Hybrid Number 2B experimenters have a considerable backlog of film now.

We feel that we could go along with the following arrangement. We can give up Fifty percent of the film after one year and the other fifty percent after eighteen months. This should give us a fighting chance to complete a reasonable fraction of the measurements. Furthermore, we want the possibility of recalling the film (1 set of 3 rolls at a time) for up to one month periods in case the need for special remeasurements arises.

Sincerely,

A handwritten signature in cursive script that reads "Gerson".

Gerson Goldhaber

GG:ml

cc: F. R. Huson  
G. Smith  
H. Bingham  
W. Fretter  
F. Winkelmann  
G. H. Trilling

Proposal File No. 215-2.13  
Master  
DG  
~~123~~

-39-

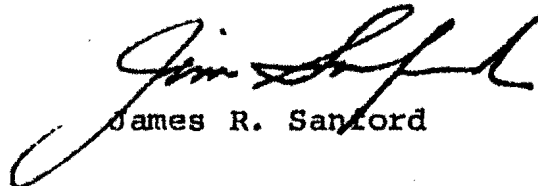
May 29, 1974

Professor Gerson Goldhaber  
Lawrence Berkeley Laboratory  
Berkeley, California 94720

Dear Gerson:

Thank you for your letter of May 10 concerning the use of the hybrid system in conjunction with your Experiment #215. The terms you propose are satisfactory both to NAL and to the spokesman for hybrid 2B. Following the  $\pi^-$  exposure that you will be running at 400 or above you expect to work on the analysis of the pictures for between twelve months and eighteen months. It is my understanding that you will give up half of the film after a year and the remaining film after eighteen months. I hope that this gives both you and the 2B group a chance to make the maximum use of that data.

Sincerely,



James R. Sanford

cc: G. Smith

REFERENCES

1. E. Bracci et al., compilation of cross sections  $I - \pi^-$  and  $\pi^+$  induced Reactions, CERN/HERA 72-1 (1972); E. L. Berger et al., CERN/D.Ph II Phys 74-26 (1974).
2. J. Whitmore, Phys. Reports 10C, 273 (1974).
3. M. Derrick et al., Phys. Rev. D9, 1215 (1974).
4. O. Benary et al., VCRL-20000 NN (1970).
5. Private communication from J. Whitmore.
6. S. Barish et al., Phys. Rev. D9, 1171 (1974).
7. "Experimental Results on Large-Angle Elastic pp Scattering at the CERN ISR", paper #488 submitted to the XVII International Conference on High Energy Physics, London, July 1-10, 1974.
8. D. Z. Freedman et al., Phys. Rev. Letters 26, 1197 (1971).
9. W. D. Shephard et al., "One-Particle and Two-Particle Distributions and Correlations in 205 GeV/c  $\pi^-p$  Inclusive Reactions" (Notre Dame-Duke-Canada) paper #760 submitted to the XVII International Conference on High Energy Physics, London, July 1-10, 1974.
10. F. T. Dao and J. Whitmore, Physics Letters 46B, 254 (1973).
11. E. L. Berger, D. Horn and G. H. Thomas, Phys. Rev. D7, 1412 (1973).
12. G. H. Thomas, Phys. Rev. D8, 3042 (1974).
13. H. Blumenfeld, et al., Physics Letters 45B, 525 (1973).
14. G. Charlton et al., Phys. Rev. Letters 29, 515 (1972); S. Barish et al., Phys. Rev. D, 9, 2689 (1974).
15. G. Charlton et al., Phys. Rev. Letters 29, 1759 (1972).
16. F. T. Dao et al., Phys. Rev. Letters 30, 1151 (1973).

17. S. R. Amendolia et al., Phys. Letters 48B, 359 (1974).
18. H. Dibon et al., Phys. Letters 44B, 313 (1973).
19. C. M. Bromberg et al., Phys. Rev. D9, 1864 (1974).
20. R. Singer et al., Physics Letters 49B, 481 (1974).
21. P. Bosetti, et al., Nucl. Phys. B54, 141 (1973).
22. E. O. Abdrakhmanov et al., Nucl. Phys. B72, 189 (1974).

FIGURE CAPTIONS

- Figure 1 - Schematic layout of the Experiment 2B hybrid system at FNAL.
- Figure 2 - Measured spark chamber track width versus time delay from coincidence.
- Figure 3 - Measured spark chamber track width versus Marx voltage for single tracks.
- Figure 4 - Single gap efficiency versus track multiplicity in the spark chambers. See text for definition of efficiency.
- Figure 5 - An eight-prong event, photographed in the bubble chamber and upstream spark chambers at 200 GeV/c.
- Figure 6 - Flow diagram used in spark chamber track reconstruction.
- Figure 7 - Point scatter (FRMS) results on beam tracks in the direct view.
- Figure 8 - Point scatter (FRMS) results on beam tracks in the 90-degree view.
- Figure 9 - Distribution of transverse coordinate of spark chamber track (extended to bubble chamber) around same coordinate of bubble chamber track for beam tracks with no magnetic field.
- Figure 10 - Flow diagram used in bubble chamber-spark chamber hookup.
- Figure 11 - Distribution of fitted beam momentum for known 200 GeV/c beam.
- Figure 12 - Distribution of fitted beam momentum for known 300 GeV/c beam.
- Figure 13 - Scatter plot of  $\pm \Delta p/p$  versus  $p$  for secondary tracks from 15 to 200 GeV/c based on (a) bubble chamber alone (open circles) and (b) hybrid system (closed circles).
- Figure 14 - Example of a one gamma-shower in the downstream spark chamber.

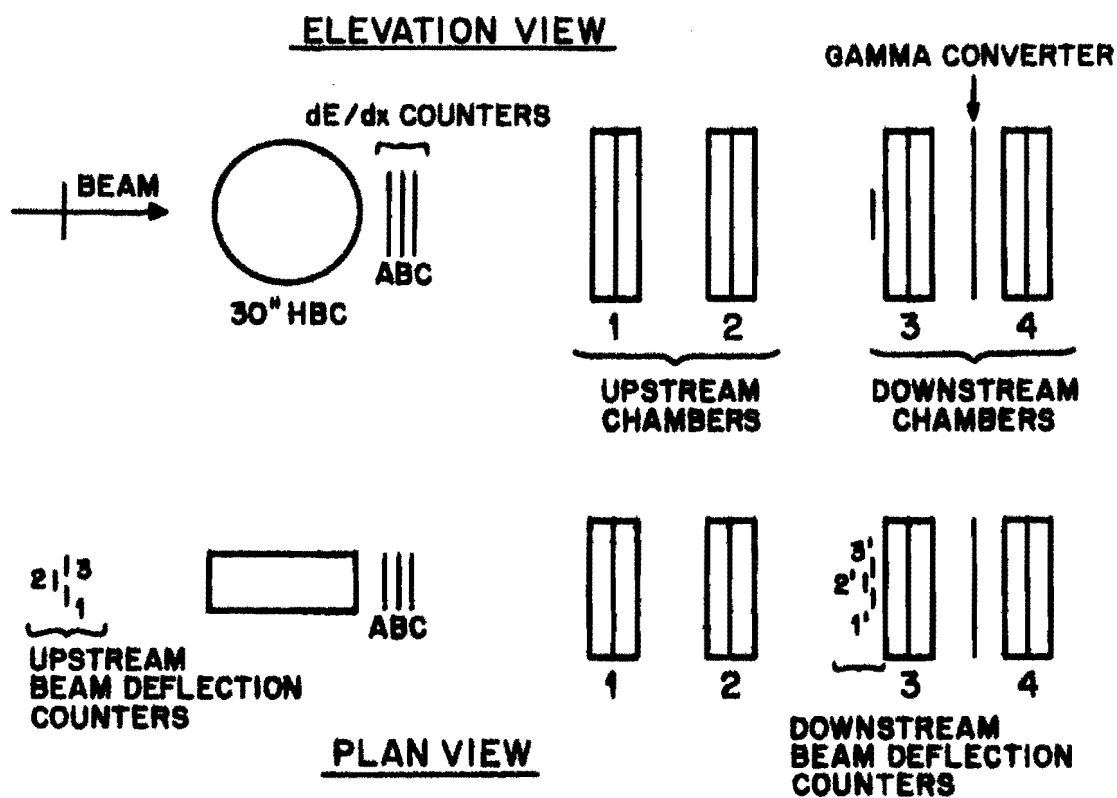
- Figure 15 - Example of a five gamma-shower in the downstream spark chamber.
- Figure 16 - Summary of cross sections for  $pp \rightarrow pp\pi^+\pi^-$  and  $\pi^-p \rightarrow \pi^-p\pi^+\pi^-$ .
- Figure 17 - Double Pomeron exchange diagrams.
- Figure 18 - Results of bare and hybrid fits to p-p elastic scattering at 200 and 300 GeV/c expressed in terms of  $MM^2$ .
- Figure 19 - Results of bare and hybrid fits to  $pp \rightarrow pp\pi^+\pi^-$  and  $pp2\pi^+2\pi^-$  at 200 and 300 GeV/c expressed in terms of  $MM^2$ .
- Figure 20 - Results of bare and hybrid fits to  $\pi^-p \rightarrow \pi^-p$ ,  $\pi^-p\pi^+\pi^-$  and  $\pi^-p2\pi^+2\pi^-$  at 100 GeV/c expressed in terms of  $MM^2$ .
- Figure 21 - Distributions of  $X = 2P_L^*/\sqrt{s}$  for protons,  $\pi^+$  and  $\pi^-$  in  $pp \rightarrow pp\pi^+\pi^-$  after fitting using hybrid data.
- Figure 22 - Distributions of  $X = 2P_L^*/\sqrt{s}$  for protons,  $\pi^+$  and  $\pi^-$  in  $pp \rightarrow pp2\pi^+2\pi^-$  after fitting using hybrid data.
- Figure 23 - Distributions in  $-t$  for elastic and inelastic two-prong events at 300 GeV/c using the bare and hybrid data.
- Figure 24 - Distributions in  $M_x^2$  for inelastic two-prong events at 200 and 300 GeV/c. Shaded events have one or more observed gamma-ray showers.
- Figure 25 - Mean number of  $\pi^0$ 's versus number of charged tracks for 205 GeV/c p-p bare experiment. The diffractive and non-diffractive contributions have been separated.
- Figure 26 - Distributions in C.M. gamma-ray rapidity versus number of prongs. The diffractive contribution has been shaded.

- Figure 27 - Contour plots showing lines of constant  $R(y_1, y_2)$  as a function of  $y_1$  and  $y_2$  for the two-particle inclusive  $\pi^-p$  reactions at 200 GeV/c: (a)  $\pi^-p \rightarrow \text{charge} + \text{charge} + \dots$ ; (b)  $\pi^-p \rightarrow \pi^- + \pi^- + \dots$ ; (c)  $\pi^-p \rightarrow \pi^+ + \pi^+ + \dots$ ; and (d)  $\pi^-p \rightarrow \pi^- + \pi^+ + \dots$ .
- Figure 28 - Distributions of  $\pi^{-2}d^2\sigma/dy_1dy_2$  as a function of  $y_2$  for various ranges of  $y_1$  in the two-particle inclusive  $\pi^-p$  reactions at 200 GeV/c: (a)  $\pi^-p \rightarrow \text{charge} + \text{charge} + \dots$ ; (b)  $\pi^-p \rightarrow \pi^- + \pi^- + \dots$ ; (c)  $\pi^-p \rightarrow \pi^+ + \pi^+ + \dots$ ; and (d)  $\pi^-p \rightarrow \pi^- + \pi^+ + \dots$ . Various ranges of  $y_1$  are indicated by different symbols as shown on the figure. The lines connecting the points are included to make it easier to follow the trend of the data.
- Figure 29 - A simulated center of mass rapidity distribution for inclusive gamma-rays produced in 200 and 300 GeV/c pp collisions. The shaded areas correspond to gamma-rays which fall within the geometrical acceptance of the lead radiator-spark chamber detector.
- Figure 30 - The normalized distribution of gamma-rays observed for pp collisions at 200 and 300 GeV/c after removing showers with three or fewer electrons.
- Figure 31 -  $\langle n_{\pi^0} \rangle$  versus  $n_c$  for the 205 GeV/c "bare" experiment and for the 200 and 300 GeV/c hybrid experiment.
- Figure 32 - Rapidity density for charged-gamma data at 200 GeV/c.
- Figure 33 - Rapidity density for charged-gamma data at 300 GeV/c.
- Figure 34 - Inclusive and semi-inclusive rapidity densities for charged-charged and charged-gamma data at 200 GeV/c.

- Figure 35 - Inclusive and semi-inclusive rapidity densities for charged-charged and charged-gamma data at 300 GeV/c.
- Figure 36 - Distributions of  $\chi(\pi^-)$  for  $\pi^-p\pi^+\pi^-$ ,  $\pi^-p2\pi^+2\pi^-$  and inelastic two-prong events in  $\pi^-p$  interactions at 100 GeV/c.
- Figure 37 - Distribution of  $d\sigma/dx(\pi^-)$  for inclusive tracks produced in 100 GeV/c  $\pi^-p$  interactions. The open circles and closed triangles represent "bare" bubble chamber and hybrid measurements respectively.
- Figure 38 - Same as Figure 37, only at 200 GeV/c.
- Figure 39 - Distribution of the invariant cross section,  $f(\chi)$ , for beam energies from 16 to 200 GeV/c.



**NAL 30-INCH BUBBLE CHAMBER-WIDE GAP  
SPARK CHAMBER HYBRID SYSTEM  
(EXPERIMENT 2-B)**



TRIGGER:  $(1+2+3) \cdot A(2) \cdot B(2) \cdot C(2)$

OR  $\left\{ \begin{matrix} 1 \\ 2 \\ 3 \end{matrix} \right\} \cdot A(1) \cdot B(1) \cdot C(1) \left\{ \begin{matrix} 1 \\ 2 \\ 3 \end{matrix} \right\}$

**APPARATUS SCHEMATIC AND TRIGGER**

Fig. 1

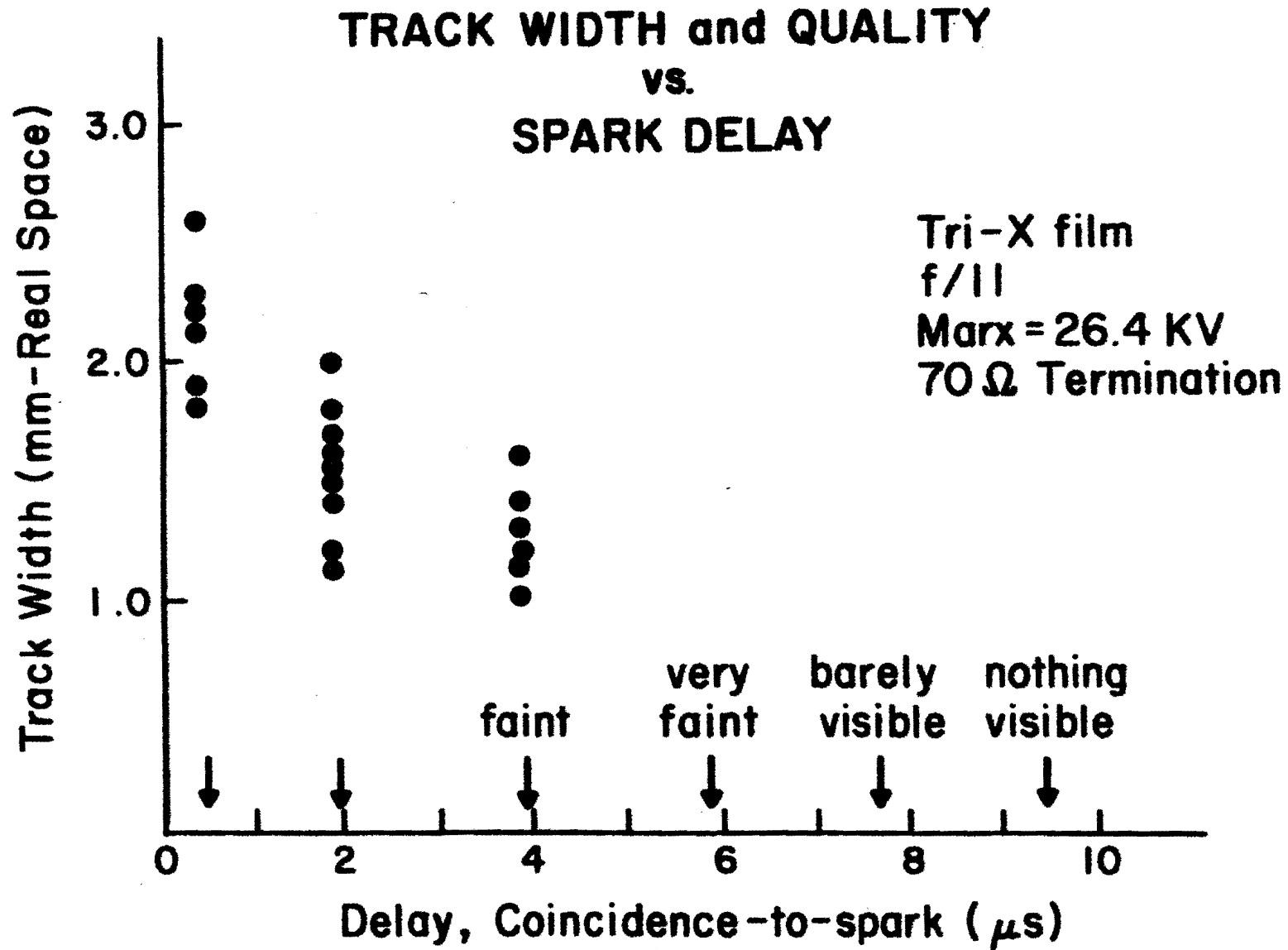


Fig. 2

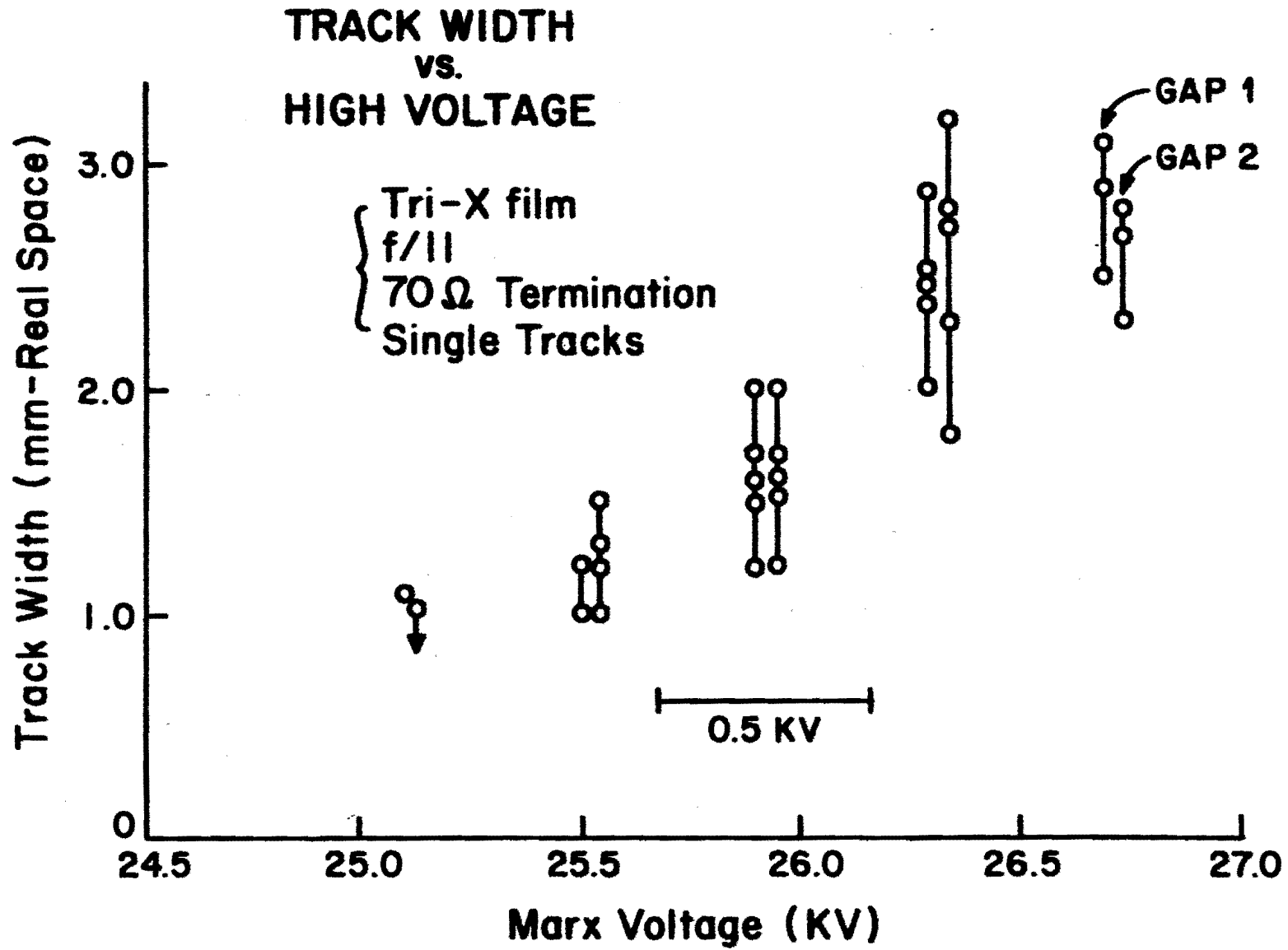


Fig. 3

**SINGLE GAP EFFICIENCY  
(AVERAGED OVER ALL EIGHT GAPS)**

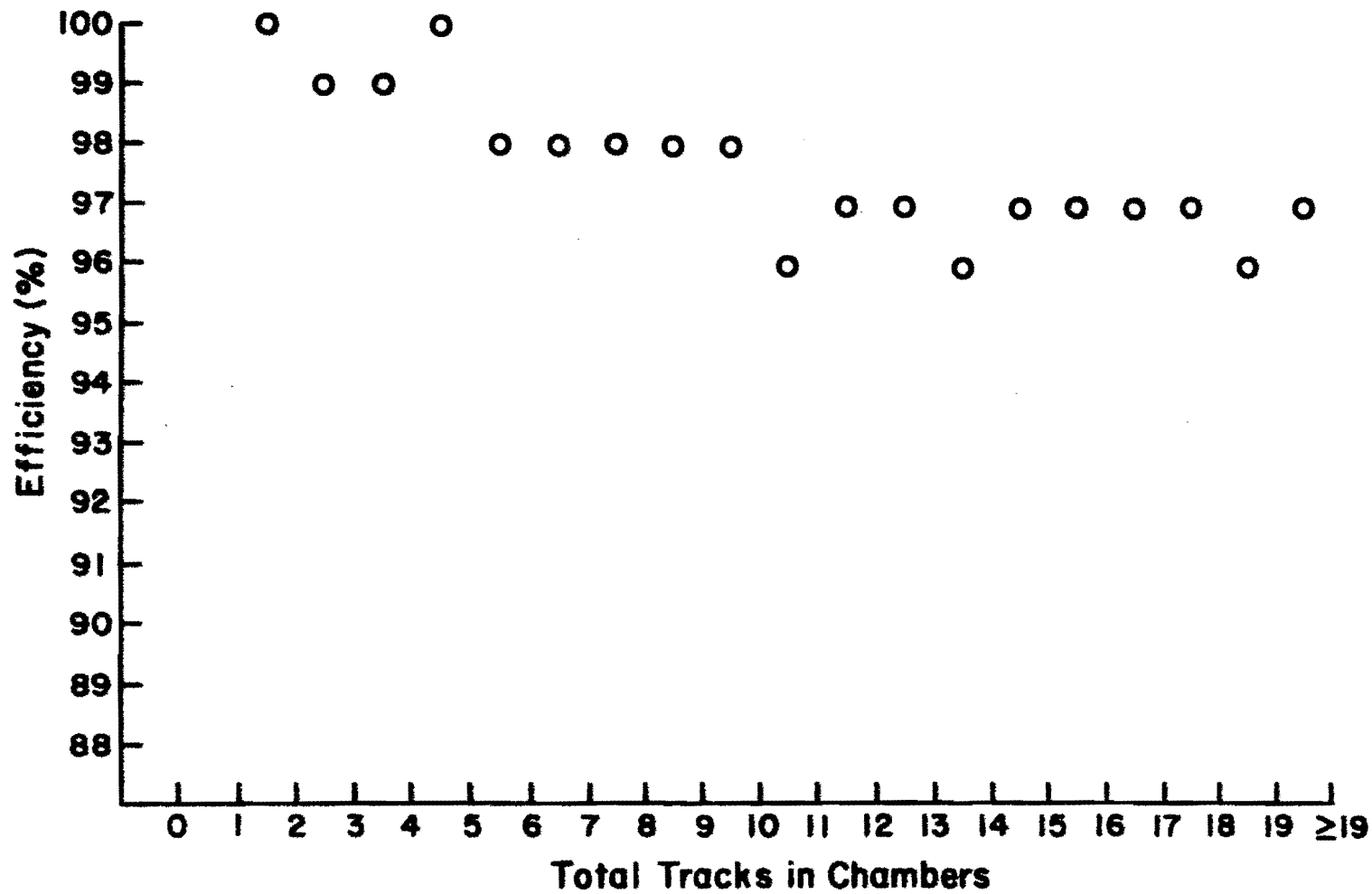
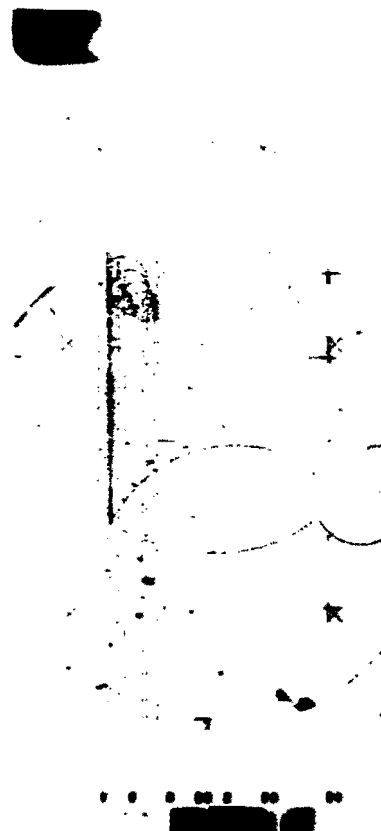
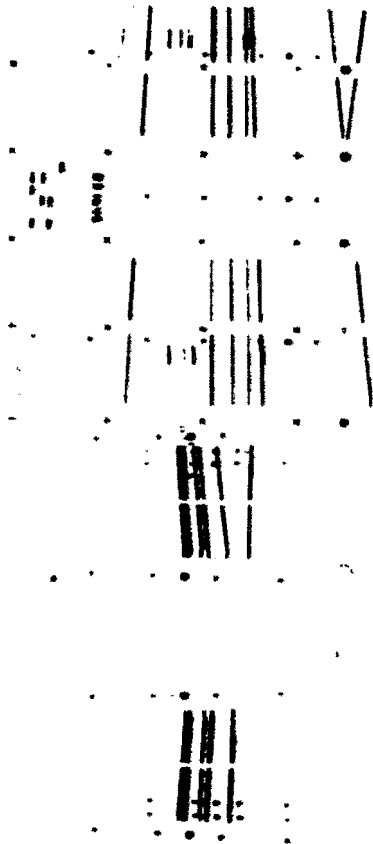


Fig. 4

Experiment 2B-200 GeV p-p  
Nov. 27-28, 1972  
(Eight Prong Event As Seen  
In Wide-Gap Spark Chambers)



Experiment 2B-200 GeV p-p  
Nov. 27-28, 1972  
(Eight Prong Event As Seen  
in Bubble Chamber)

Fig. 5

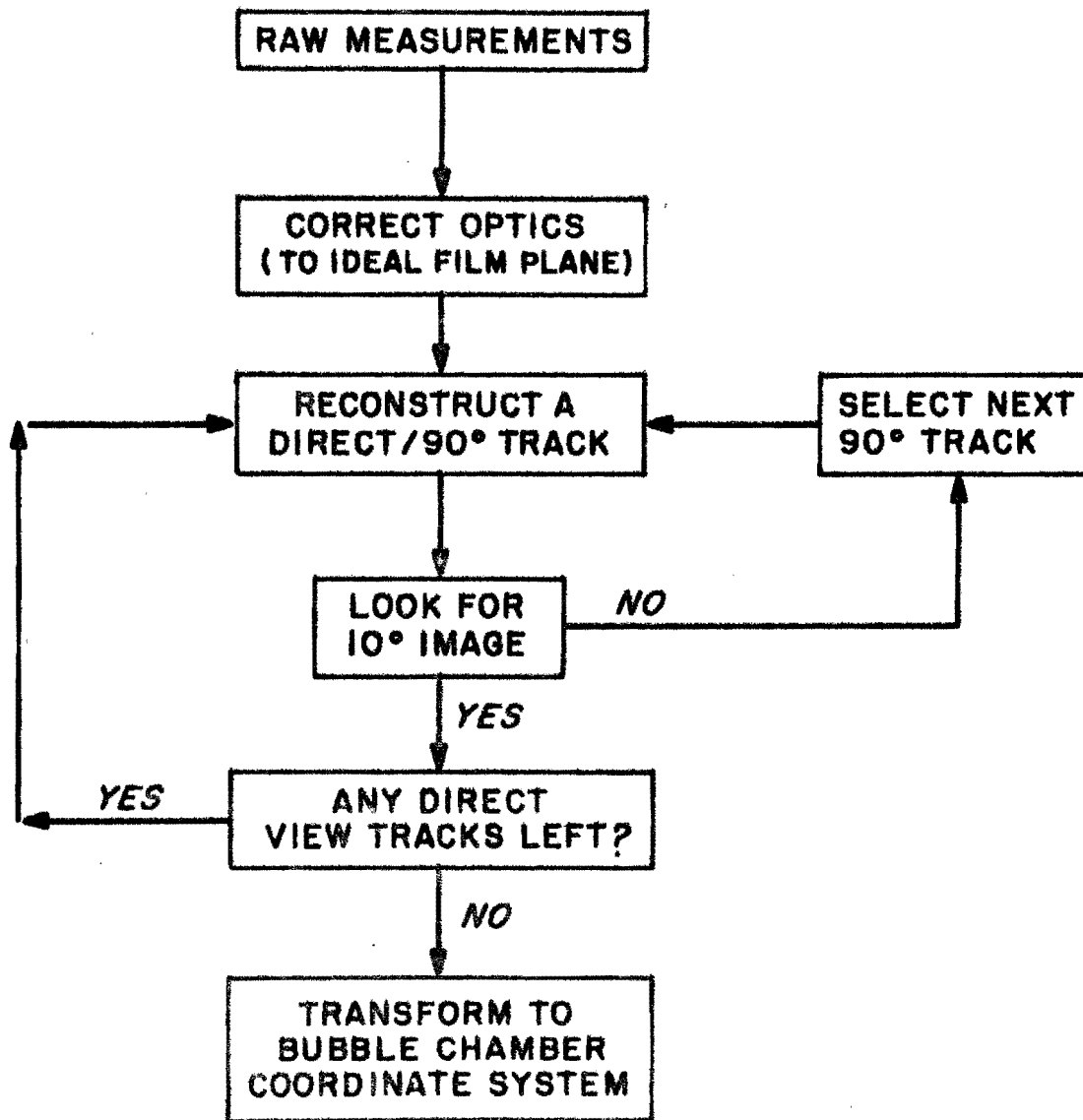
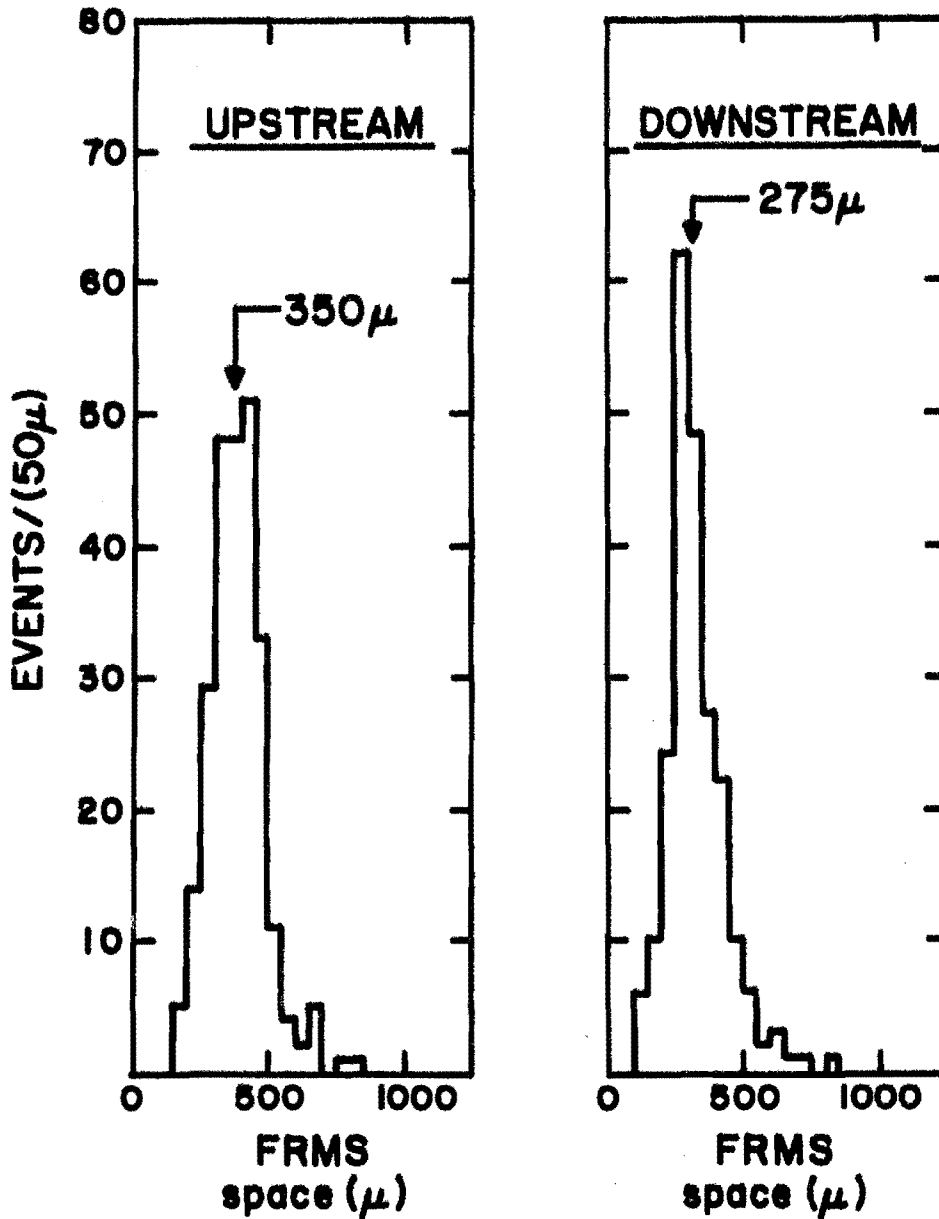


Fig. 6

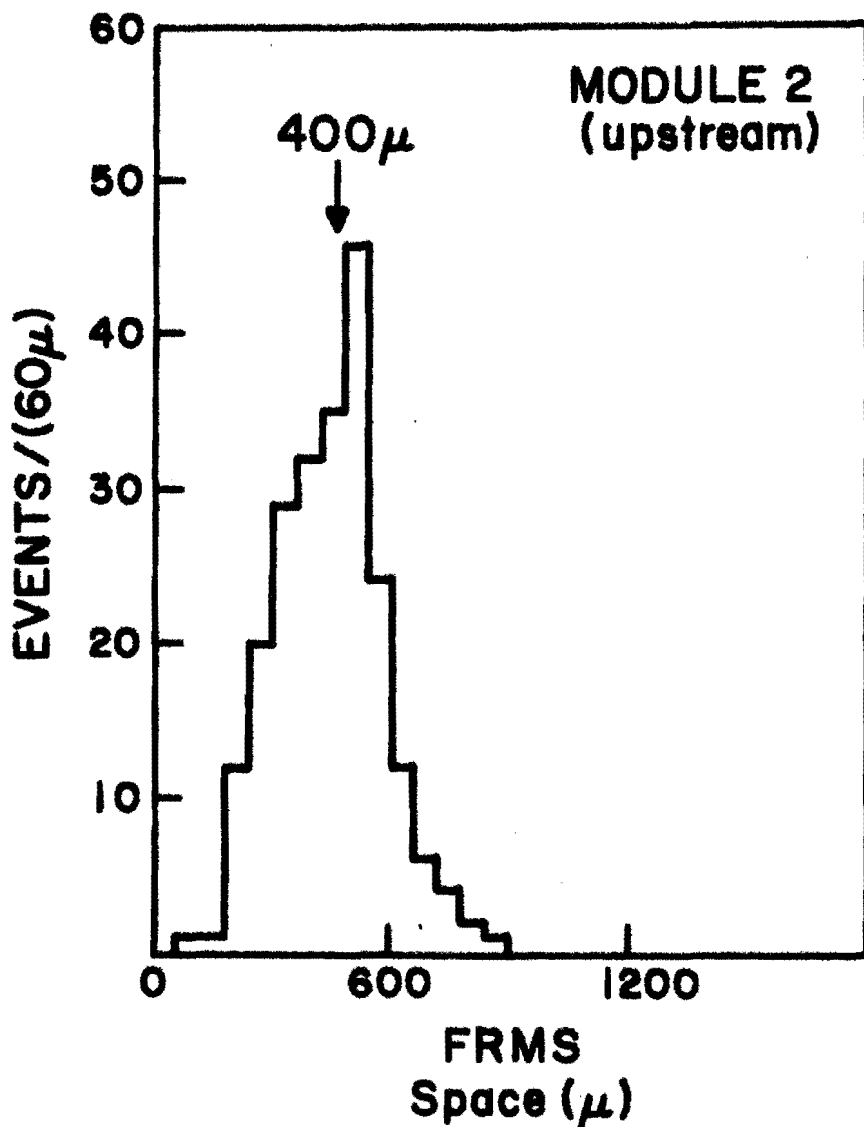
**NAL 30-INCH BUBBLE CHAMBER-WIDE GAP  
SPARK CHAMBER HYBRID SYSTEM  
(EXPERIMENT 2-B)**



**SPARK-CHAMBER POINT SCATTER (FRMS)  
(DIRECT VIEW)**

Fig. 7

**NAL 30-INCH BUBBLE CHAMBER-WIDE GAP  
SPARK CHAMBER HYBRID SYSTEM  
(EXPERIMENT 2-B)**

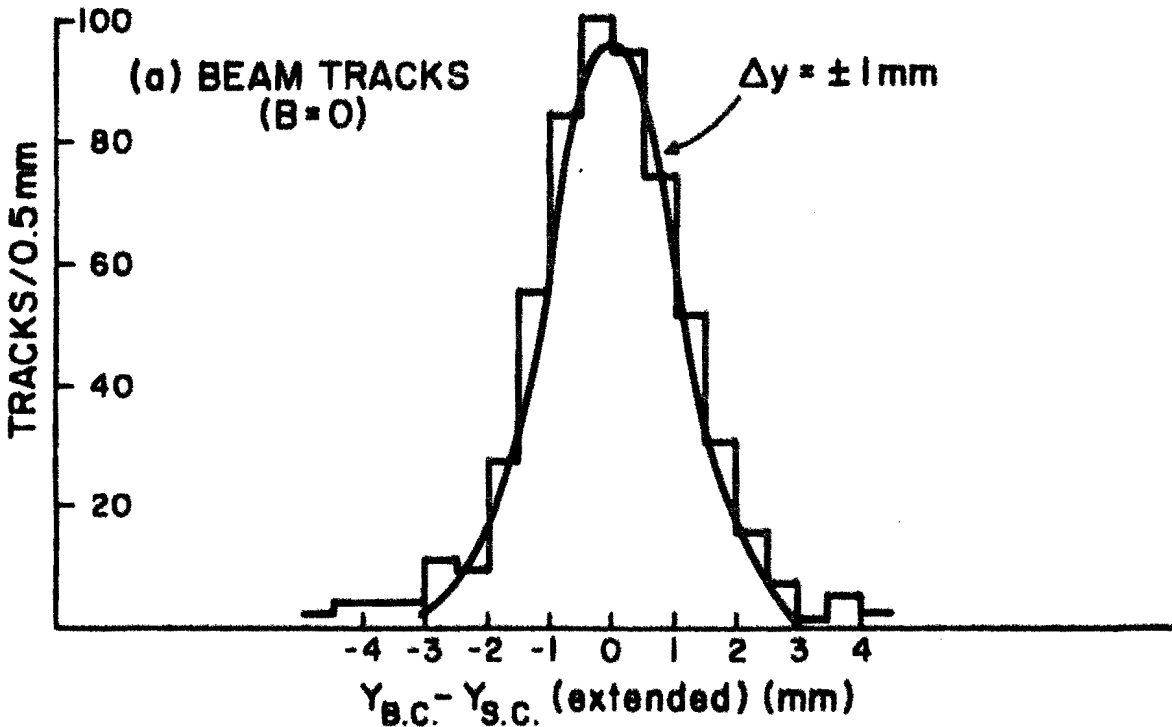


**SPARK-CHAMBER POINT SCATTER (FRMS)  
(90-DEGREE VIEW)**

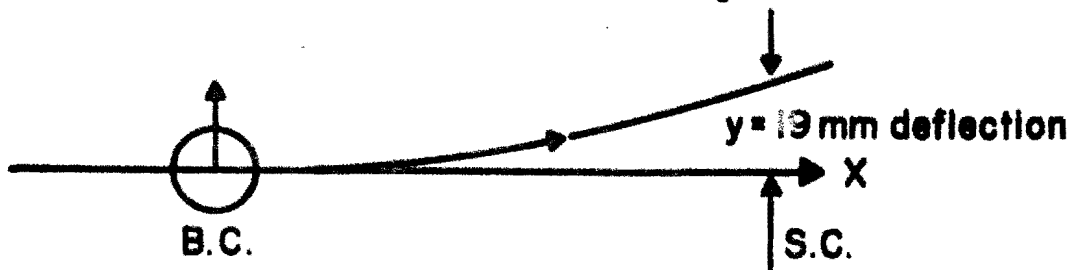
Fig. 8



NAL 30-INCH BUBBLE CHAMBER-WIDE GAP  
SPARK CHAMBER HYBRID SYSTEM  
(EXPERIMENT 2-B)



(b) 200 GeV BEAM TRACKS (B=30 Kg)



$$\frac{\Delta p}{p} = \frac{\Delta y}{y} = \pm \frac{1\text{mm}}{19\text{mm}} = \pm 0.053$$

$$\therefore \pm \frac{\Delta p}{p} (\%) = 0.026p (\text{GeV}/c)$$

Fig. 9

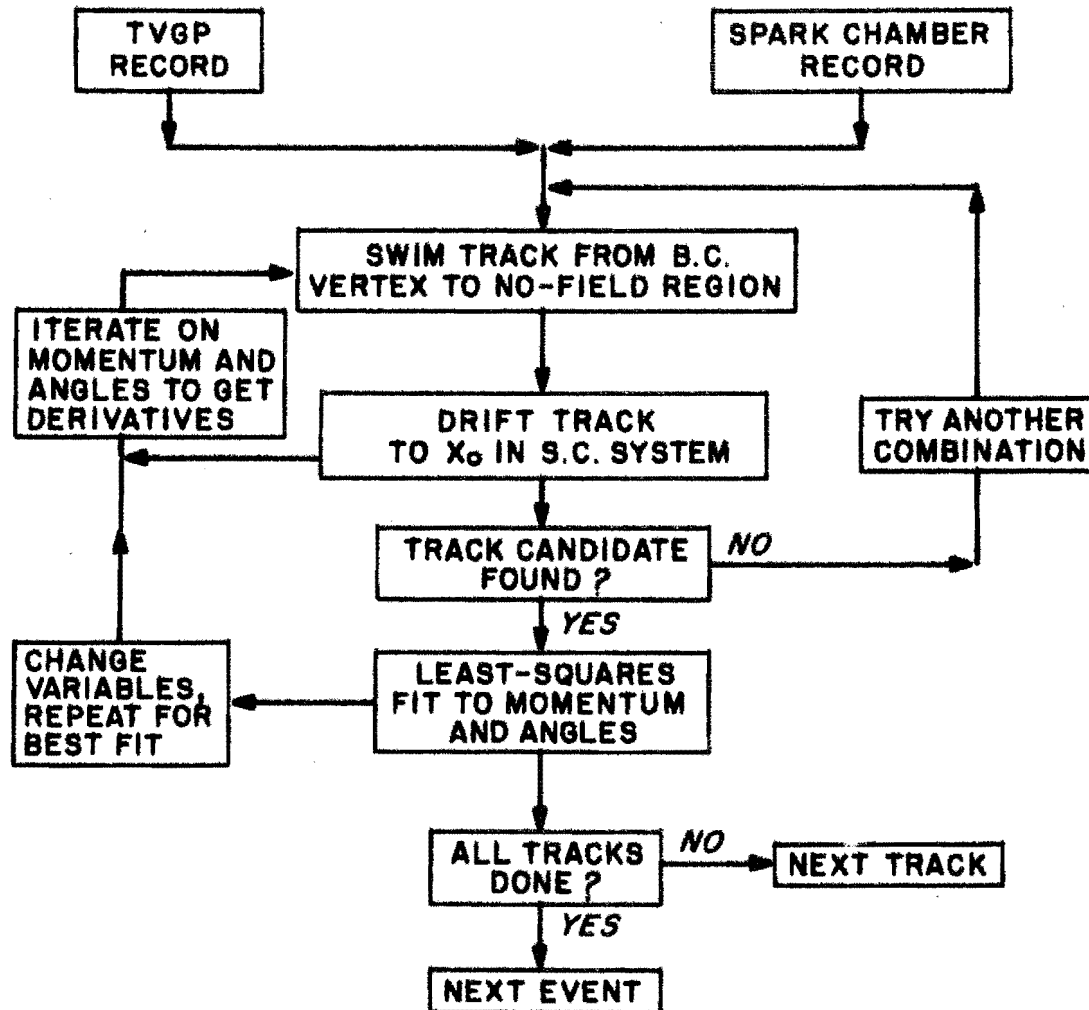
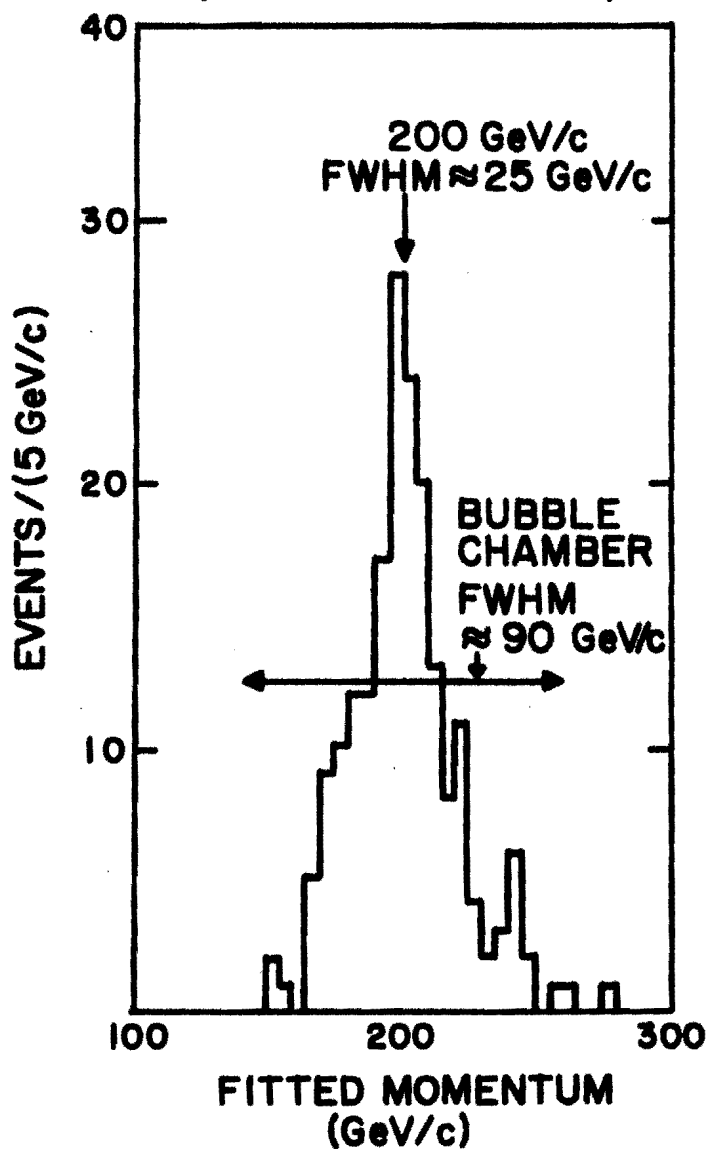


Fig. 10

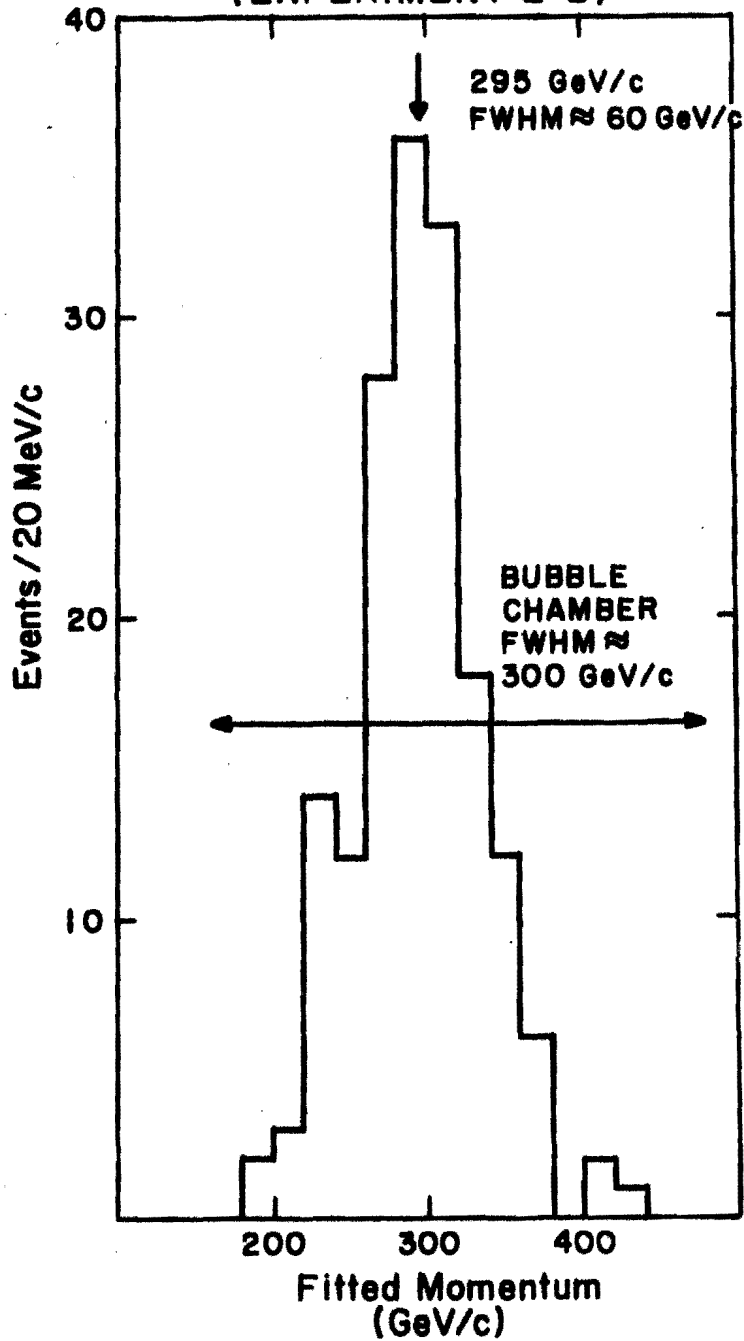
**NAL 30-INCH BUBBLE CHAMBER-WIDE GAP  
SPARK CHAMBER HYBRID SYSTEM  
(EXPERIMENT 2-B)**



**FITTED BEAM MOMENTUM USING  
BUBBLE CHAMBER - SPARK CHAMBER  
HOOK-UP DATA**

Fig. 11

NAL 30-INCH BUBBLE CHAMBER-WIDE GAP  
SPARK CHAMBER HYBRID SYSTEM  
(EXPERIMENT 2-B)



Fitted Beam Momentum using Bubble-  
Chamber-Spark Chamber Hook-up data

Fig. 12

NAL 30-INCH BUBBLE CHAMBER-WIDE GAP  
SPARK CHAMBER HYBRID SYSTEM  
(EXPERIMENT 2-B)

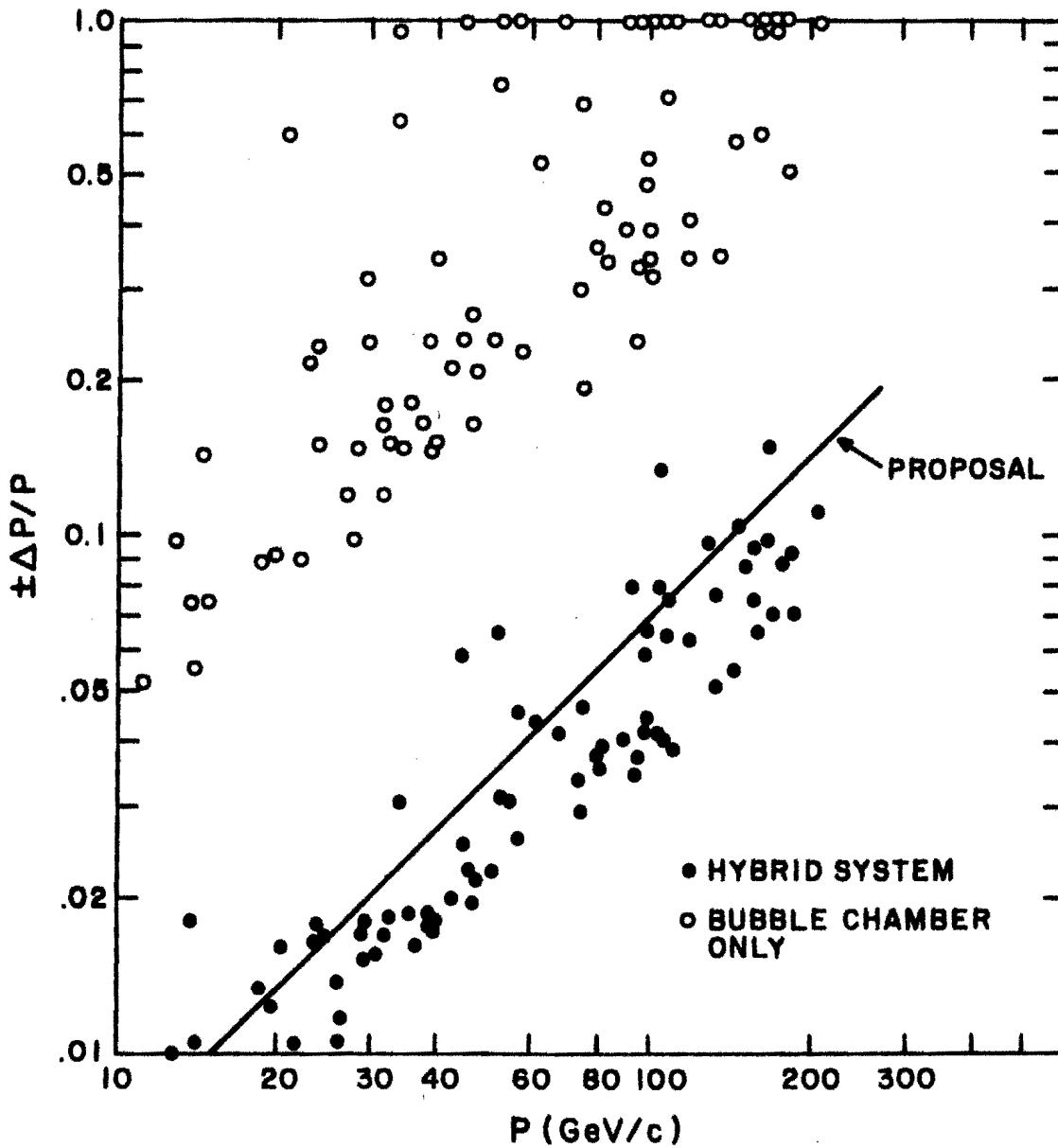


Fig. 13

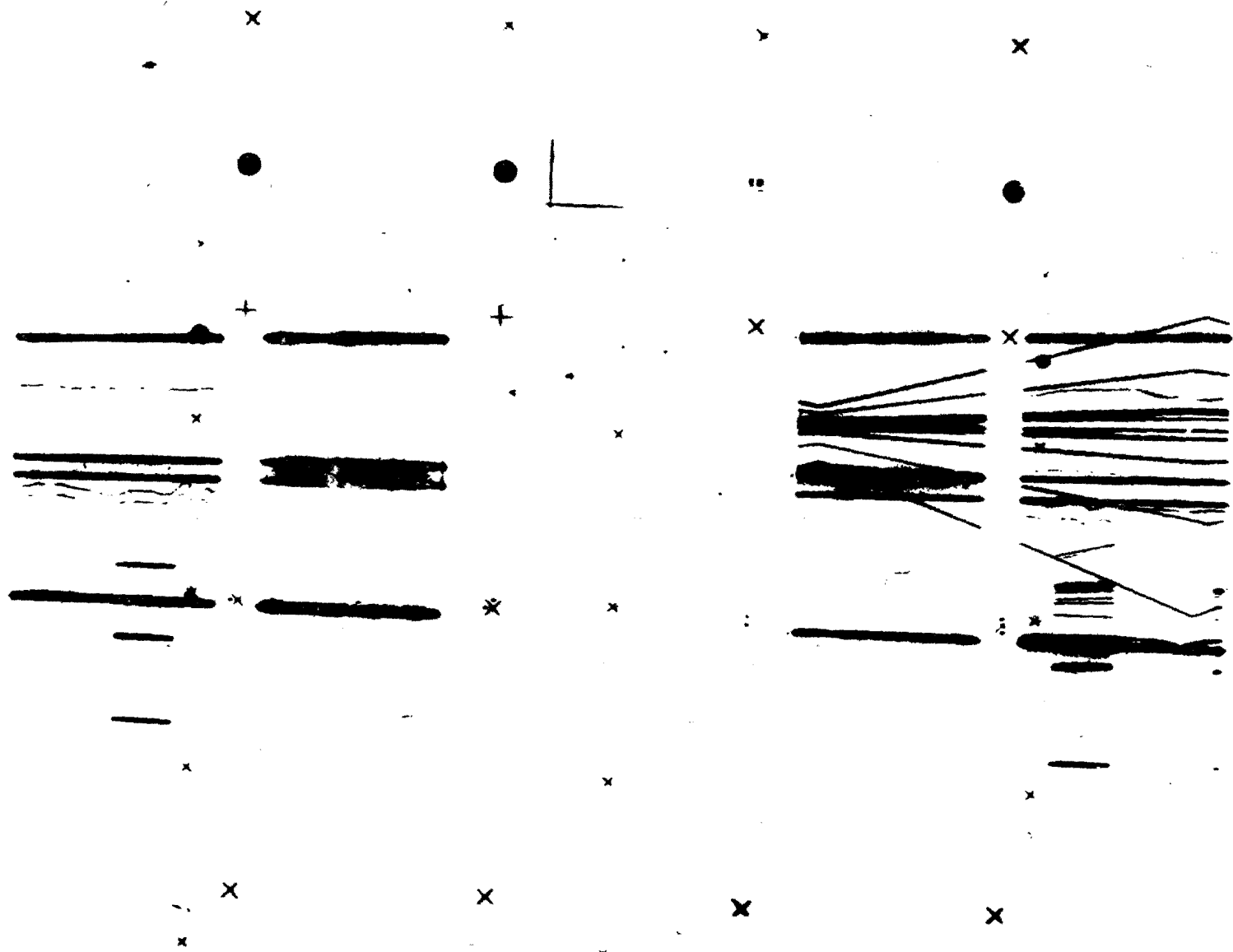


Fig. 14

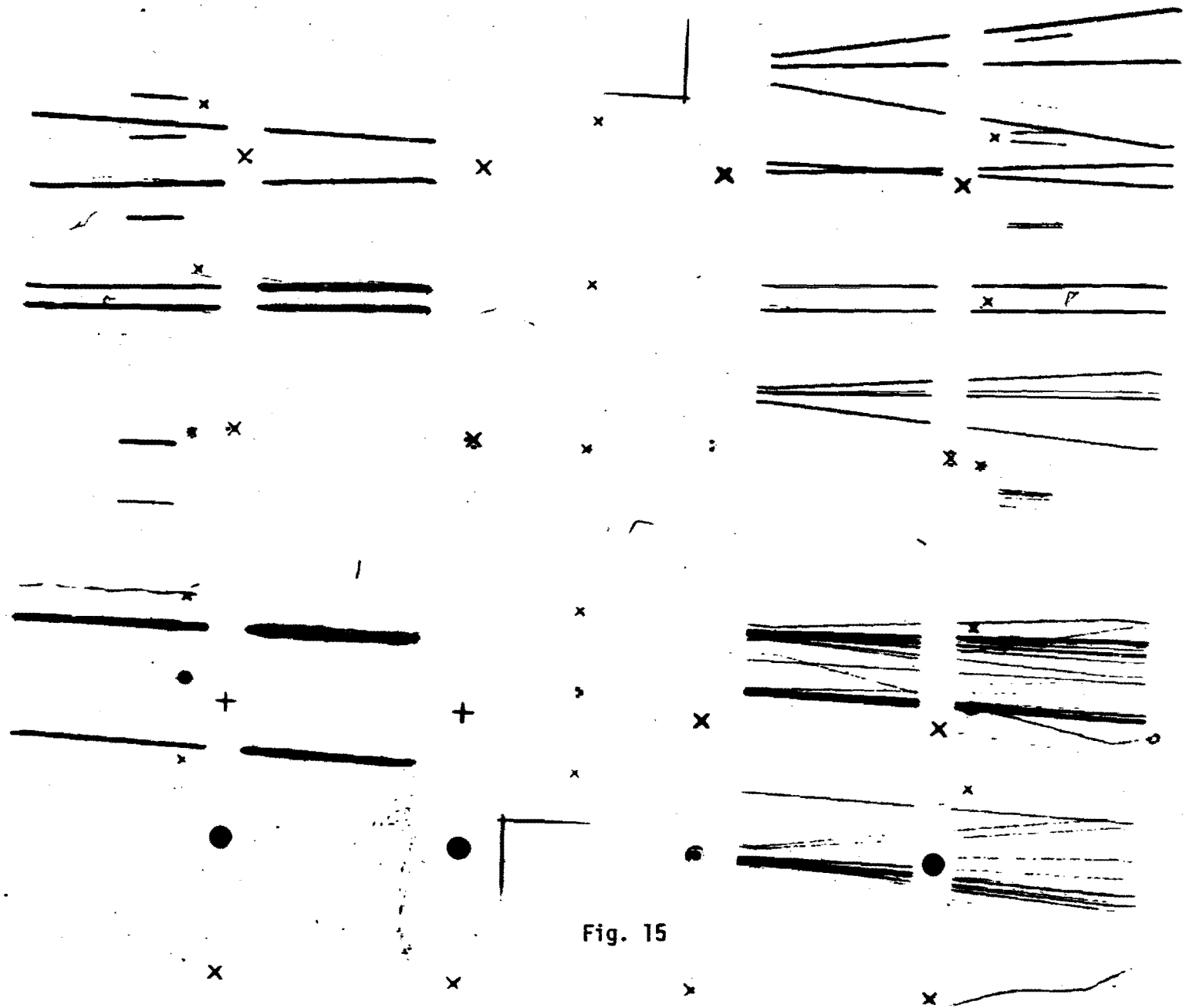


Fig. 15

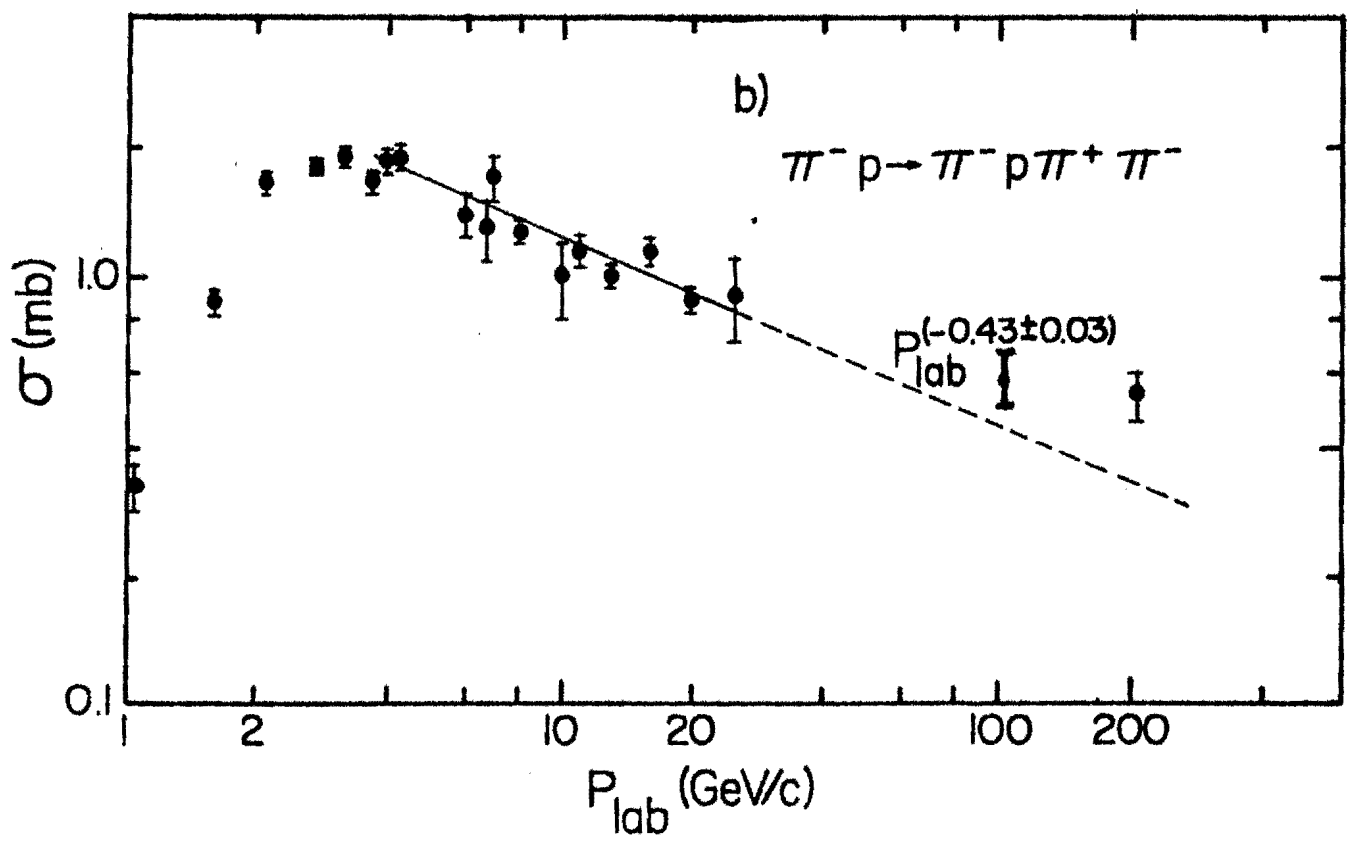
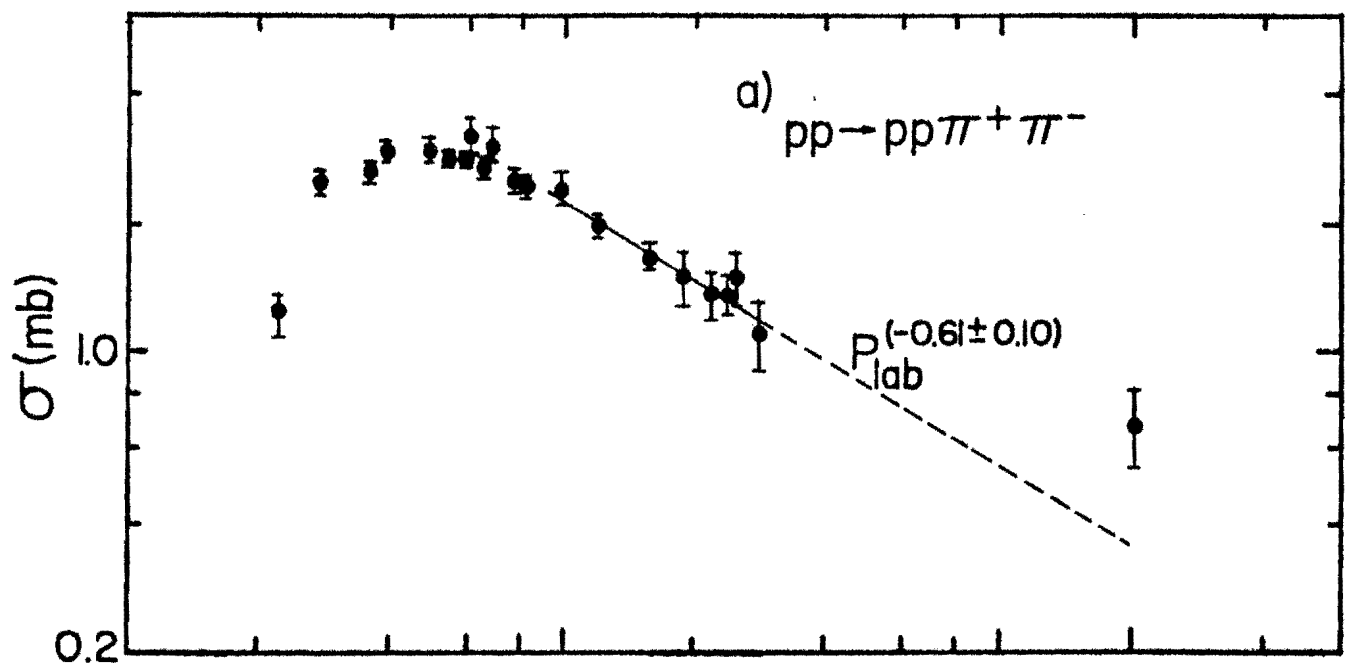
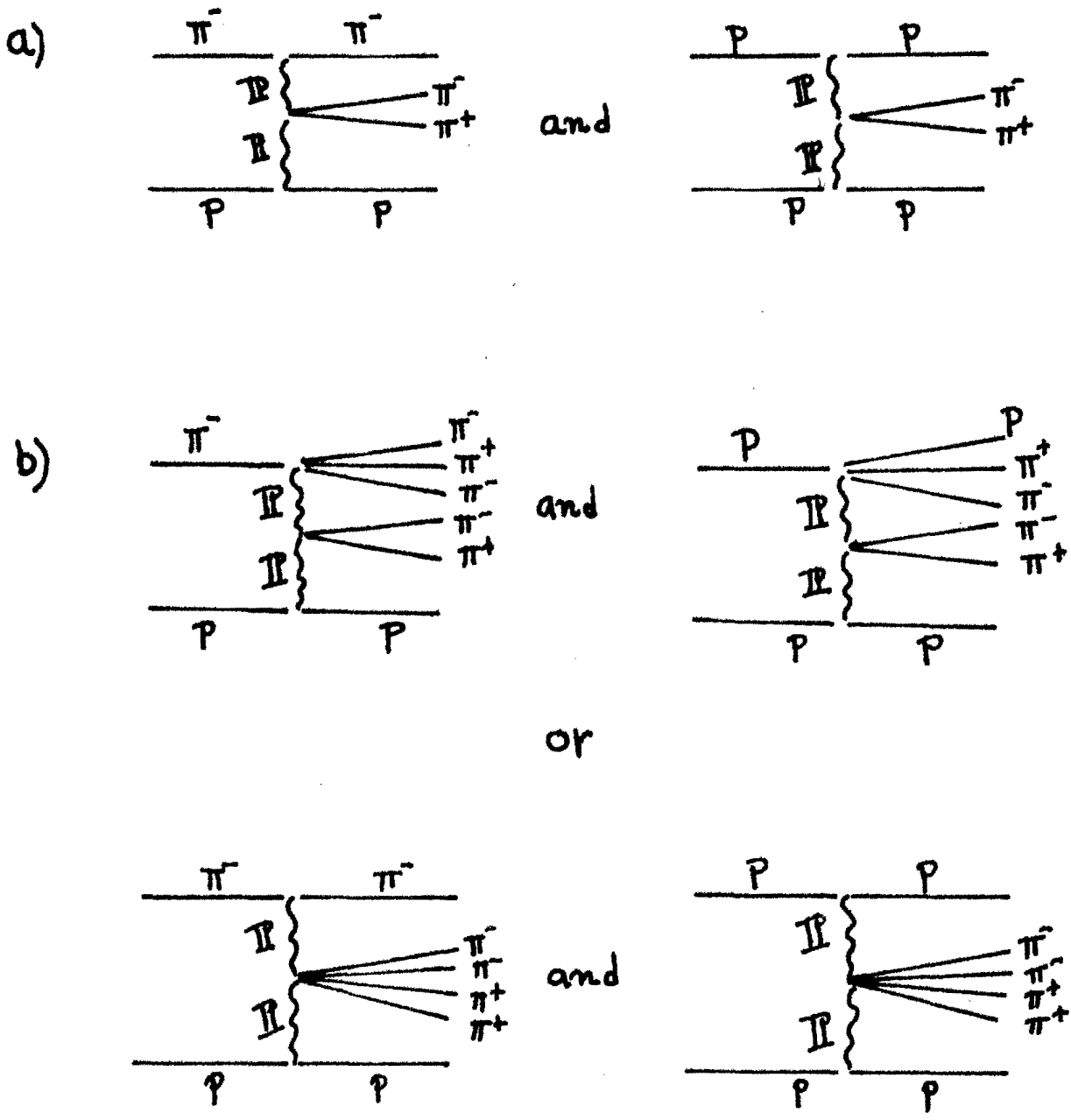


Fig. 16



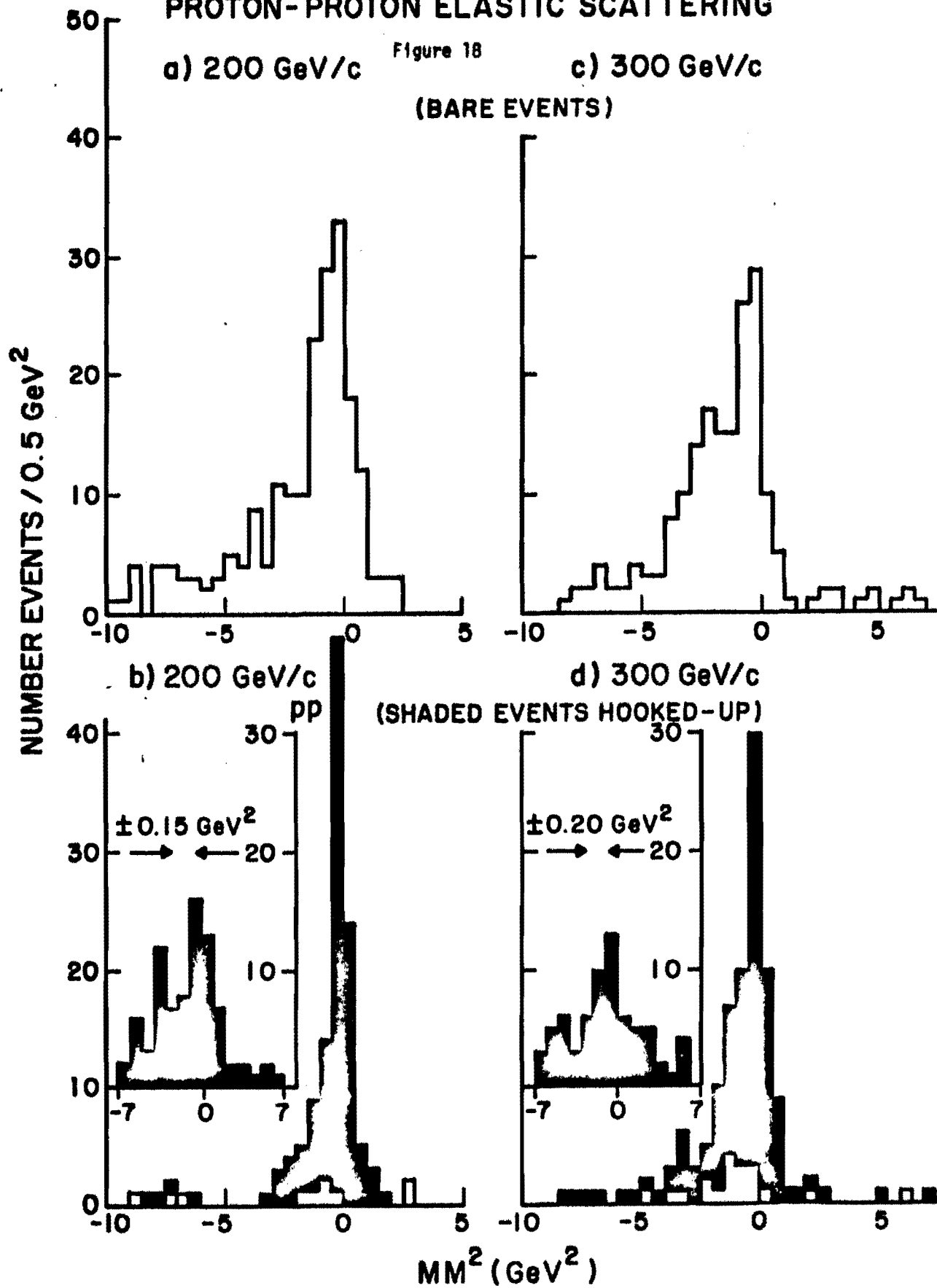


# DOUBLE POMERON EXCHANGE DIAGRAMS

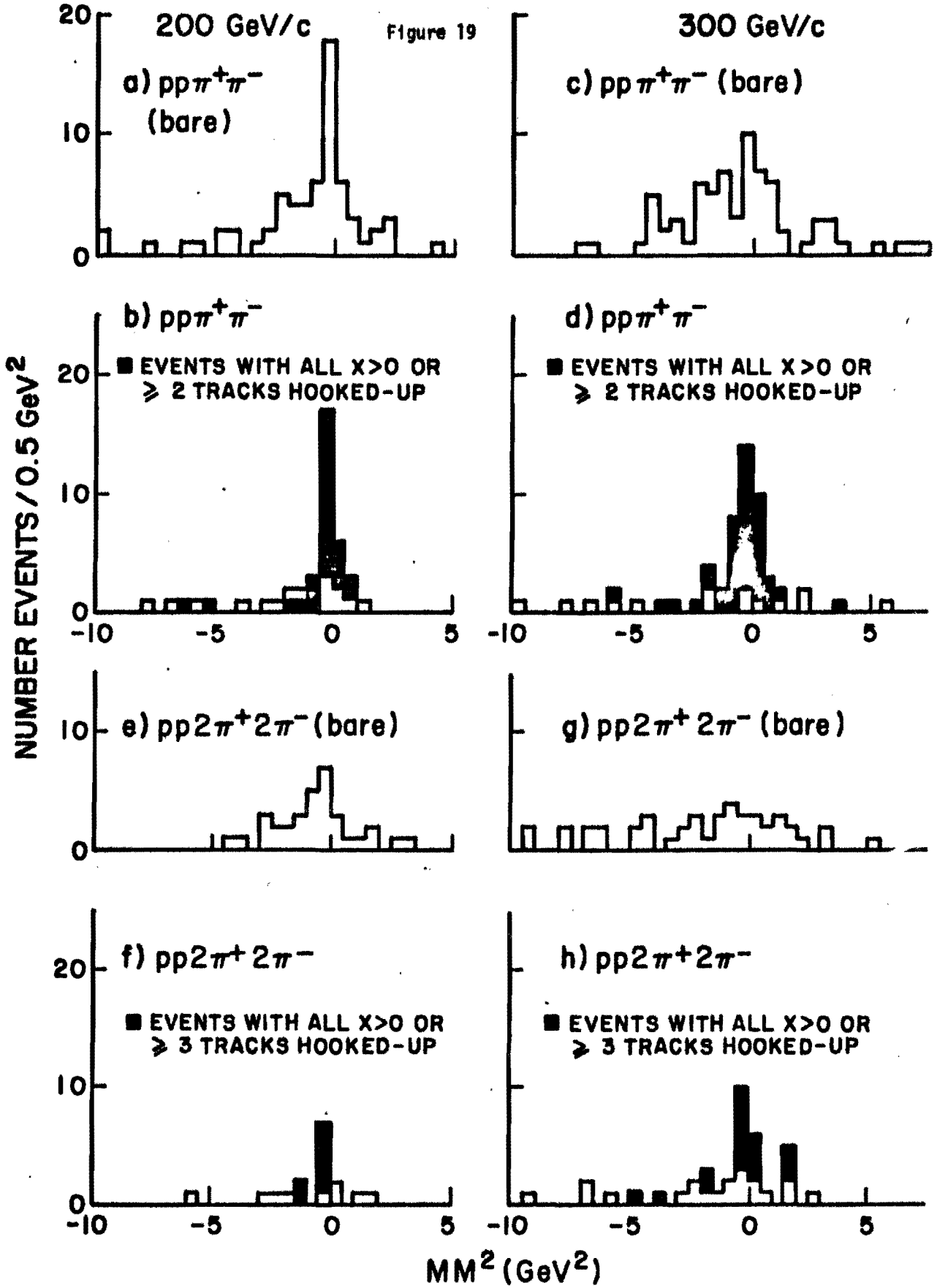
Figure 17

# PROTON-PROTON ELASTIC SCATTERING

Figure 18



**$p-p \rightarrow pp\pi^+\pi^-$  and  $pp2\pi^+2\pi^-$  EVENTS**



100 GeV/c  $\pi^-p$

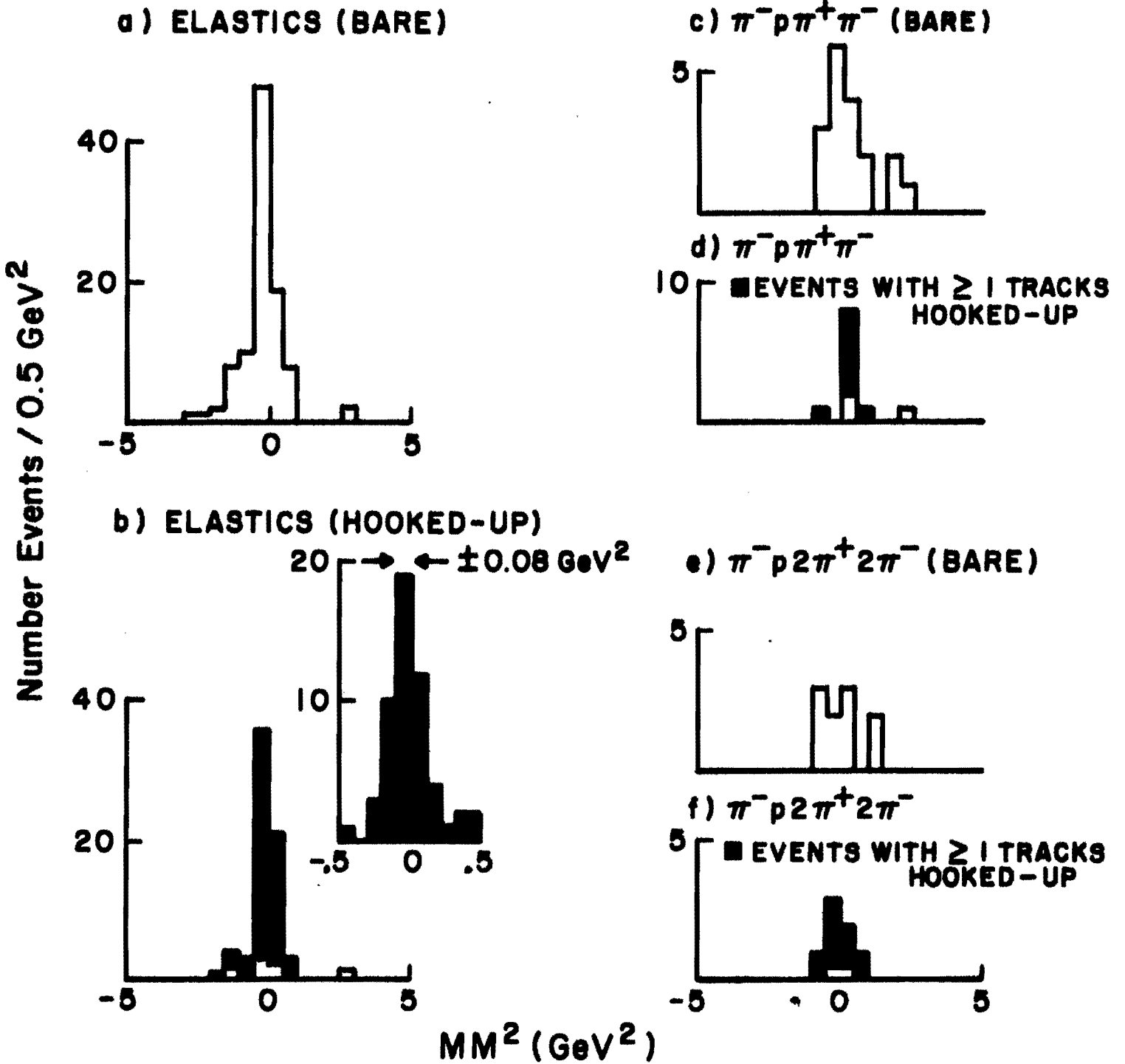


Figure 20

$pp \rightarrow pp\pi^+\pi^-$

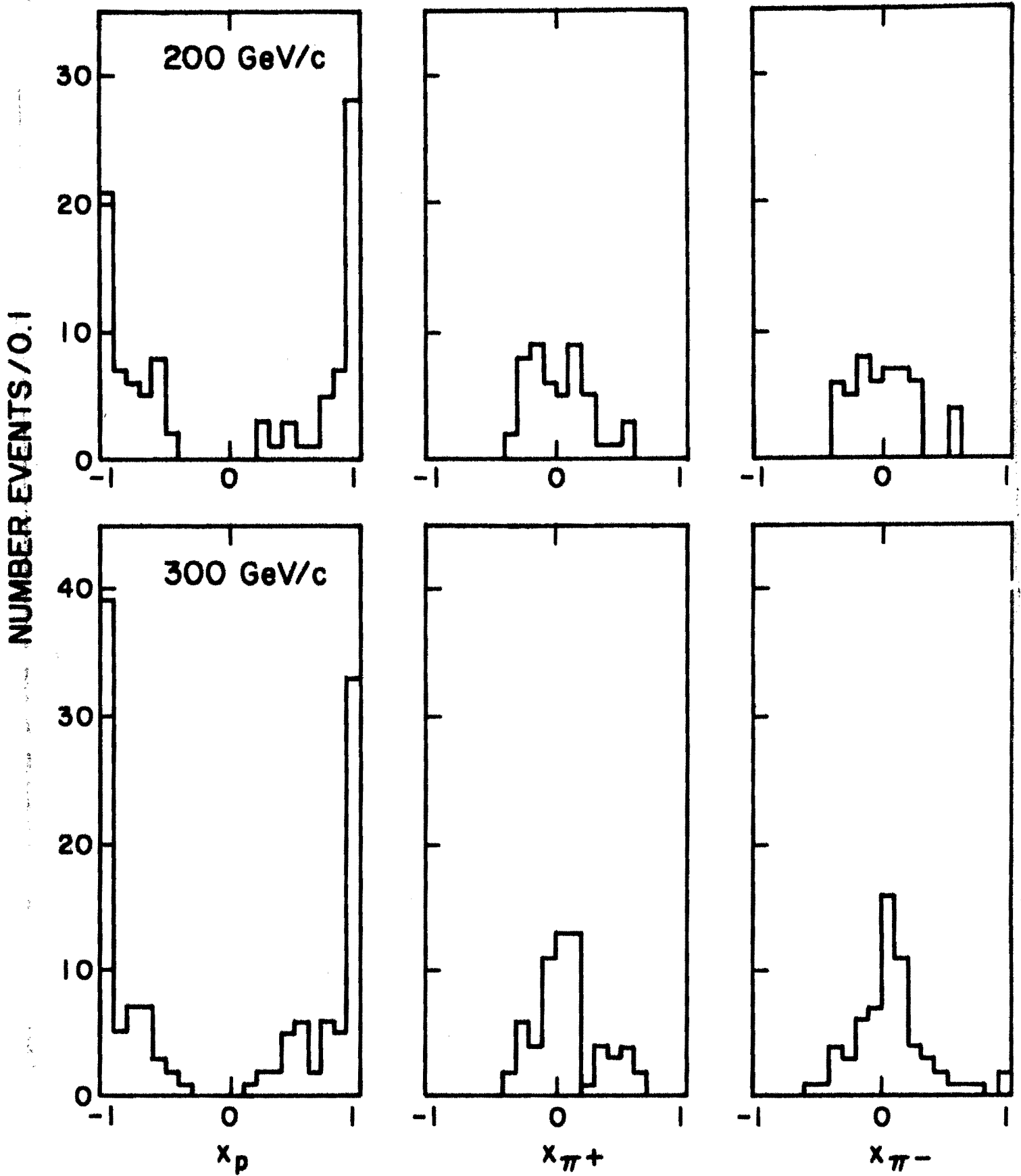


Figure 21

NUMBER EVENTS / 0.1

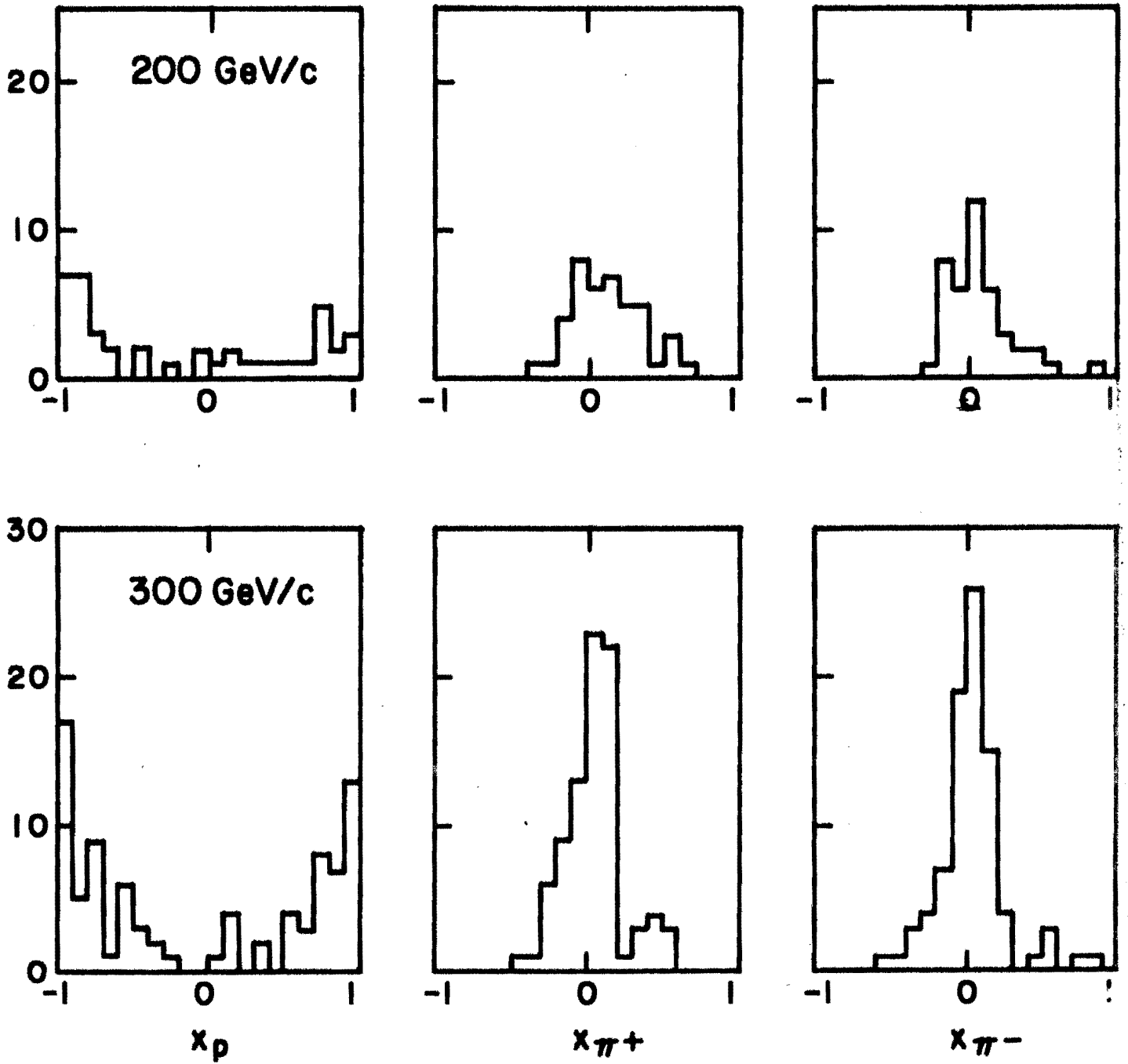
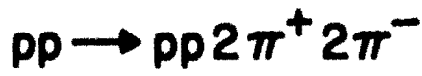


Figure 22

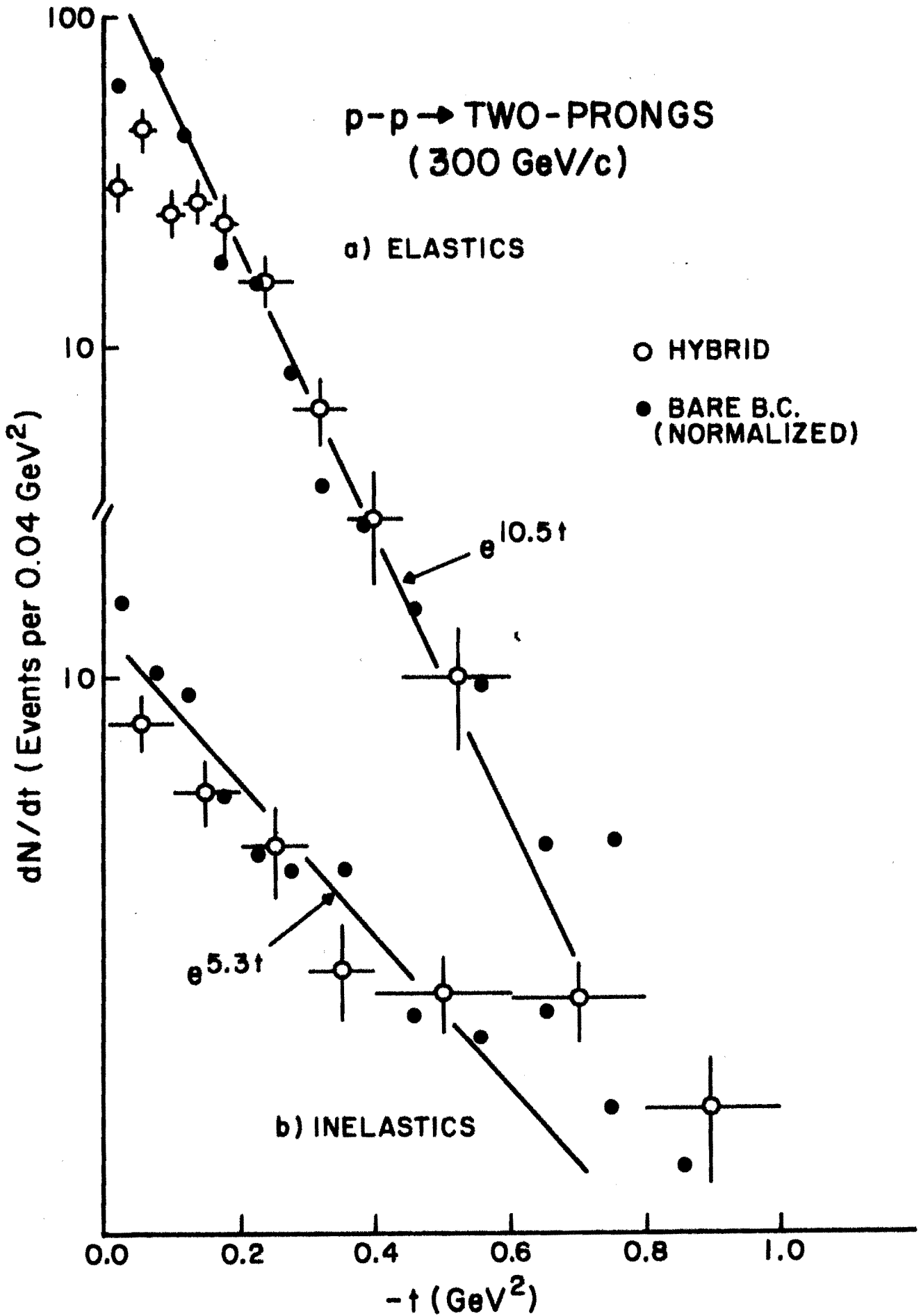


Figure 23

$pp \rightarrow pX$  (200 and 300 GeV/c Two-Prongs)

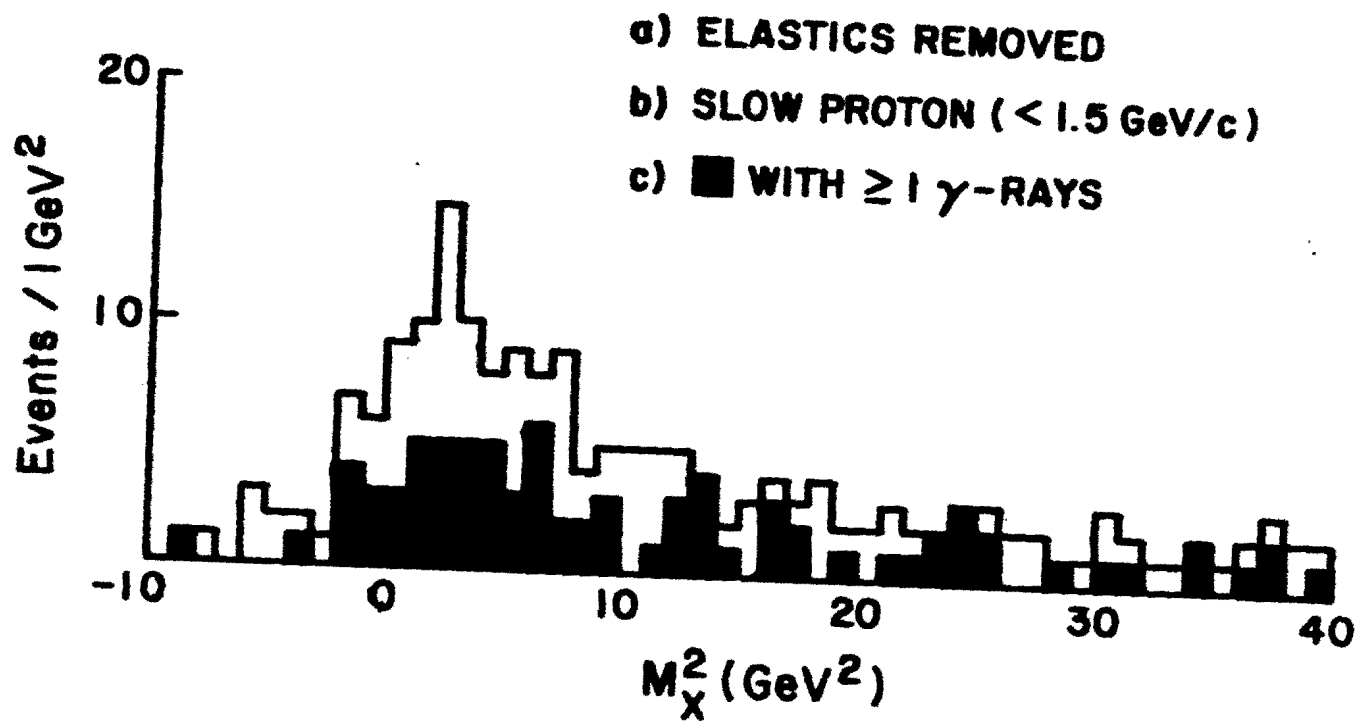


Figure 24



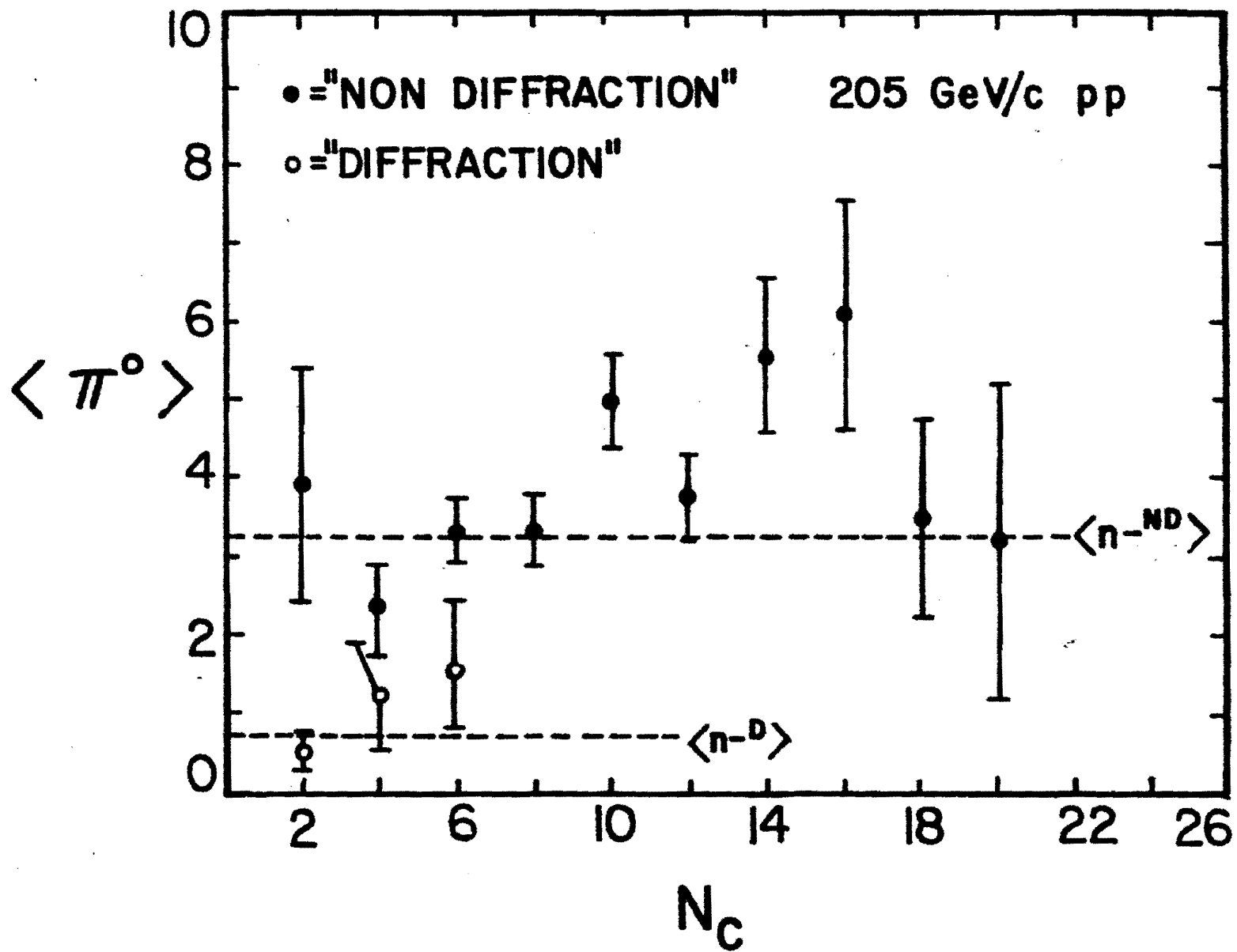


Figure 25

$pp \rightarrow \gamma X$  (200 GeV/c)

■ "DIFFRACTIVE" EVENTS  
( $M_X^2 < 50 \text{ GeV}^2$ )

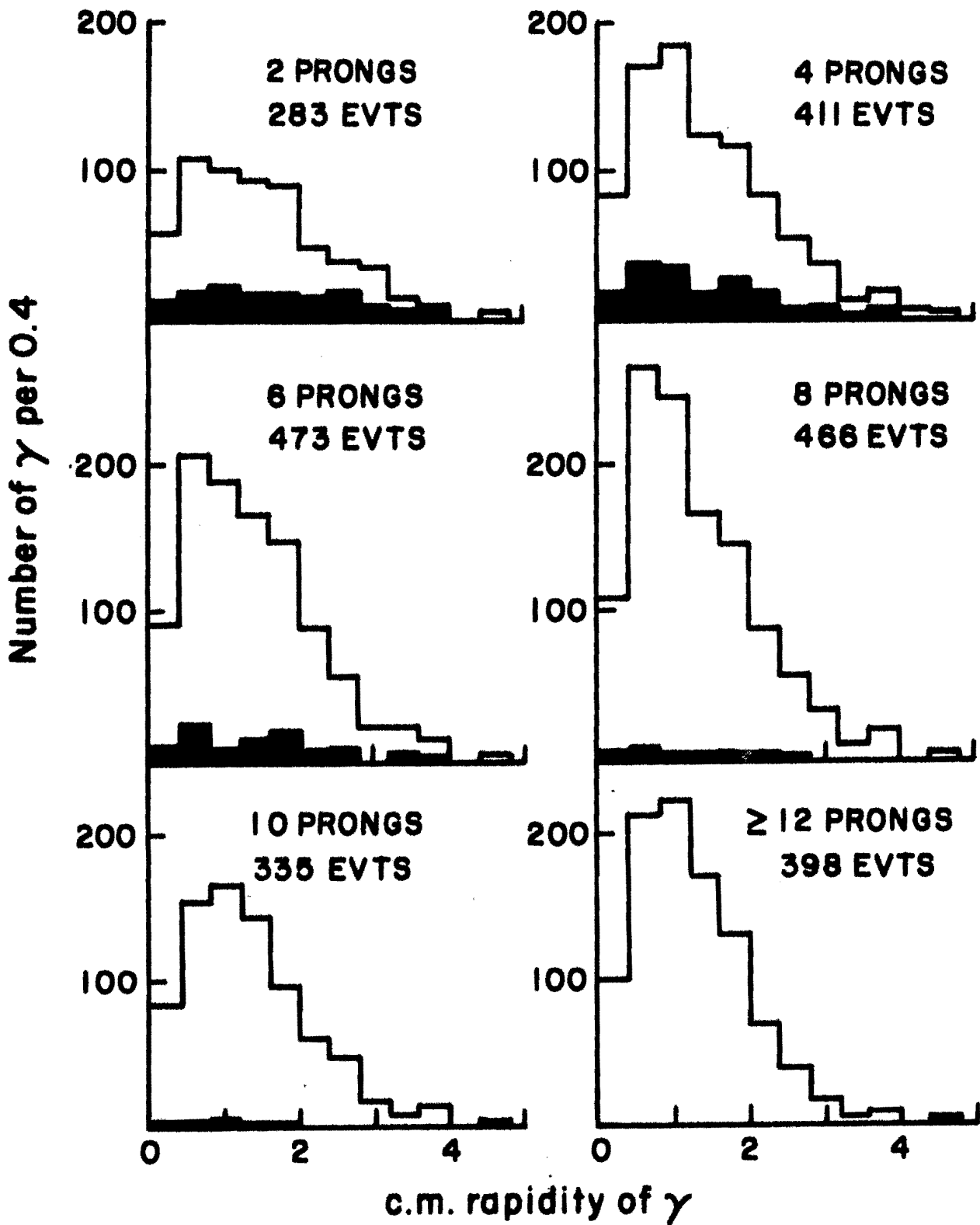
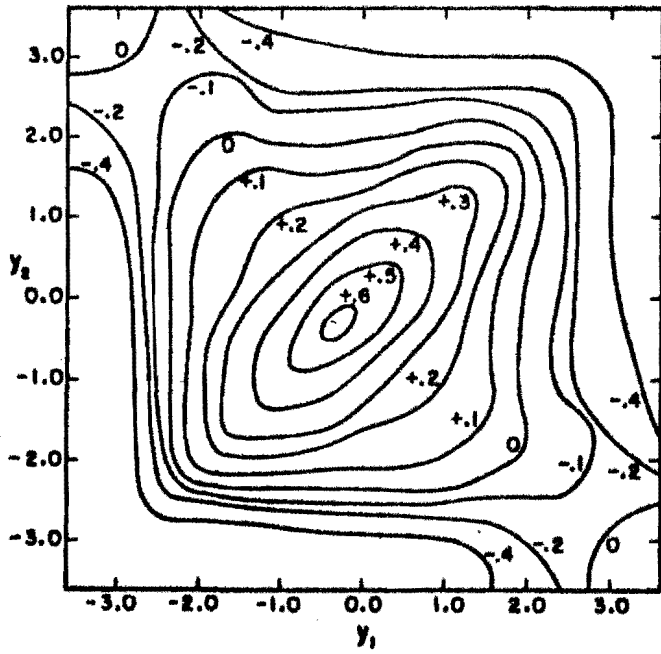
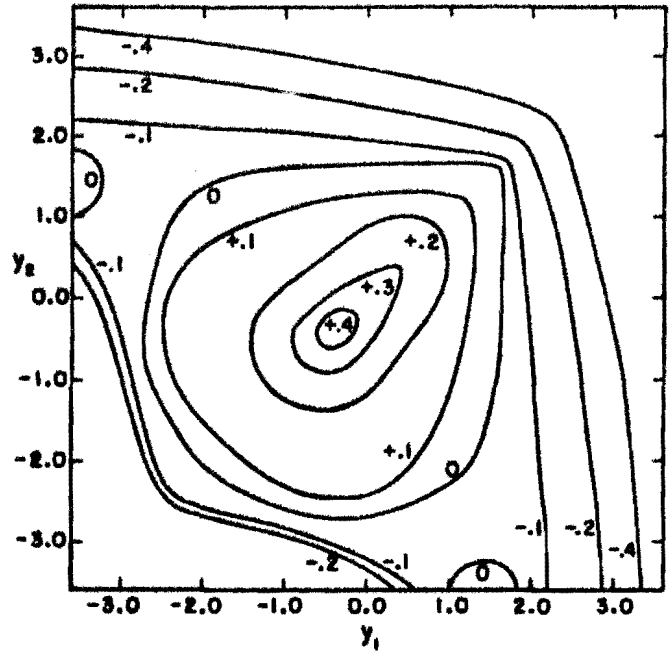


Figure 26

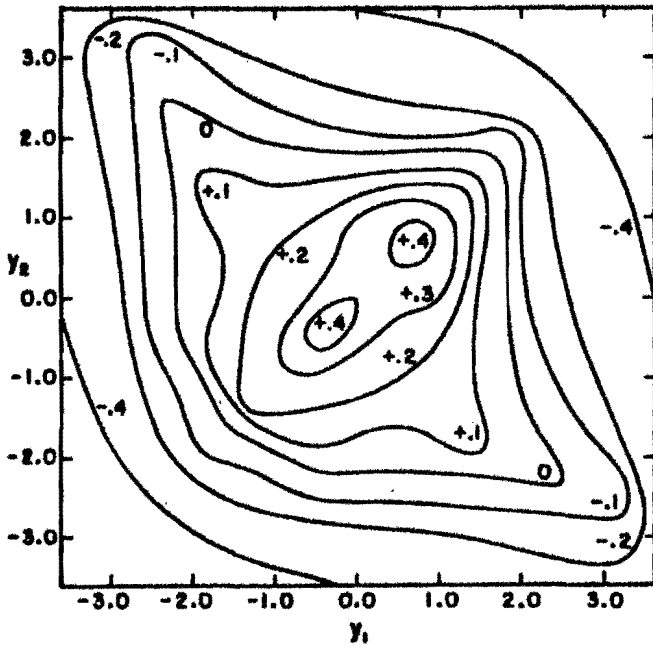
205 GeV/c  $\pi^-p$  (All Charged Particles)  
Notre Dame - Duke - Canada



205 GeV/c  $\pi^-p \rightarrow \pi^- + \pi^- + \dots$   
Notre Dame - Duke - Canada



205 GeV/c  $\pi^-p \rightarrow \pi^+ + \pi^+ + \dots$   
Notre Dame - Duke - Canada



205 GeV/c  $\pi^-p \rightarrow \pi^- + \pi^+ + \dots$   
Notre Dame - Duke - Canada

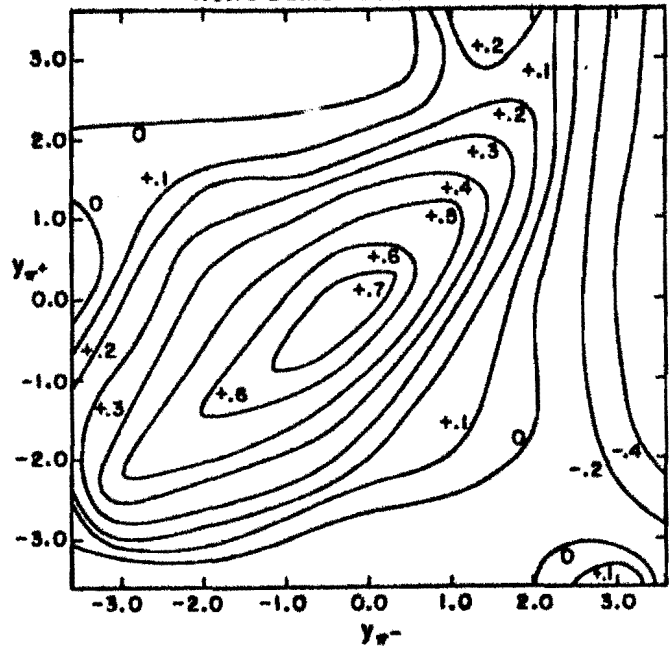


Figure 27

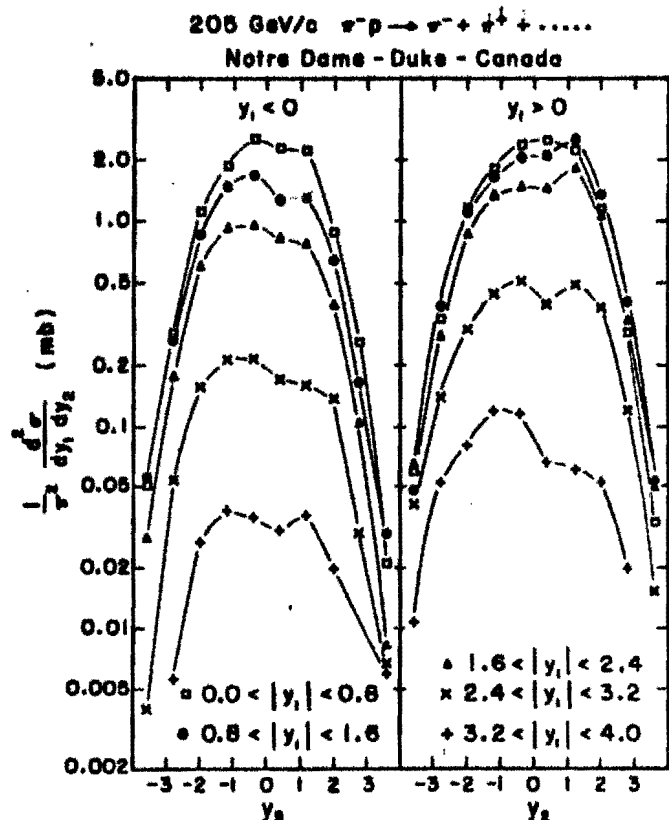
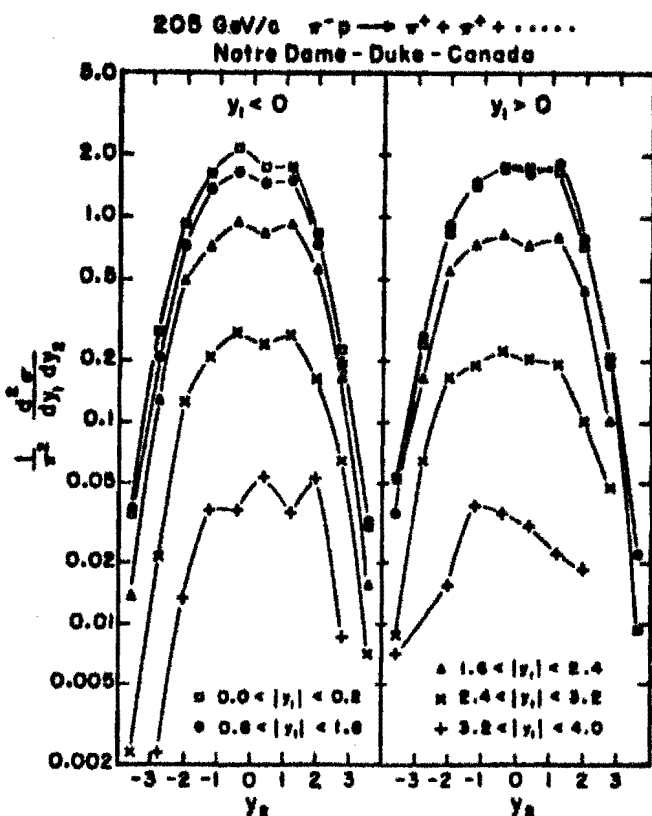
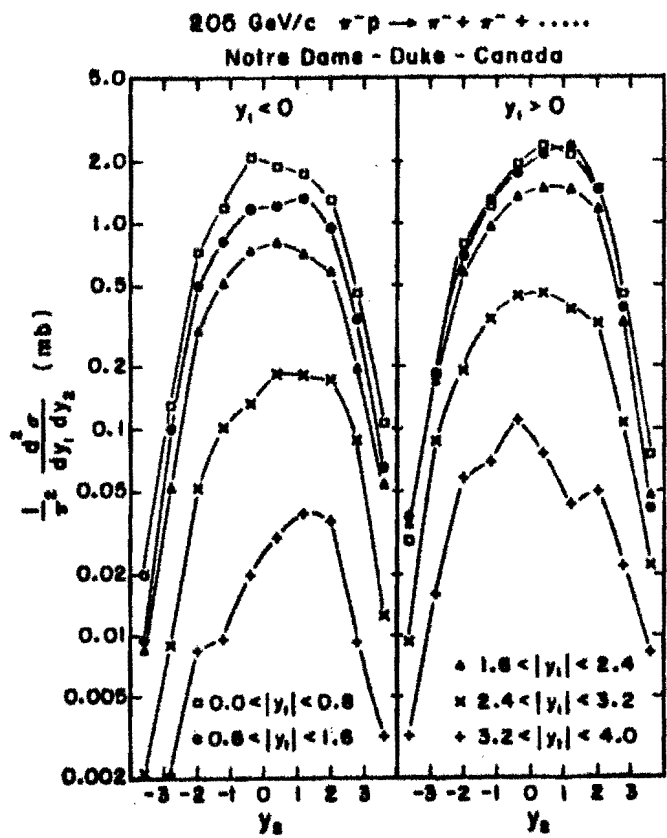
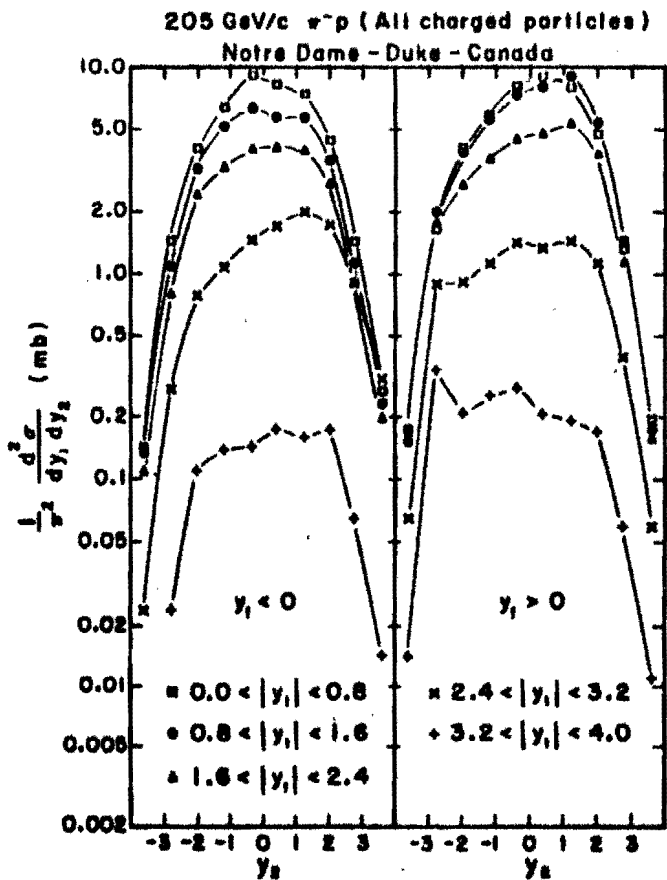


Figure 28

# GAMMA-RAY RAPIDITY DISTRIBUTIONS (Proton-Proton) AND ACCEPTANCE

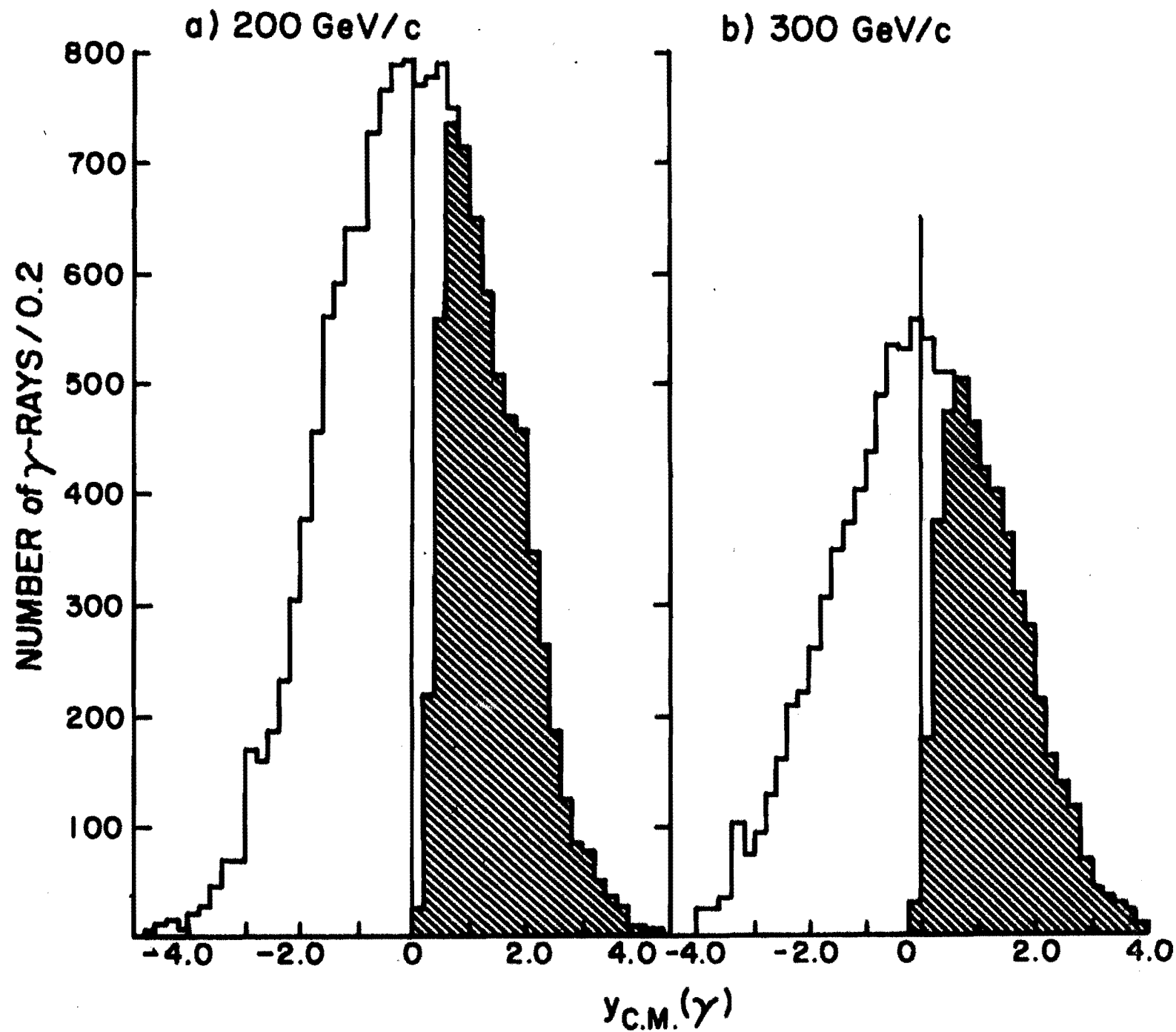


Figure 29

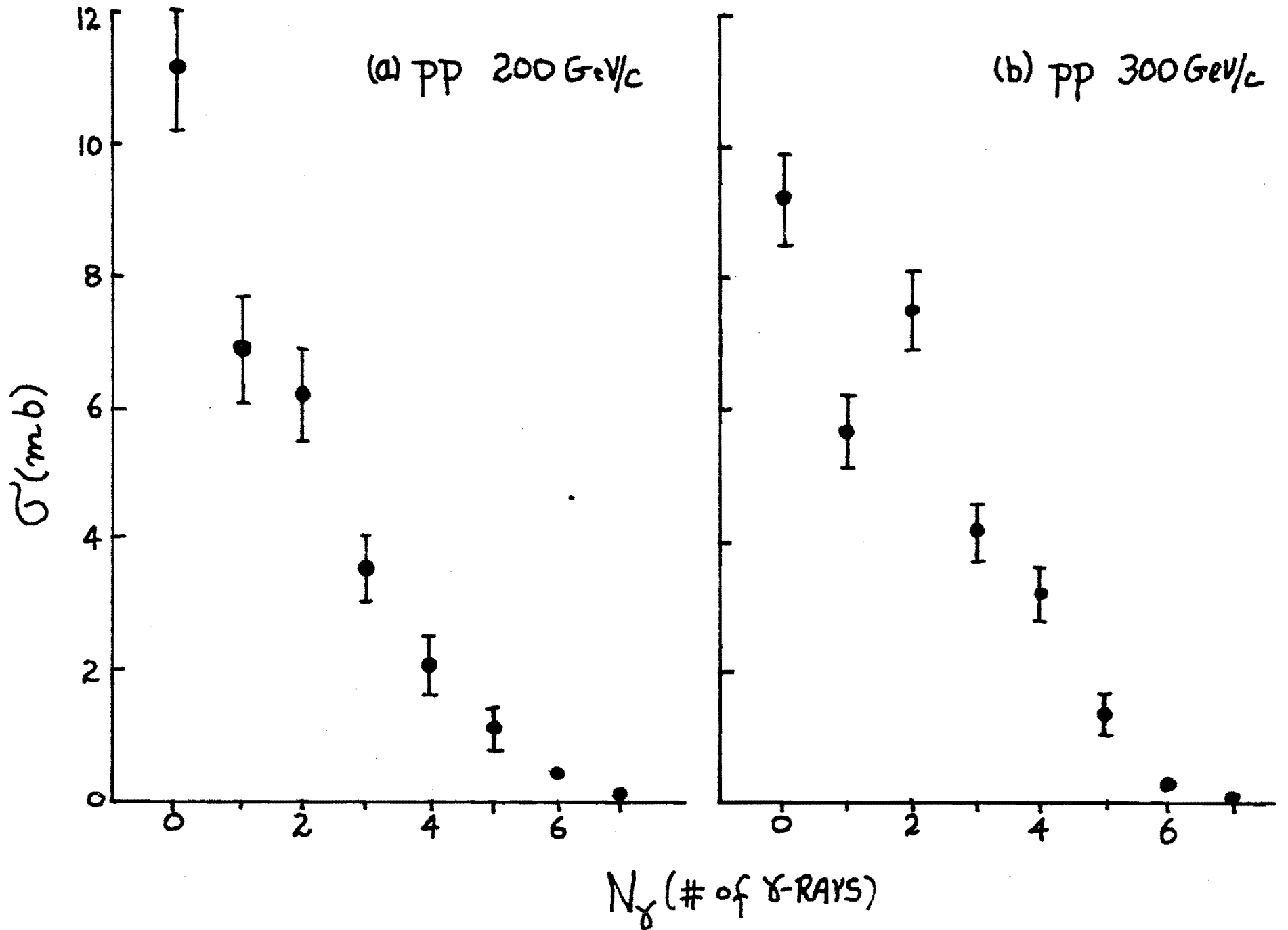


Figure 30

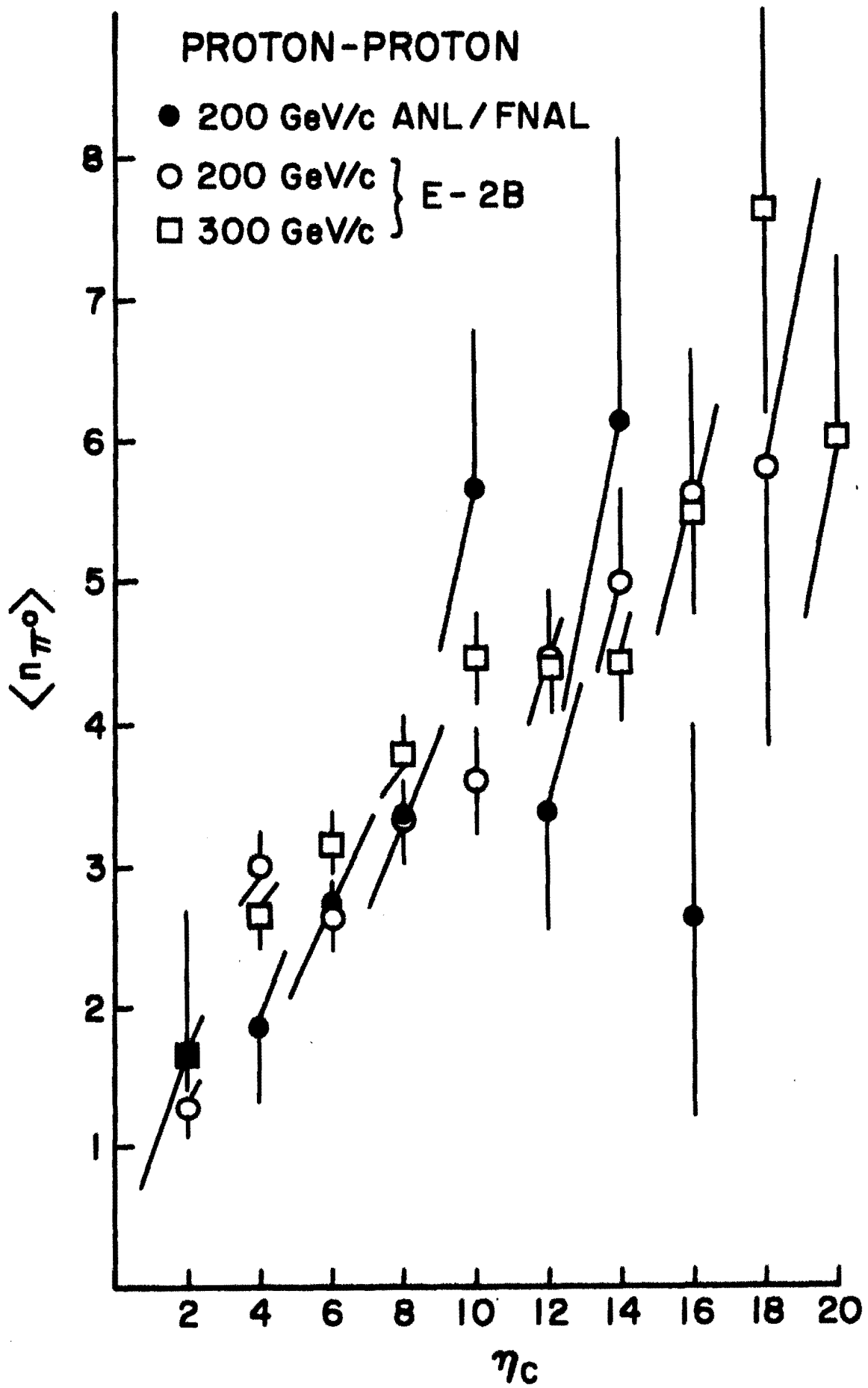


Figure 31

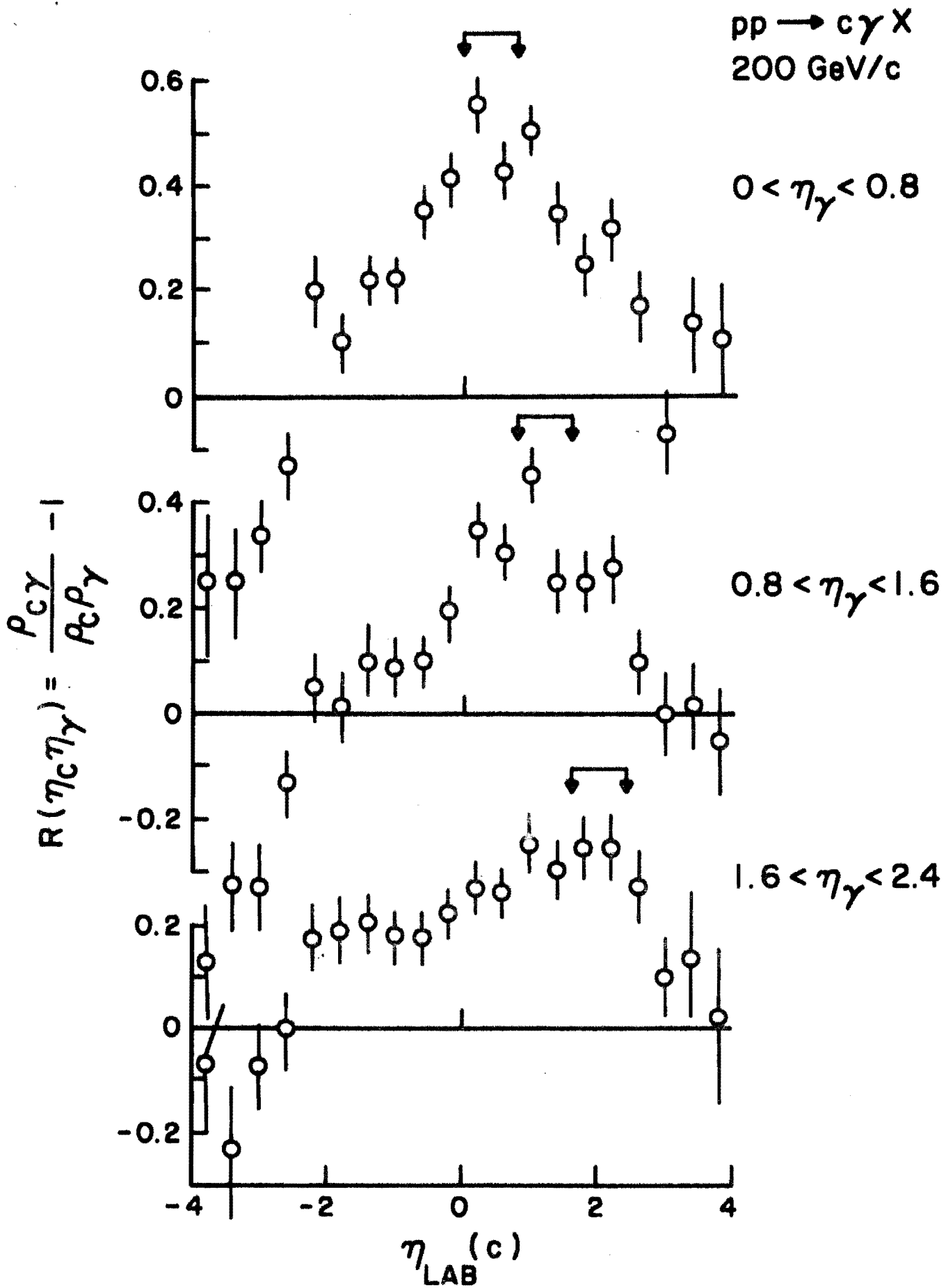


Figure 32



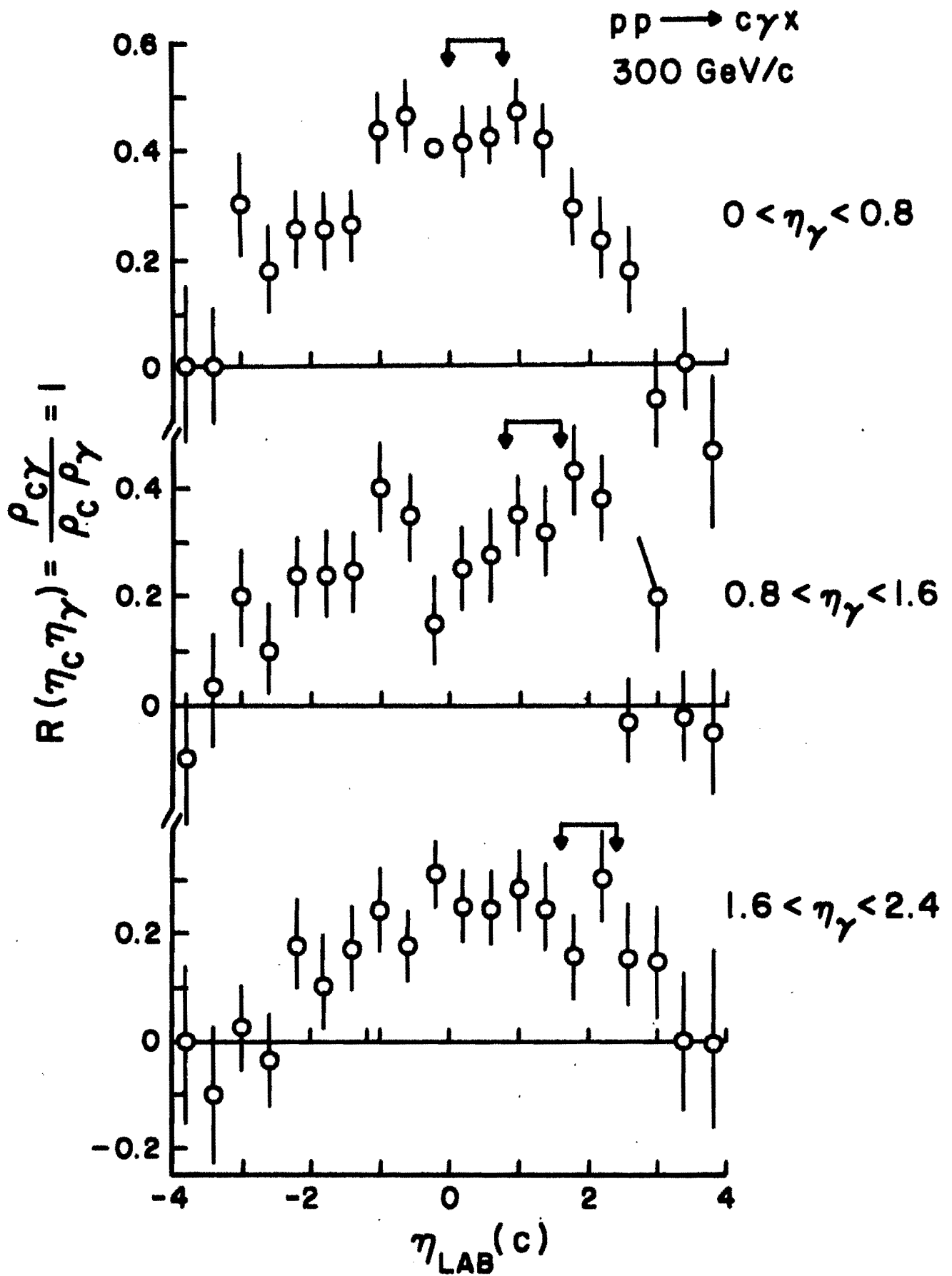


Figure 33

Figure 34

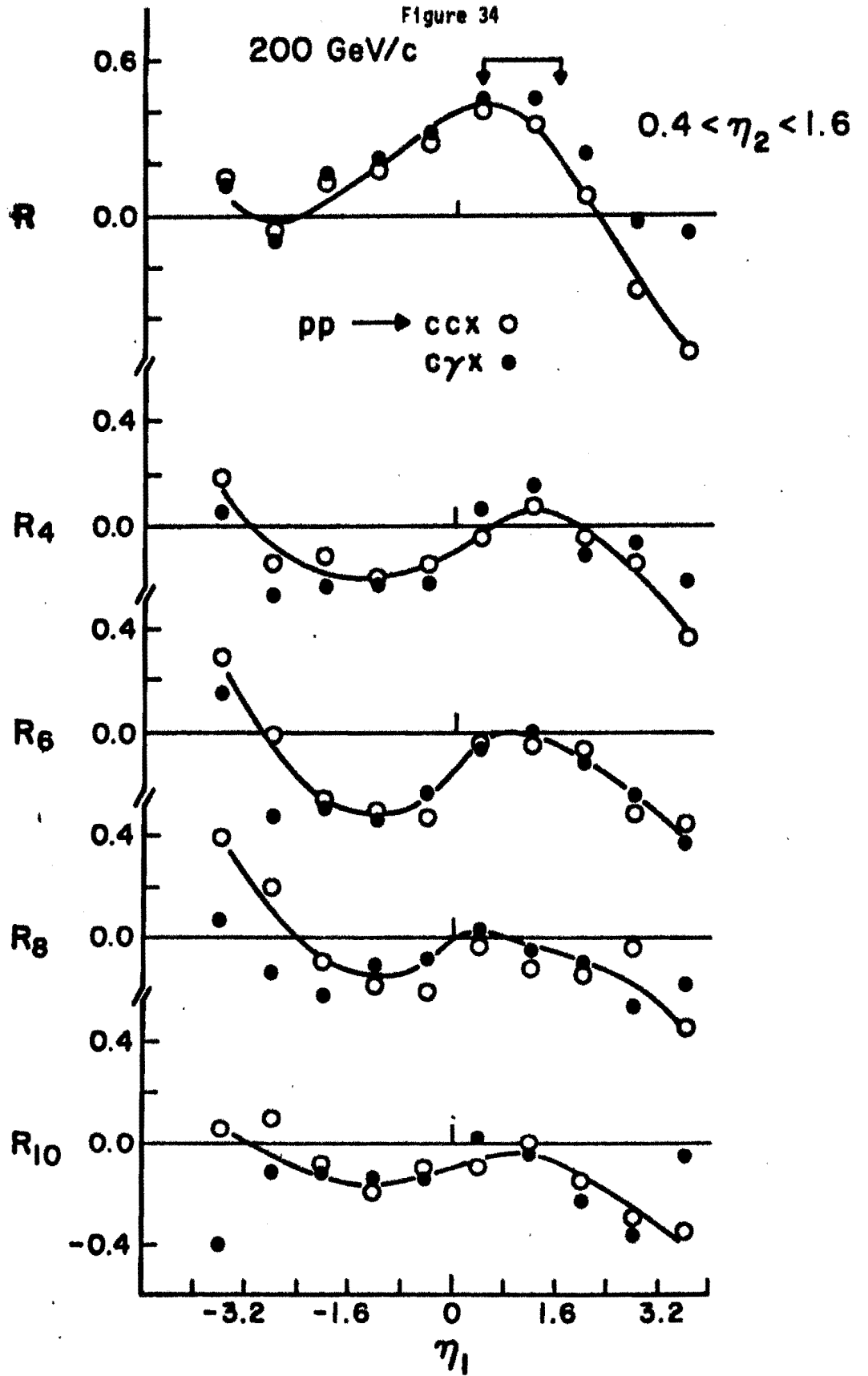


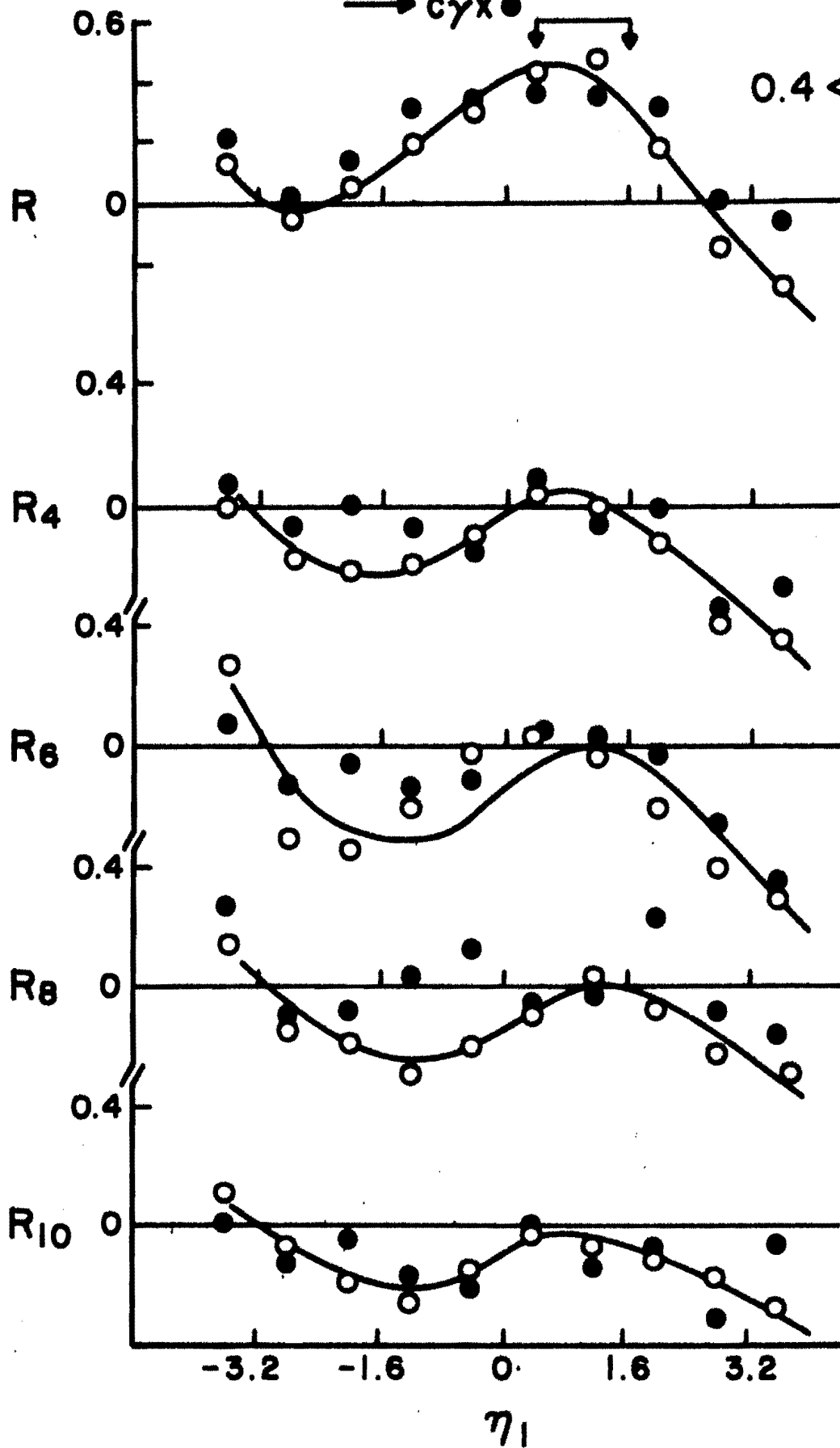
Figure 35

pp → CCXO

300 GeV/c

→ CγX●

$0.4 < \eta_2 < 1.6$



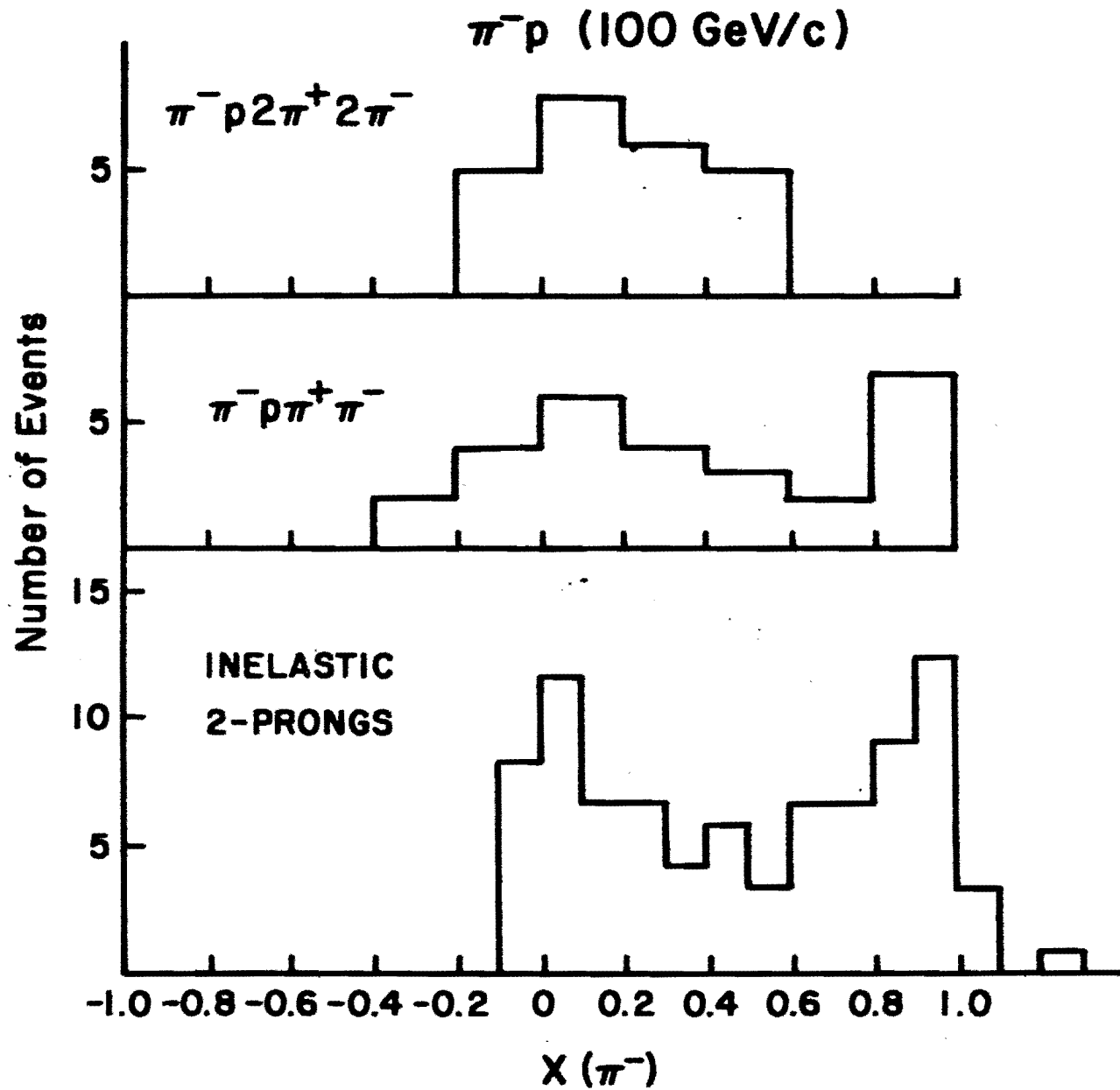


Figure 36

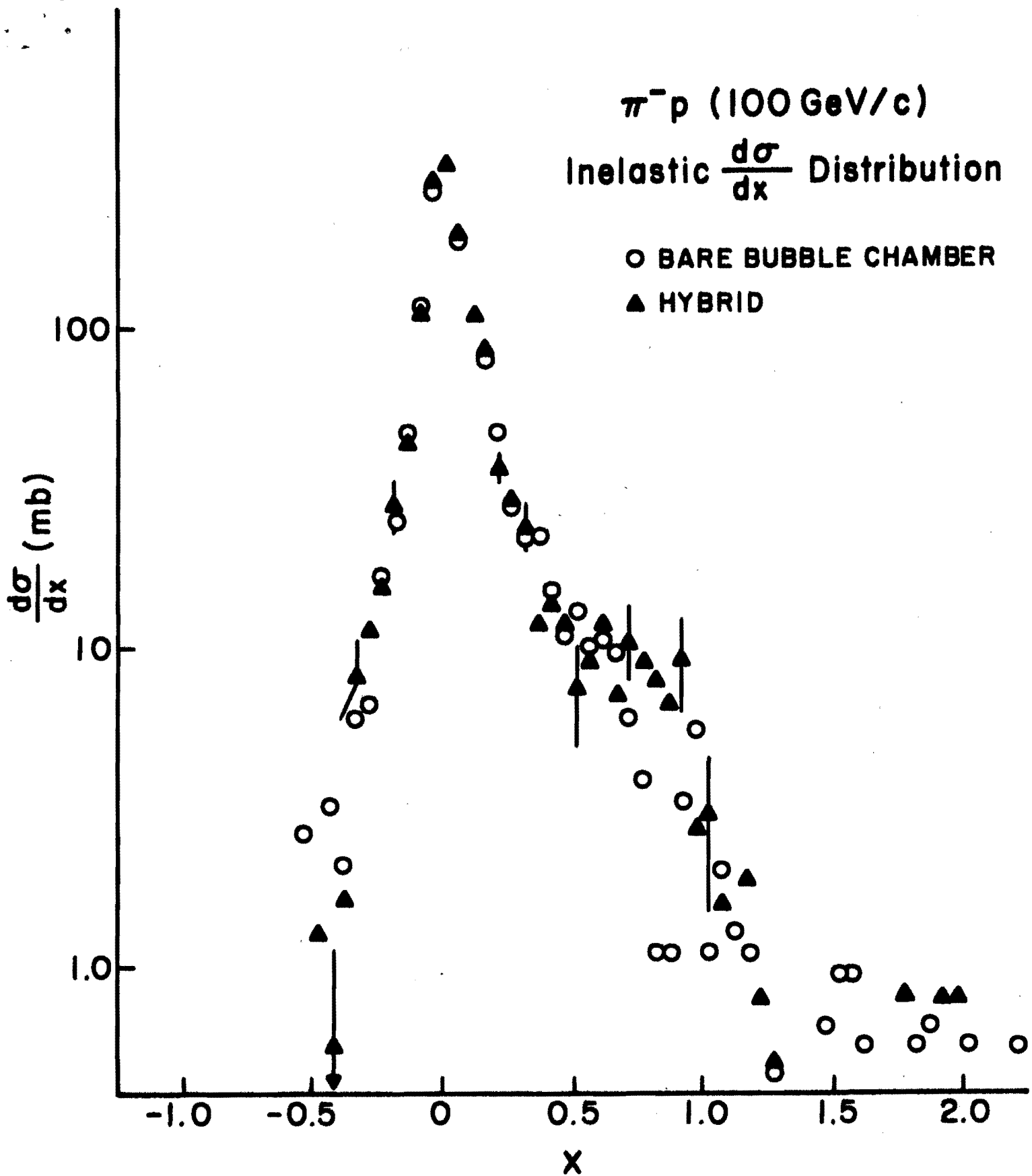


Figure 37

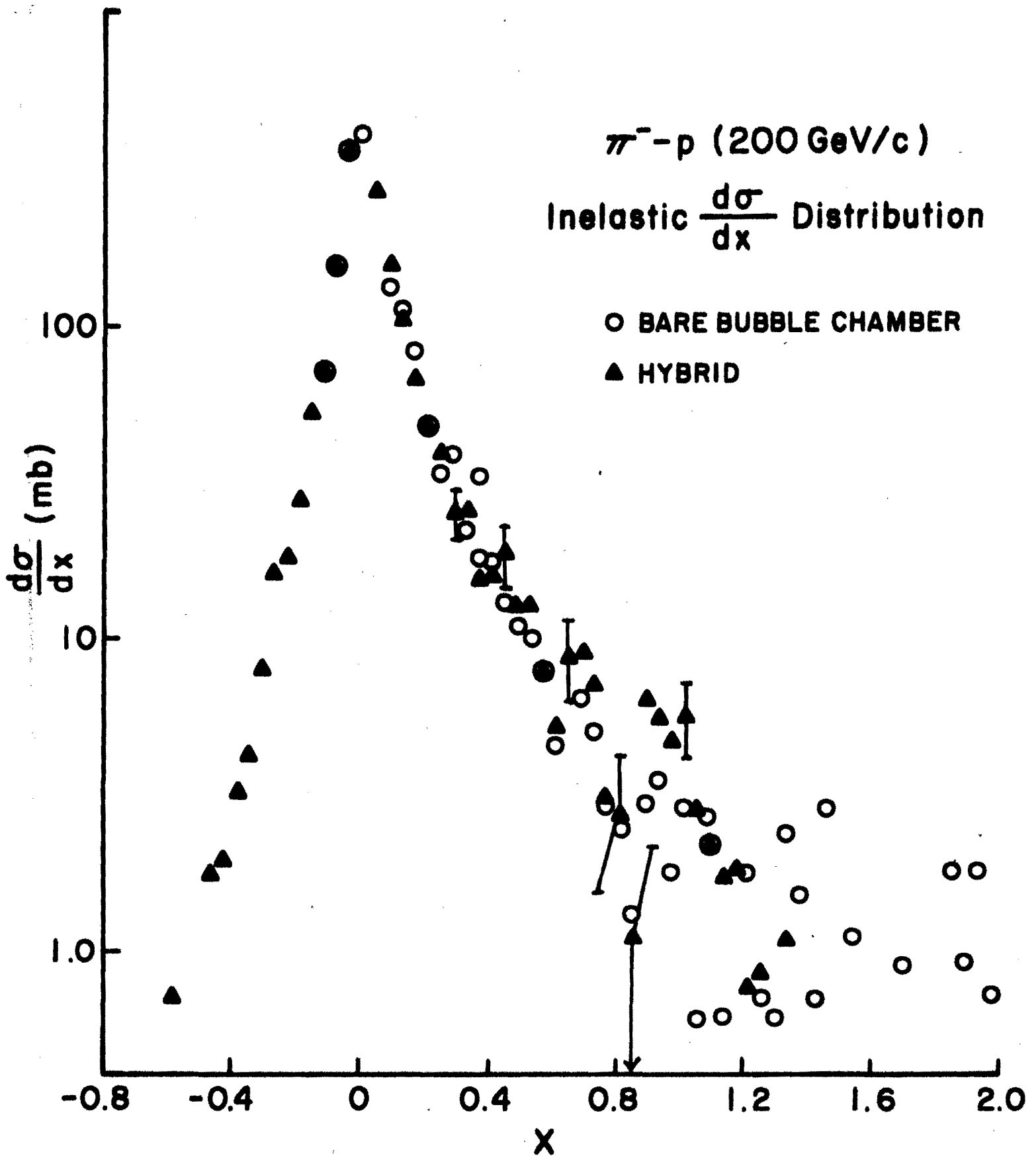


Figure 38

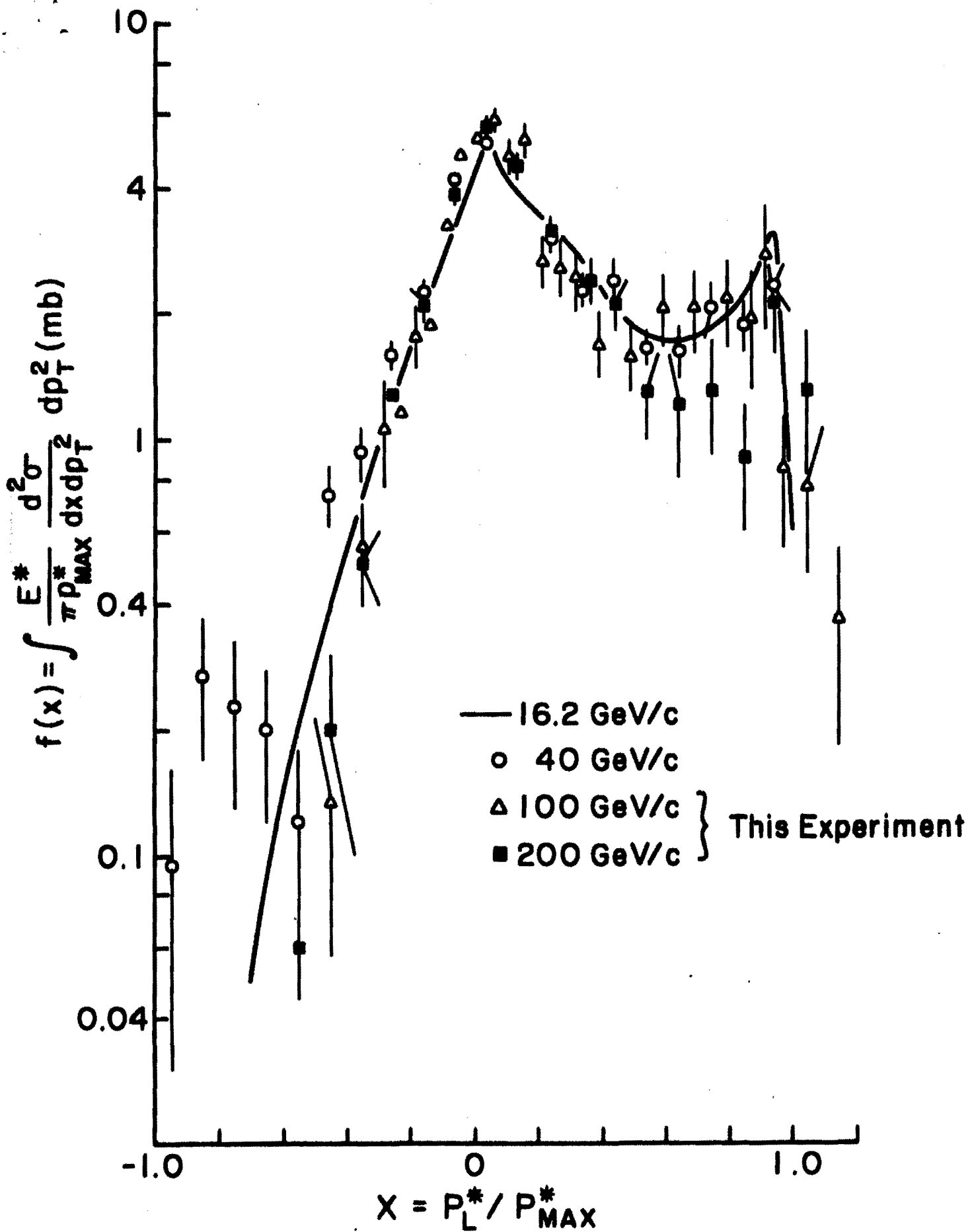


Figure 39